UNIVERSITY OF CALIFORNIA
RIVERSIDE

Direct Interactions Between Bacterial Ribosomes and RNA Polymerase

A Dissertation submitted in partial satisfaction
of the requirements for the degree of

Doctor of Philosophy

in

Biochemistry and Molecular Biology

by

Adam Conn

December 2020

Dissertation Committee:

Dr. Gregor Blaha, Chairperson

Dr. Russ Hille

Dr. Seán O'Leary

The Dissertation of Adam Conn is approved:

Committee Chairperson

University of California, Riverside

Acknowledgments:

Writing an acknowledgments section feels completely unreal. It's such a strange thing. It reads as a list of people who were impactful to my own development and survival throughout the Ph.D. process, which is great and important and so very much needed. All these folks and definitely more (I am far too forgetful to list everybody and I apologize if you missed the list, I mean no disrespect!) should be honored for how they made this all possible.

…

But in forming that list, in acknowledging how I could not have achieved what I had without the aid of all these wonderful people, it also demands some self-recognition that this feat is worthy of praise. And that's the hard one to swallow.

I did a thing.

I was far from confident I would make it this far, yet here I am. Still standing, still writing, still pushing forward. So to everybody, thank you so much for keeping me on this path. It truly means the world to me that I have this opportunity to write this excerpt, to be able to look myself in the mirror and confidently say I have done something worth celebrating and that you all were the ones to make it possible. Thank you.

And now, the actual list!

Let me start by thanking my committee members, past and present: Dr. Hille, Dr. O'Leary, Dr. Song, Dr. Hai, thank you for being a source of knowledge to draw upon, wisdom in approaching both science and the academic process, and a thorn in my side when I wanted to take shortcuts. It's far too easy for me to get complacent and think I have finally "gotten it," but if I took anything away from this entire process, it'd be that there is never a "getting it," just new questions to ask and ideas to explore with each new piece of data added to the ever growing puzzle.

To my lab mates, thank you all for the help over the years, trading off cleaning up preps for starting cultures so I could leave before the sun went down and you all wouldn't have to come in before the sun came up. Special thanks to Steve Diggs, Joseph Hahm, Tim Tam, and Carlos Rodriguez. I seriously would have been lost on so many occasions without your guidance and assistance with lab work, technique, theory, not going insane, most everything really.

To my PI, Dr. Blaha, it's hard to overstate how much help you have been over the years. Honestly, I probably would not have even started the Ph.D. process at all if it hadn't been for you. Being told upfront by some people after I was accepted to the program that I should drop out immediately had me reaching for the door. You were the first person to slam that door right back shut and tell me to step up and prove them wrong. Even if I still have a long road ahead of me, I am at least glad I have held on this long and buried the idea that I could never be a biochemist. Thanks for all the support, guidance, chips, and chocolate.

To my family, Hi Mom! Hi Dad! Hi Morgan! Hope you survived this far! I know you all said you'd read this cover to cover, but it's going to get a fair bit denser coming up and I wouldn't blame you for stopping about here. The shorthand of it all is I did some science, there is still a bunch more to do on the topic, but at least the field is now looking at this topic and taking it seriously whereas it seemed to be relatively disregarded in the recent past. Cool! Thanks for the support. Thanks for believing in me even if you weren't sure what in the world I was actually doing. Knowing you all were always there to turn to was vital to my persistence.

To Ada, I don't think there has been a day since I started graduate school that you hadn't been there with me: talking, supporting, comforting, cheering. This entire process would have stunk without you always being there by my side. High or low, I always had you to turn to. I can't wait to see what the future has in store for us, but I have a feeling it is going to be great.

To Maria Fletcher, I think you were the one that started this journey for me. Twelve years in the making, the first one to not only say I should go to college, but that I should try to go all the way, that I had a chance to pursue a doctorate and earn it. Thanks for believing in me and pushing me in the right direction. I look forward to earning that degree and being able to come back and show you I finally made it.

To my friends old and new, there are honestly far too many of you to list here. Thank you for being you, spending your time, keeping me from falling victim to the college grind and losing my motivation to continue. Thank you for laughs, the games, the fun.

I would also like to thank Nucleic Acids Research for originally printing Fan H, Conn AB, Williams PB, et al. Transcription-translation coupling: direct interactions of RNA polymerase with ribosomes and ribosomal subunits. *Nucleic Acids Res*. 2017;45(19):11043-11055. [PMID: 28977553] and Oxford University Press for publishing it. Thank you for allowing me to reprint this work for my dissertation. To our collaborators on this project, thank you for your support and insight to bring this publication to life.

I would also like to thank the International Journal of Molecular Sciences for printing: Conn AB, Diggs S, Tam TK, Blaha GM. Two Old Dogs, One New Trick: A Review of RNA Polymerase and Ribosome Interactions during Transcription-Translation Coupling. *Int J Mol Sci*. 2019;20(10):2595. Published 2019 May 27. [PMID: 31137816]. Thank you for the opportunity to reprint this work.

Lastly, to everyone else who has made it this far, thank you for reading this, whether you are friends, companions, colleagues that I might have missed, or a reader I haven't met before. I hope you have found or will find something in here that you find interesting. Whether it be for curiosity, interest in transcription and translation, or happenstance, thanks for giving this dissertation a read.

ABSTRACT OF THE DISSERTATION

Direct Interactions Between Bacterial Ribosomes and RNA Polymerase

by

Adam Conn

Doctor of Philosophy, Graduate Program in Biochemistry and Molecular Biology
University of California, Riverside, December 2020
Dr. Gregor Blaha, Chairperson

The coupling of transcription and translation is more than mere translation of an mRNA that is still being transcribed, it is critical to the control of gene expression in bacteria. Despite the recognition of its importance to the cell's physiology and metabolism, a detailed and comprehensive understanding of its mechanistic underpinning has remained elusive.

In my thesis, I aimed to uncover potential routes of crosstalk between RNA polymerase and ribosome, the key players of transcription and translation, respectively. In my *in vitro* work, I identified direct interactions between both of these nanomachines as potential element for the regulation of the coupling of both processes. Using several methods I was able demonstrate the existence and specificity of this interaction and in collaboration with my colleagues from the Blaha and Wang laboratories, I was able to narrow the RNA polymerase binding interface on the ribosome to the head region of the small ribosomal subunit.

All this progress in our understanding of transcription-translation coupling depended on a reliable method of separating free from ribosome-bound RNA polymerase. To this end I have established a reliable analytical procedure using sucrose gradient centrifugation followed by SDS polyacrylamide gel electrophoresis. Recently, I improved this procedure by replacing the sucrose gradient centrifugation with native gel electrophoresis, thus reducing the time and the amount of material required for the analysis of the interactions between RNA polymerase and ribosomes.

To place my finding of the direct interaction between RNA polymerase and ribosomes in context of the resurgence of interest in the mechanism of coupling, I have included in this thesis the review I co-authored that summarizes the recent literature of the field. In this review, we integrate the presented data of the literature and of my work into a dynamic model of transcription-translation coupling in which the interactions between RNA polymerase and ribosomes are repeatedly formed and broken. The careful comparison of the effects of the direct interactions between RNA polymerase and ribosomes with those mediated by transcription factors NusG and RfaH leads us to propose two distinct modes of coupling: a factor-free and a factor-mediated coupling.

Table of Contents

List of Figures

Chapter 1: Introduction

Chapter 2: Methodologies, Optimizations, and Standardizations

Chapter 3: *E. coli* Ribosome and Ribosomal Subunits Direct Coupling to RNAP

List of Tables

Chapter 3: *E. coli* Ribosome and Ribosomal Subunits Direct Coupling to RNAP

Chapter 1:

Introduction

Introduction:

As much as we like to describe *Escherichia coli* and other bacteria as simple bags of loose enzymes, recent work has demonstrated that these "bags of enzymes" actually regulate all enzymatic activity by employing sophisticated temporal and spatial programs. It is therefore unsurprising that the two processes central for the expression of genes, transcription and translation, display more complexity in the context of the cell than the individual processes in isolation would suggest. In the following chapters, I will explore this complexity by studying the interactions between RNA polymerase and ribosomes, the central nanomachines of transcription and translation, respectively. As I provide in my discussion an extensive overview of the current knowledge of transcription and translation coupling itself, and to avoid unnecessary redundancy, I will provide here only a description of transcription and translation itself.

Transcription:

Transcription is the process that transforms the genetic information encoded in the form of DNA into RNA using the enzyme RNA polymerase (RNAP). RNAP is a 379 kDa multi-subunit complex consisting of two α subunits, a β subunit, a β' and an ω subunit known as the core complex. The two α subunits assemble through a dimerization domain, acting as a platform for the folding of the β subunit. Similarly, the ω subunit acts as a folding chaperone for the β' subunit. The assembly of the $(\alpha)_2\beta$ and ωβ' subcomplexes results in the formation of transcriptionally competent core enzyme of RNAP. Once bonded together into the core enzyme, the β and β' subunit form a cleft

through which the upstream double stranded DNA will be directed towards the active site of the polymerase. Before reaching the active site, the double stranded DNA is separated; The template strand continues towards the active site of the polymerase while the non-template strand reroutes towards the surface of the polymerase. At the active site, the nascent RNA is extended in a template strand-dependent fashion forming a DNA:RNA hybrid duplex of 8-9 nucleotides length. At the end of this duplex, the RNA and template DNA are separated from one other and exit the polymerase through a separate path. After exiting the polymerase, the template DNA strand recombines with the non-template strand to form the downstream double-stranded DNA (Figure 1.1).

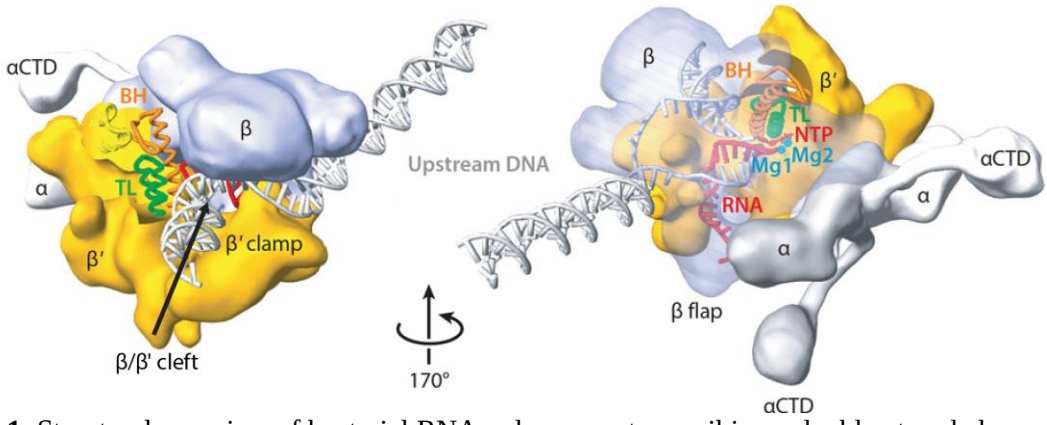

Figure 1.1: Structural overview of bacterial RNA polymerase transcribing a double-stranded DNA. Double-stranded DNA, in white, enters into the active site of the RNAP through a cleft between the β and β' subunits. The template DNA splits from the non-template DNA and is fed into the active site. The appropriate rNTP enters through a secondary channel controlled by the trigger loop, coordinated to two active site magnesium ions. Upon synthesis, the DNA:RNA hybrid is formed. The translocation of the polymerase along the DNA allows the process of nucleotide addition to reiterate. Near the β flap, the DNA•RNA hybrid breaks down, allowing the nascent RNA to exit the RNAP though the exit channel. Figure adapted from Belogurov and Artsimovitch, 2015.

To initiate transcription, the core RNAP recruits σ^{70} to form a 449 kDa holoenzyme (Finn, Orlova et al 2000). As a holoenzyme, the RNAP adopts the 'closed state' in which the cleft between the β and β' subunit narrows from 25 to 15 Ångstrom (Murakami, Masuda et al 2002). At the end of the transcription initiation phase, this cleft will accommodate the downstream double-stranded DNA of the gene being transcribed.

σ^{70} is a four-domain protein responsible for recognizing the -35 and -10 promoter elements upstream of the transcription start site. Once σ^{70} binds as part of the holoenzyme to these DNA elements, the duplex DNA undergoes several conformation changes. Domain 2 of σ^{70} interacts with the -10 element -- with a consensus 5' TATAAT-3' sequence -- , while domain 4 interacts with the -35 element -- consensus 5' TTGACA-3' sequence -- resulting in around 36 degrees of bending of upstream DNA relative to the downstream DNA (Hawley, McClure et al 1983, Murakami, Masuda et al 2002, Campbell, Muzzin et al 2002). In addition, domain 4 interacts cooperatively with the C-terminal domains of the two α-subunits to the UP DNA element (upstream of the -35 element), bending the upstream DNA even more towards the RNAP. This bending of the DNA is thought to facilitate the melting of the double stranded DNA and facilitate conformational changes in the RNAP that enable the formation of the so called "open complex", RP_o, in which the DNA region at the transcription start site melts to form a transcription bubble (Figure 1.2, Ruff, Thomas Record, Jr. et al 2015).

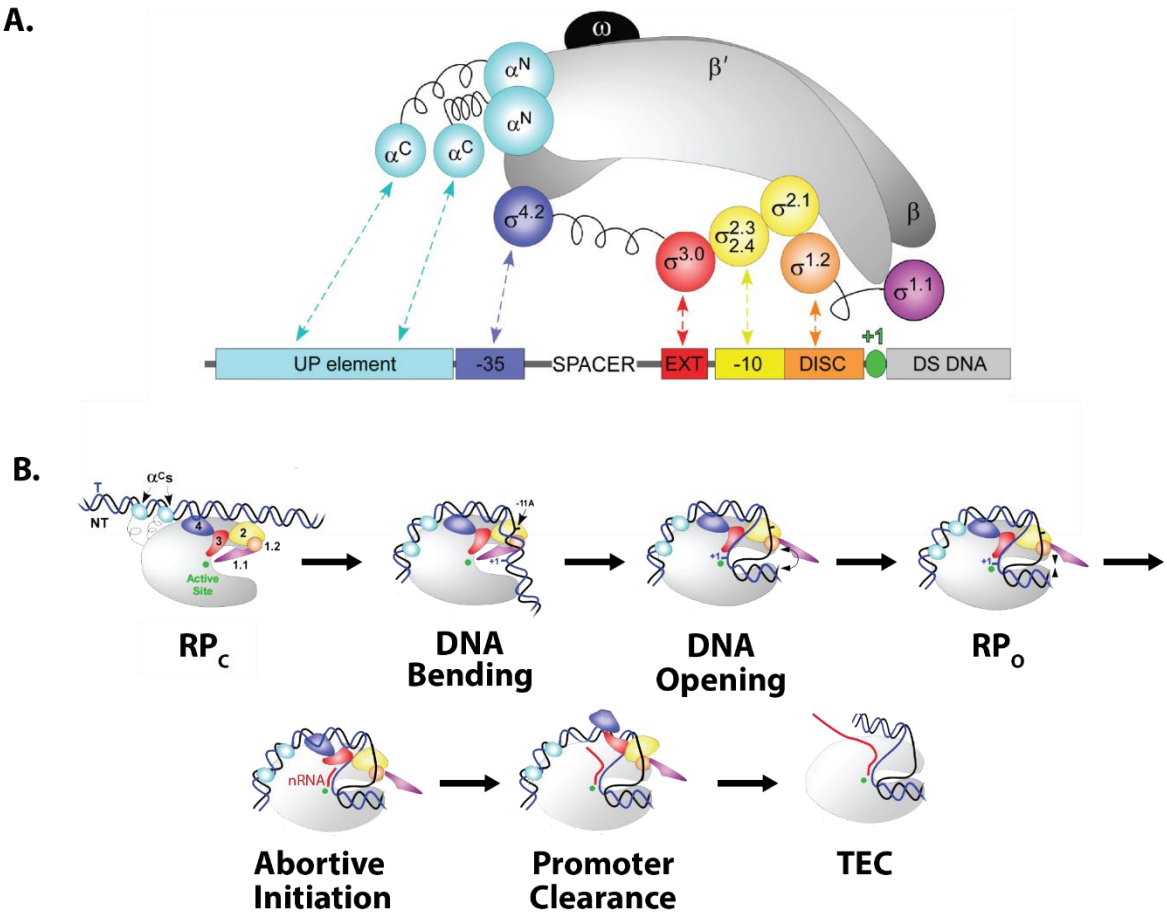

Figure 1.2: Transcription initiation. **A)** Interactions between the promoter and specific σ^{70} RNAP regions. UP element in cyan, -35 element in blue, extended -10 in red, -10 element in yellow, discriminator region in orange, transcription start site in green. **B)** Schematic representation of the steps of transcription initiation from DNA binding the RNA polymerase (RNAP) in the closed state (RP_C) to the formation of the transcription elongation complex (TEC). RNAP binds with the double-stranded DNA along the promoter region through specific interactions mediated by σ^{70} and the α-subunit. Upon doing so, the DNA is bent and unwound, with the template strand being oriented towards the active site. Upon strand separation, the RNAP is able to enter an open state (RP_O), facilitating elongation. With the start site in place, RNAP begins a process of abortive initiation, forming short strands of nascent RNA (nRNA). Once a long enough stretch of DNA:RNA hybrid forms and is able to push past region 3 of σ^{70}, the RNA is able to enter the exit tunnel. Thus, the promoter is able to be cleared and σ^{70} to be released, forming a functional TEC. Figure adapted from Ruff, Record Jr., 2015.

As the duplex DNA is sufficiently destabilized, the -10 element is able to bend into the cleft formed by β and β', with the -11 non-template A (the most conserved base of the -10 element) base flipping out into a complementary binding pocket within region 2.3 of σ^{70} resulting in a 90 degree turn of the DNA between the -11 and -10 positions, (Feklistov, Darst et al 2011) stabilizing the strand separated state (Feklistov, Darst et al 2011, Zhang, Feng et al 2012, Basu, Warner et al 2014, Murakami, Darst et al 2003). At this point, region 1.1 of σ^{70} assists in preventing non-promoter DNA from entering the active site while the remainder of the DNA is loaded into the polymerase in preparation for strand separation. Upon loading DNA into the active site, the 13 bp (-11 to +3) transcription bubble is able to melt open and transition into a stable RP_o state, driven by RNAP affinity towards the open state rather than external energy input (Feklistov, Darst et al 2011).

The final transition from an unstable to stable open complex involves the placement of the +1 nucleotide of the template strand in the RNA polymerase active site (Murakami, Masuda et al 2002). As the first nucleotide is fed through a positively charged tunnel (Murakami, Darst et al 2003) to the active site of the polymerase, the non-template strand is loaded into its binding track (Saecker, deHaseth et al 2011). Thus, the fully stabilized open complex can enter the nucleotide addition cycle where RNA is synthesized one nucleotide at a time. Each nucleotide addition cycle begins with the RNAP in the pre-translocated state, where both active sites, *i* and *i* + 1, are occupied with the nascent DNA:RNA hybrid (Mishianina, Palo et al 2017). Translocation of the DNA:RNA hybrid not only opens the *i* + 1 site of the polymerase for the addition of

another ribonucleotide, but also places the 3′ OH group of the nascent RNA within the coordination sphere of a Mg^{2+} ion bound in the *i* site. This interaction with the Mg^{2+} ion prepares the 3′ OH group for a nucleophilic attack on the α-phosphate group of the ribonucleotide triphosphate (rNTP) upon its accommodation into the *i* + 1 site (Steitz 1998). The rNTP enters the active site through a secondary channel and its binding to the active site leads to site closure. This closing assists in dehydrating the active site, orienting the two catalytic Mg^{2+} ions, and aligning the 3′ OH of the nascent RNA with the α-phosphate of the incoming NTP (Windgassen, Mooney et al 2014) while also reducing the dimensions of the secondary channel (Vassylyev, Vassyleyeva et al 2007). After phosphodiester bond formation has been achieved, the pyrophosphate dissociates from the polymerase through the secondary channel the rNTP had entered the active site through. Once the pyrophosphate exits, the active site reopens for another cycle of nucleotide addition.

As nucleotide addition continues, the growing nascent transcript must eventually push past the σ^{70}'s domain 3.2 loop which blocks the exit channel for the DNA:RNA hybrid on the polymerase. Whenever the nascent DNA:RNA hybrid is unable to the dislodge the domain 3.2 loop, the nascent RNA dissociates from the polymerase and a new nascent RNA synthesis is initiated in the process known as abortive initiation (Murakami, Masuda et al 2002). Once the nascent RNA reaches a length of 13-15 nt (7-9 nt DNA:RNA hybrid), it can successfully free itself from the 3.2 loop, clearing the promoter, releasing σ^{70}, and beginning the cycle of transcription elongation (Vassylvev, Vassylveva et al 2007). During this transition from the initiation to elongation phase, the

nucleic acids replace their contacts to σ^{70} with interactions to β and β' subunits. This remodeling of the nucleic acid interactions along with proper positioning of several key structural elements of the polymerase prepares the RNAP for the elongation cycle.

Transcription elongation does not proceed monotonously through repeat cycles of nucleotide addition, but is prone to pausing (Weixlbaumer, Leon et al 2013) as frequently as every 200 nucleotides (Adelman, La Porta et al 2002). These frequent, brief pauses were suggested to provide time for the proper folding of the nascent RNA (Pan, Artsimovitch et al 1999), to allow transcription factors to bind the elongation complex (Artsimovitch, Landick et al 2002), and to coordinate the rate of transcription and translation of the nascent RNA (Landick, Carey et al 1985). Some of these brief, elemental pauses can evolve into permanent pauses due to backtracking of the polymerase along the DNA:RNA hybrid or due to formation of nascent RNA hairpins in the RNA exit channel of the polymerase at hairpin pause sites and intrinsic termination sites.

During backtracking along the DNA:RNA hybrid, the polymerase extrudes the 3′ end of the nascent RNA through the secondary channel, thus blocking the entry of rNTPs into the active site of the polymerase (Ray-Soni, Bellecourt et al 2016). Backtracked polymerases are rescued from their arrested state by either forward translocating all of the extruded sequence, thus pulling the 3′ end of the nascent RNA back into the active site, or by cleaving the extruded RNA off the polymerase with the aid of transcription factor GreA or GreB. This cleavage produces a free 3′ end in the active site, enabling the RNA

polymerase to enter another round of nucleotide addition (Lowery-Goldhammer, Richardson et al 1974)

Elongation may cease in a variety of ways, canonically through reaching the RNA's intrinsic terminator sequence. The intrinsic terminator consists of a G-C rich dyad followed by an 7-8 nt U-rich stretch on which the polymerase pauses. Stalling on the U-stretch gives the G-C rich sequence sufficient time to form a hairpin loop within the RNAP exit channel which in turn enables the DNA:RNA hybrid to melt, destabilizing the elongation complex and thereby terminating transcription (Lubkowska, Maharjan et al 2011).

Alternatively, termination can be achieved through Rho factor. Rho is homohexameric ATP-dependent helicase capable of binding and translocating along nascent RNA. It preferentially binds the nascent RNA at Rho utilization sites (rut), an 80-90 nt long C-rich/G-poor stretch of RNA lacking any secondary structure (Lowery-Goldhammer, Richardson et al 1974). The binding of Rho to the rut sequence involves all six monomers of Rho, enabling Rho factor to translocate along the RNA. Rho-dependent termination is thought to be brought about when the Rho factor contacts the RNA polymerase at its RNA exit channel by hyper-translocating the RNAP, leading to translocation of the DNA:RNA hybrid without nucleotide addition (Park, Roberts et al 2006), through hybrid-shearing, where continued ATP hydrolysis shears the DNA:RNA hybrid (Richardson, 2002), or by inducing a conformational change on the RNA polymerase that leads to the melting the DNA:RNA hybrid within the polymerase.

As termination proceeds, the transcription of the gene/operon ceases, allowing the polymerase to dissociate from the DNA and initiate another round of transcription by binding a σ^{70} factor and finding a new promoter site on the DNA.

Translation:

Translation is the process in which the genetic information encoded on the messenger RNA is translated into protein. The key player in this process is the ribosome, a several megadalton large ribonucleoprotein particle which, with the aid of amino-acyl transfer RNAs (tRNAs), decodes the mRNA and synthesizes the encoded protein.

In bacteria, the fully active ribosome, the 70S ribosome, is composed of two ribosomal subunits, the large and the small ribosomal subunit, i.e., 50S and 30S subunit, respectively. The 50S subunit consists of two RNAs, the 23S and 5S ribosomal RNA (rRNA) and approximately 30 ribosomal proteins (L1-L36). The 30S subunit consists of the 16S rRNA and about 20 ribosomal proteins (S1-S21) (Schmeing, Ramakrishnan et al 2009).

The structure of the 50S subunit consists of a large body from which three protuberances extend, the L1-stalk, the central protuberance, and the L7/L12 stalk while the 30S subunit appears to have a more irregular shape, consisting of several features that can be identified even at low resolutions such as the head, platform, body, neck, shoulder, and toe(Figure 1.3).

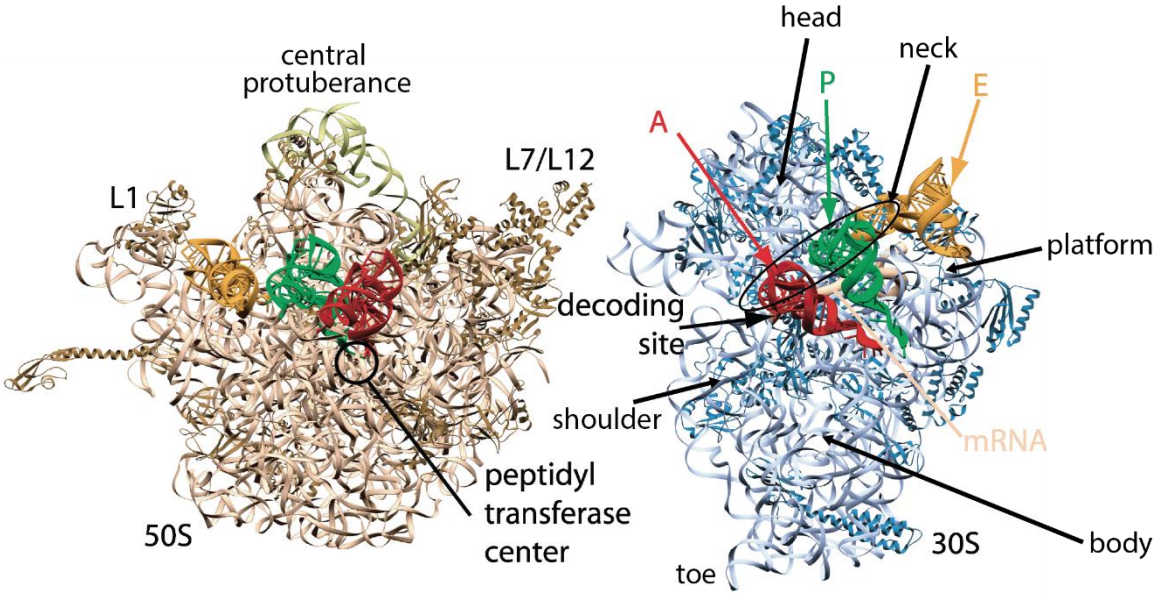

Figure 1.3: Structure of the large and small ribosomal subunits .View from the interface between the 50S ribosomal subunit (left) and 30S ribosomal subunit (right), highlighting the A- (red), P- (green), and E-(yellow) site tRNAs and structural features of both subunits. The components of the 50S subunit, 23S rRNA, 5S rRNA and ribosomal proteins are shown in beige, yellow, and gold, respectively. The 50S subunit consists of three protuberance, the L1 stalk, the L7/L12 stalk and the central protuberance. The peptidyl transferase center is housed within the main body. On the right panel is the 30S subunit displayed with bound mRNA, in wheat, and one tRNA in each of the three tRNA bindings sites. The components of the 30S subunit, 16S rRNA and ribosomal proteins are shown in light blue and dark blue, respectively. The 30S subunit consists of a head, that swivels about the neck, which connects the head to the 30S body. Molecular figures were made using RIBBONS (Carson, 1991), MOLSCRIPT (Kraulis, 1991) and RASTER3D (Merrit and Bacon, 1997). This figure was adapted from Ramakrishnan, 2002.

During translation, the tRNA steps through three tRNA binding sites on the ribosome, the “A”, “P”, and “E”-sites. Both ribosomal subunits contribute to each tRNA binding site, anchoring the acceptor arm of the tRNA via its 3′ terminal CCA to the 50S subunit and to the 30S subunit via base pairing interactions between the tRNA’s anticodon loop and a three nucleotide stretch of mRNA known as the codon. In the A-site, the incoming aminoacyl tRNA is selected before being accommodated. After accommodation, the peptidyl chain on the tRNA in the P-site is transferred onto the aminoacyl group of the A-site tRNA, thereby extending the peptidyl chain by one amino acid. The peptidyl tRNA in the A-site is translocated into the P-site of the ribosome where it awaits the arrival of another aminoacyl tRNA into the A-site. The now deacylated tRNA in the P-site progresses into E-site from where it exits the ribosome.

This process of protein synthesis can be subdivided into three phases: initiation, elongation, and termination (Figure 1.4).

During translation initiation, the 30S subunit binds mRNA, initiation factors IF1, IF2, IF3, and fMet-$tRNA_i$ to form the 30S initiation complex (Ramakrishnan 2002). Each factor fulfills a different critical function during translation initiation.

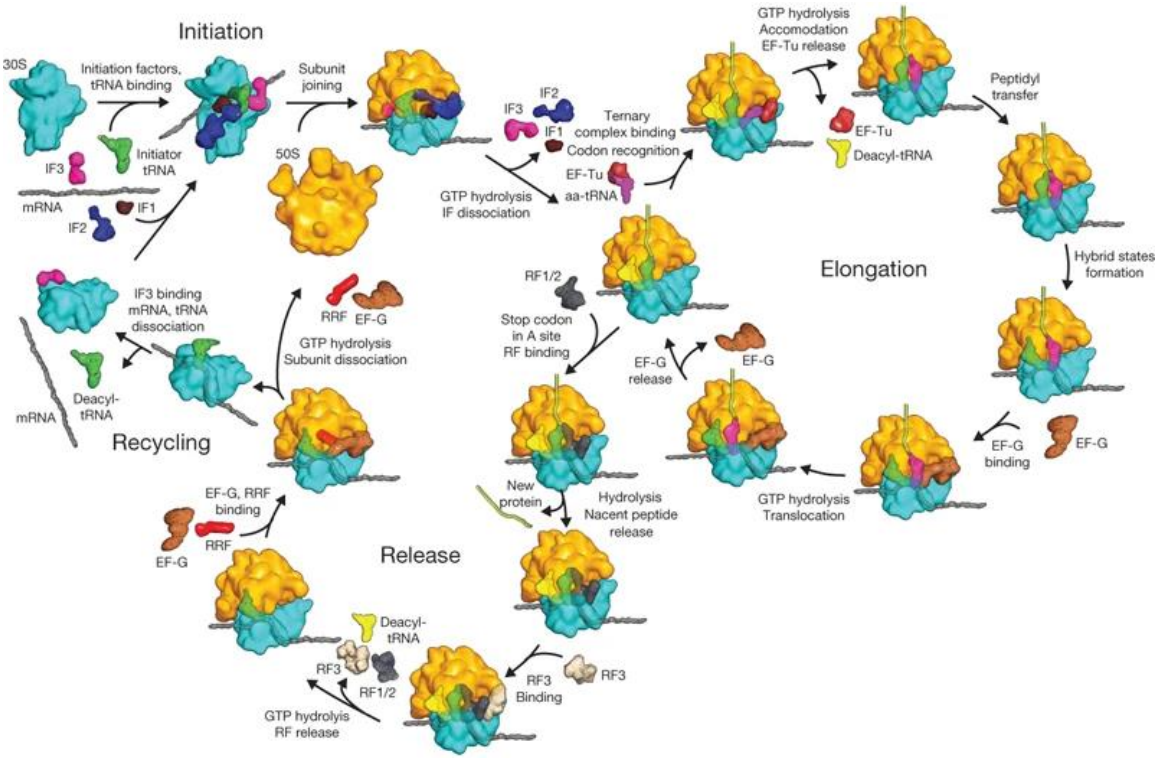

Figure 1.4: Overview of bacterial translation including initiation, elongation, termination, release, and recycling. The 50S subunit is displayed in yellow, while the 30S subunit is in cyan. Figure adapted from Schmeing, Ramakrishnan, 2009.

IF3 prevents the binding of tRNAs other than fMet-tRNA$_i$ to the P-site of the 30S subunit (Gualerzi, Pon 1990, Sussman, Simons et al 1996). It is composed of two domains, the N-terminal and C-terminal domain, which are connected by a linker region. The N-terminal domain interacts with the 30S platform close to the E-site, while the C-terminal domain reaches all the way into the P-site (Ayyub, Dobrival et al 2017). In addition to selecting the tRNA for binding into the P-site, IF3 stimulates the release of the mRNA and deacylated tRNAs from the 30S subunit and inhibits the binding of 50S subunit to the free 30S subunit (Karimi, Pavlov et al 1999).

IF1 binds within the A-site of the 30S subunit, interacting with helix 44 and ribosomal protein S12, occluding tRNAs from accessing the A-site until it's dissociation (Carter, Clemons Jr. et al 2001).

IF2 facilitates the binding of fMet-tRNA$_i$ to the 30S subunit and of the 50S subunit to the 30S initiation complex. It is composed of an N-terminal domain close to the A-site, responsible for binding tight to the 30S subunit (Gualerzi, Pon 2015), and a C-terminal half containing the "G" domain which loosely binds the 50S subunit, but more importantly includes the GTP binding site/GTP hydrolysis activity as well as domains C1 and C2. The C2 domain is responsible for recognizing the formylated methionine on the fMet-tRNA$_i$ and protecting it from hydrolysis (Eiler, Lin et al 2013, Peterson, Kruse et al 1981).

Canonically, mRNA is recruited to the 30S subunit through binding of its Shine-Dalgarno sequence, a 4-6 nucleotide long A/G rich region of mRNA located 6-12

nucleotides upstream of the translation start site, to the anti-Shine-Dalgarno region at the 3′ end of the 16S rRNA (Xia, Santa-Lucia et al 1998). This interaction assists in aligning the start codon (AUG, GUG, or UUG) into the P-site of the 30S subunit (Sussman, Simons et al 1996).

With the 30S initiation complex formed, the 50S subunit can dock to form the 70S initiation complex, leading to the release of IF3 (Grigoriadou, Marzi et al 2008). After GTP hydrolysis by IF2, fMet-tRNA$_i$ is accommodated into the peptidyl transfer center on the 50S subunit, thereby readying the 70S complex for the first-round of peptide elongation (Tomsic, Vitali et al 2000).

The elongation cycle begins with an empty A-site, awaiting the correct aminoacyl tRNA to be delivered in the form of a ternary complex with bound EF-Tu and GTP. The correct aminoacyl tRNA is selected through the codon-anticodon base pairing of the incoming tRNA with the mRNA in the A-site of the 30S subunit. The geometry of the first two codon-anticodon base pairs is monitored through minor groove interactions with two bases of the 16S rRNA, A1492 and A1493. This observation is consistent with the third base of the codon being a wobble base which can engage in more than just Watson-Crick interactions with its counterpart on the anticodon loop (Ogle, Ramakrishnan 2005). The recognition of the correct codon-anticodon interaction induces a closing of the 30S subunit shoulder, introducing a kink into the anticodon loop of the tRNA which forces the acceptor arm of the tRNA and its bound EF-Tu•GTP towards the A-site of the 50S subunit (Schmeing, Voorhees 2009). This straining of the tRNA pushes the GTPase site of the EF-Tu onto the GTPase associated center on the 50S subunit,

allowing the α-sarcin/ricin loop within the GTPase associated center to activate the GTPase activity of the EF-Tu (Schmeing, Voorhees 2009, Shi, Khade et al 2012). Upon GTP hydrolysis, EF-Tu is released from the ribosome and the tRNA is accommodated into the A-site. The CCA tail of the A-site tRNA is bound into the peptidyl transfer center (Valle, Zavilov et al 2003), placing the α-amino group of its attached amino-acyl group in the ideal position to perform a nucleophilic attack at the C-terminus of the peptidyl chain attached to the peptidyl tRNA bound in the P-site (Schmeing, Huang et al 2005). By the end of the nucleophilic attack, the peptidyl chain is transferred to the aminoacyl tRNA in the A-site, extending the nascent peptidyl chain by one amino acid and deacylating the tRNA in the P-site.

To enable another cycle of elongation, the peptidyl tRNA in the A-site must translocate into the P-site. With translocation of A-site peptidyl-tRNA to the P-site, the deacylated tRNA in the P-site is translocated into the E-site. The translocation reaction is catalyzed by another GTPase, elongation factor G (EF-G) (Shoji, Walker et al 2009).

After the peptidyl-transferase reaction, the 30S subunit samples multiple conformational states where it rotates relative to the 50S subunit and its head swivels relative to its body. This freedom of motion allows tRNAs to sample two binding states on the ribosome, the classical and the hybrid state. In the classic binding state, the tRNA binds to the same site on the 30S and 50S subunit, e.g., a tRNA bound in the classical A-site is bound to the A-site on the 30S and on the 50S subunit, referred to as the A/A state where the first letter indicates tRNA binding on the 30S subunit and the second letter on the 50S subunit. In the hybrid state, a tRNA is bound to different sites on the 30S and 50S

subunit, e.g., a tRNA can be bound to the A-site on the 30S subunit and to the P-site on the 50S subunit, referred to as the A/P state. In order for the tRNA to adopt the hybrid state, the 30S subunit rotates relative to the 50S subunit while the 30S head swivels around the neck, connecting the head to the body of the 30S subunit, referred to as the rotated or ratcheted state (Figure 1.5).

The ribosome starts oscillating between the ratcheted and non-ratcheted states causing the tRNAs to oscillate between the classical and the hybrid states as well (the peptidyl tRNA between the classical A/A and the hybrid A/P state and the deacylated tRNA between the classical P/P and the hybrid P/E state). The binding of EF-G•GTP to the ribosome stabilizes the ratcheted state of the 30S subunit and the hybrid state of the tRNAs. Through GTP hydrolysis, the body of the 30S subunit is able to relax into the non-ratcheted state while the head of the 30S subunit maintains the ratcheted state, resulting in a tRNA state in which the tRNA binds on the 30S subunit into two separate sites, one linked to the 30S head and one linked to the 30S body. The peptidyl tRNA is bound on the 50S subunit and on the 30S subunit body in P-site while on the 30S subunit head in the A-site. This state is referred to as the ap/P state where the first small cap indicates the tRNA binding site on the head and the second on the body of the 30S subunit. Only upon EF-G release does the 30S head relax back into the non-ratcheted state and with it the tRNA bound to the 30S head is translocated, completing the translocation of the tRNA from ap/P and pe/E to pp/P and ee/E tRNA binding sites (Ratje, Loerke et al 2010). The ee/E-site tRNA is now free to dissociate and another round of elongation can commence.

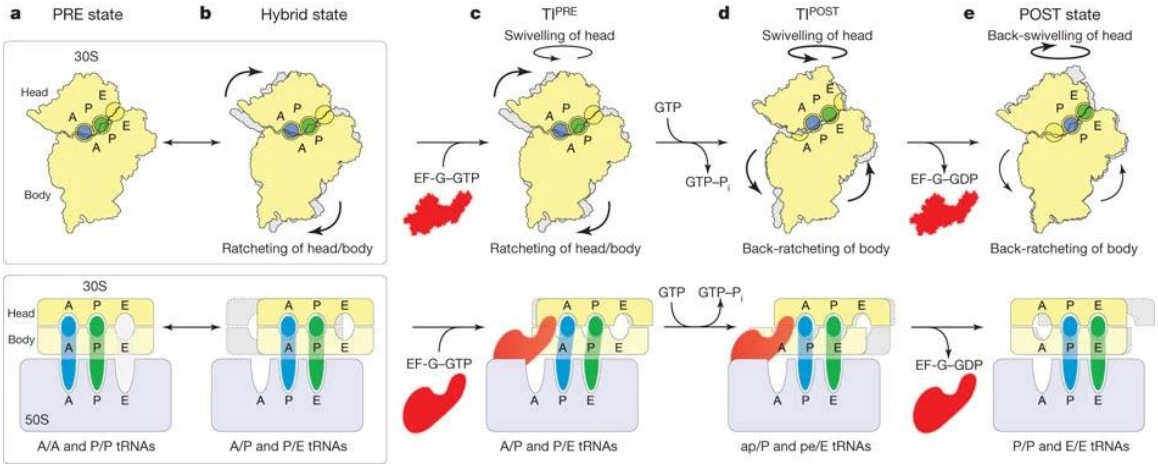

Figure 1.5: Schematic diagram of translation translocation through hybrid states. **a-b)** During elongation, the ribosome is in a dynamic equilibrium between classical (A/A, P/P) and hybrid states (A/P, P/E) where the head and body of the 30S subunit are swiveled and rotated, respectively. **c)** Upon binding of EF-G•GTP, the 30S subunit is stabilized in the ratcheted or hybrid states (A/P corresponds to aa/P and P/E to pp/E in the extended hybrid nomenclature used here and explained in the text). **d)** GTP hydrolysis allows the 30S body to relax while the 30S head is maintained in the ratcheted state, (aa/P progresses to ap/P, pp/E to pe/E upon GTP hydrolysis). **e)** Dissociation of EF-G•GDP allows the 30S head to rotate back, relaxing the ribosome back to classical states (ap/P progresses to pp/P or P/P and pe/E to ee/E or E/E). The E-site tRNA is able to dissociate and a new tRNA may enter the A-site. Figure adapted from Ratje, Loerke, et al., 2010.

The elongation cycle is signaled to end once the mRNA stop codon (UAA, UAG, UGA) enters the A-site (aka A/A or aa/A site). With no matching anticodon, the ribosome stalls on these codons until a class I release factor binds within the A-site to cleave the nascent polypeptide chain from the peptidyl tRNA in the P-site. *E. coli* has two class I release factors, RF1 and RF2. While RF1 recognizes specifically the UAG codon and RF2 the UGA, they both also recognize the UAA codon (Buckingham, Grentzmann et al 1997). Post-cleavage, RF3 accelerates the release of RF1 or RF2 from the ribosome by binding to the ribosome•RF1 or ribosome•RF2 complex in the GDP form, where RF1 or RF2 act as a guanine exchange factor for RF3 (Zavialov, Buckingham et al 2001). Once RF3 is bound with GTP, GTP hydrolysis leads to the release of both release factors from the ribosome.

With the mRNA and P-site tRNA still bound, the ribosome enters the recycling phase in which ribosome recycling factor (RRF) is recruited. Binding of RRF stabilizes the 30S ratcheted state, placing the remaining tRNA into the hybrid P/E site (Dunkle, Wang et al 2011). Afterwards, EF-G appears to bind, and through GTP hydrolysis activity, stimulates subunit dissociation (Fu, Kaledhonkar et al 2016). The free 50S subunit is available for binding a new 30S initiation complex, however, the 30S subunit needs to dissociate the deacylated tRNA as well as the mRNA. Through IF3 binding, the tRNA and mRNA are able to dissociate (Karimi, Pavlov et al 1999), resulting in a free 30S subunit and thus enabling a new round of translation initiation.

Chapter 2:

Methodologies, Optimizations, and Standardizations

Introduction:

Utilizing sucrose gradient centrifugation for determining binding affinities was derived from classical ribosome studies and purification protocols. The methodology behind the separation of ribosomes using a sucrose gradient had been well established since the 1960s (Britten, Roberts 1960) and was refined over the decades to result in efficient preparation of polysomal (Ron, Kohler et al 1968), vacant (Robertson and Wintermeyer, 1981), and reassociated ribosomes (Blaha 2000) depending on experimental need. However, despite the general recognition that ribosomes and complexes thereof sediment through the sucrose gradient and is extensively used for purpose of purifying ribosome particles (Mangiarotti and Schlessinger 1966), the use of this principle to determine the binding affinity of factors to purified ribosomes was mostly avoided. Considering much of the early ribosome purification work was riddled with setbacks and confusions with regard to ribosomal stability brought in part about by subjecting the material to approximately 100,000g-forces for 15+ hours (Noll, Hapke et al 1973), it is no surprise that other methods were favored for this purpose, even if separation of free and ribosome bound factors by sucrose gradient centrifugation was in plain view all along.

In fact, our own group did not begin study the RNA polymerase-ribosome interaction with this method either, favoring instead to use gel filtration chromatography as a more robust, simpler to monitor, and more ‘precise’ method to determine the strength of interactions. Though gel filtration was able to separate free RNA polymerase from ribosome-bound polymerases confirming complex formation (Figure 2.1), it had a

pronounced loss in resolution with increasing concentrations of RNA polymerase and ribosomes due to peak tailing and the increased trapping of material on the column. To eliminate the contamination of individual gel filtration runs, the system had to be reconditioned between each sample, which introduced significant variability in the separation of ribosome-bound and free RNAP. Automation of some of the steps of chromatography during data collection such as autoinjection of samples may have improved the resolution variability between samples. However, due to the increased use of the size exclusion column, a more rapid deterioration of the separation power of the column was expected. Given the scope of the project, multiple column replacements during its duration would have occurred, a significant expense and hurdle in our lab setting. Instead, the capability of separating up to 6 samples of RNA polymerase-ribosome mixtures in parallel under nearly identical conditions, while also being relatively hands off throughout the separation made sucrose gradient centrifugation a more preferable option.

Therefore, one of my first tasks after joining the Blaha laboratory was to develop a reliable and reproducible procedure for density gradient centrifugation and its quantification of the free and ribosome-bound RNA polymerase by SDS polyacrylamide gel electrophoresis (SDS-PAGE).

Once optimized and explored, our lab decided to expand the scope of our study to focus on transcription/translation direct interactions more intensely, focusing specifically on interactions with regard to the functional states of RNAP and ribosome. For my part, I was tasked with refining and quantifying our native gel system.

Size Exclusion Chromatography

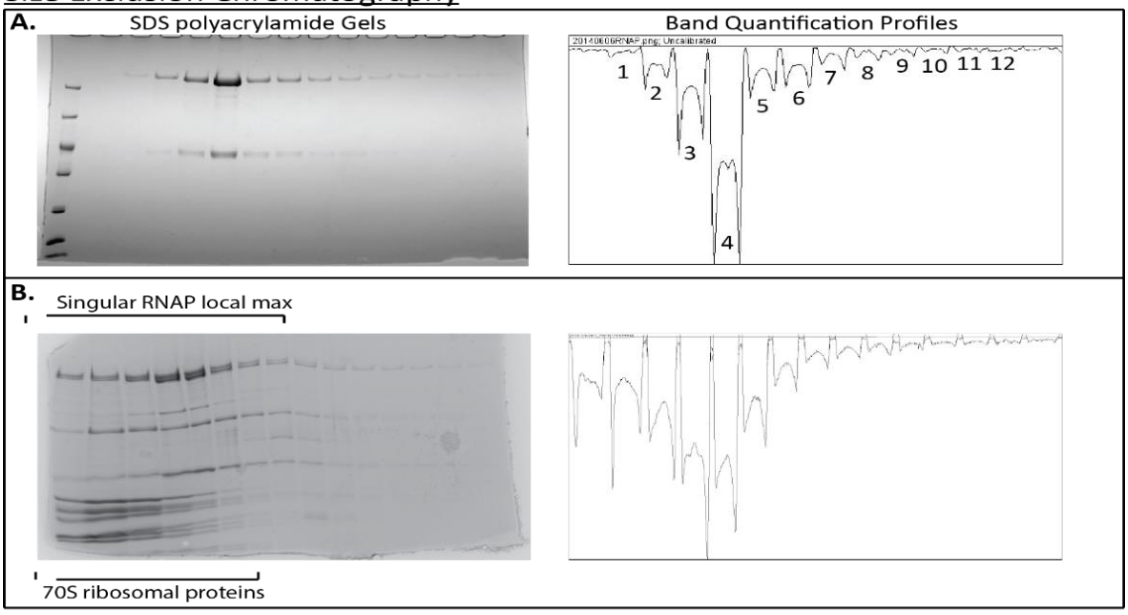

Sucrose Gradient Centrifugation

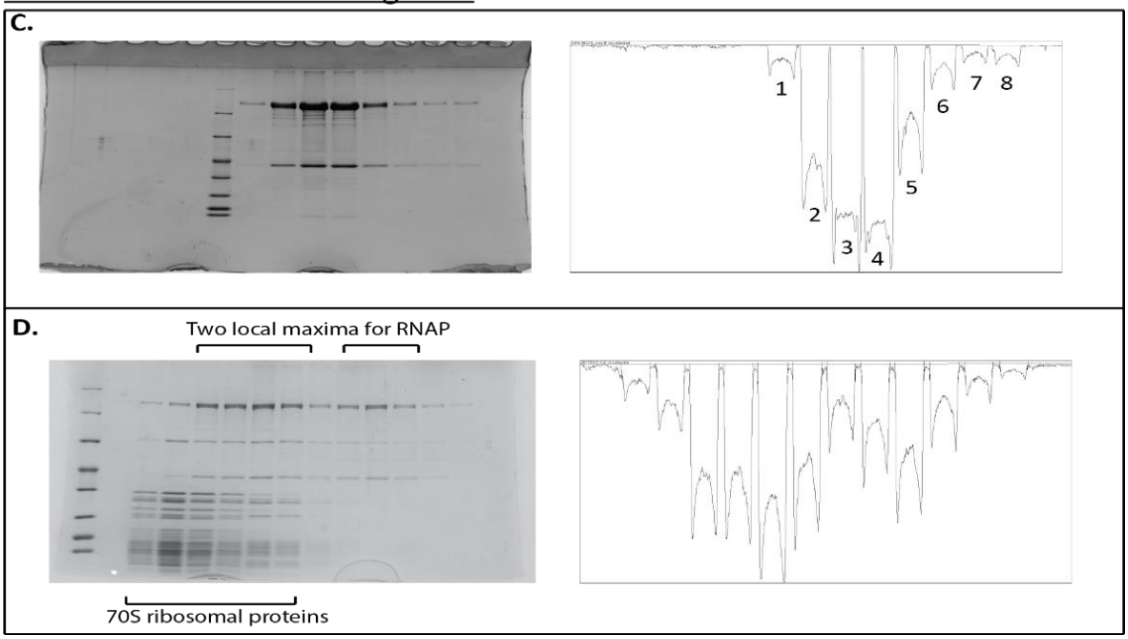

Figure 2.1: Size exclusion chromatography and sucrose gradient centrifugation comparison. Comparison of representative SDS polyacrylamide gels of RNAP collected through size exclusion chromatography (A and B) and sucrose gradient centrifugation (C and D). β/β' were quantified and the band profiles are displayed right of their associated gels, with each lane/fraction of quantifiable RNAP labeled beneath each peak. **A)** RNAP on SEC: Of the 13 lanes, RNAP was detected in 12 lanes as per the gel profile. **B)** 70S•RNAP complex analyzed by SEC: When the complex is formed there is a singular RNAP peak despite two populations of RNAP existing (bound and unbound), making quantification of bound RNAP difficult. **C)** RNAP on sucrose gradient centrifugation: Of the 13 lanes, RNAP was detected in 8, resulting in much less tailing and a sharper signal overall. **D)** 70S•RNAP complex analyzed by sucrose gradient centrifugation: When mixed with ribosomes, two local maxima are detected, one corresponding to the bound fraction of RNAP and one representing the unbound fraction of RNAP, facilitating analysis and quantification.

Optimization and Standardization of the Analysis of Free and Ribosome-bound RNAP by Sucrose Gradient Centrifugation and SDS-PAGE:

In this section I am detailing my efforts to optimize and standardize our analysis procedure for free and ribosome-bound RNAP. This included the selection of the density gradient, i.e., sucrose versus glycerol, optimization of the SDS-PAGE, i.e., more consistent and better resolving gels, and optimization and standardization of data processing and handling.

Sucrose vs. Glycerol Gradient Ultracentrifugation.

In order to dissuade the idea that sucrose in the sucrose gradient may influence the complex formation during the spin, I decided to replace the sucrose with glycerol. In order to accommodate for the differences in viscosity (particles sedimentation coefficients are dependent on viscosity of the solution) and density of the two reagents at 4°C (Lide, 2008), the linear gradient was adjusted from a 10-40% gradient in sucrose to a 10-50% gradient in glycerol, while maintaining all other run time conditions (SW32.1 rotor at 4°C. 13hr. at 28K RPM). The results yielded comparable profiles to that of the sucrose gradients and in separation of the free RNA polymerase from ribosome-bound RNA polymerase, helping establish the interactions we were finding to not be influenced by the chemical forming the gradient. Since both types of gradients yielded similar results, I proceeded to use sucrose for the remainder of my studies as it is the standard for the ribosome field and is more cost effective. (See Figure 2.2)

Sucrose Gradient

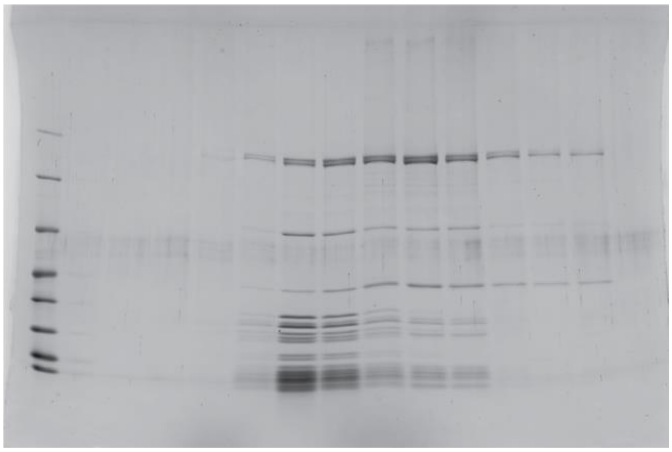

Glycerol Gradient

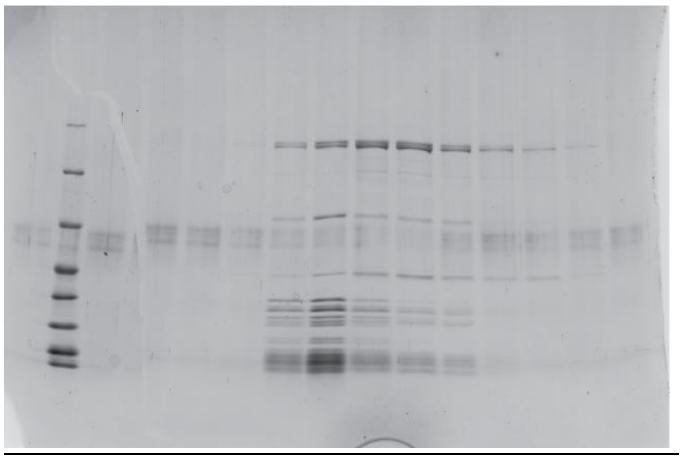

Figure 2.2: Comparison between sucrose gradient and glycerol gradient sedimentation. Both gradients were loaded with the same solution of 70S and RNAP, incubated and loaded onto the same rotor before being spun and fractionated under the same settings. The SDS polyacrylamide gels showed a similar degree of penetration and pattern.

Optimization and Standardization of the Quantification of Free and Ribosome-bound RNAP separated by Gradient Centrifugation:

Quantification of free and ribosome-bound RNA polymerase was achieved through fractionizing the density gradients, precipitating each fraction with one-tenth volume of 100% trichloroacetic acid solution, followed by SDS-PAGE. Since free RNAP was unable to penetrate through the sucrose gradient as effectively as the ribosome (70S or ribosomal subunits), we could measure the ratio of free vs ribosome-bound RNAP based on the profile of the β/β' band on the SDS polyacrylamide gels. If the β/β' band appeared in fractions that penetrated further into the gradient than the free RNAP could penetrate on its own, then it was concluded that some other component in the reaction mixture must be complexed with the polymerase, enabling it to progress deeper into the gradient. The amount of β/β' in each fraction was estimated from the Coomassie-stained SDS polyacrylamide gels through densitometry using the ImageJ software (Schneider, Radband et al 2012)

However, our preliminary results using this quantification method for RNA polymerase in each density gradient fraction had a higher level of variance than we would have desired. This variance was derived in part from the SDS polyacrylamide gels as well as the stability of the RNAP complexes resisting traditional denaturation conditions. Both conditions interfered with the entry of β/β' proteins into the polyacrylamide gel matrix. The quantification of the β/β' bands after Coomassie-staining was further complicated by the unevenness of the background noise across individual gels, requiring a new method of gel preparation to avoid even further loss of resolution.

Improving the resolution and reliability of SDS-PAGE – Optimization of the Gel Preparation and Loading Procedure.

Previously, our homemade SDS polyacrylamide gels were individually poured at a single acrylamide concentration. Given that approximately twenty gels were being run weekly, this process was far too slow. Furthermore, the single percentage gel had a lower amount of resolving power than desired since the range of proteins being analyzed extended from 10 kDa to 175 kDa. To improve this process, we switched to a multicasting system, enabling us to establish a protocol to pour 12 continuous 6-25% polyacrylamide gradient gels simultaneously. These gradient gels were more shelf stable and were much simpler to produce, making the SDS-PAGE analysis of the RNAP•ribosome complex more efficient.

However, as we investigated the effects of more components on complex formation, the need for a more robust and higher resolving gel system became apparent. Many of the ribosomal subunit proteins are of similar size to other key components of transcription and translation such as NusG, RfaH, and Initiation Factors 1 and 3. With the minimal separations of the small molecular weight proteins in the continuous gradient gels, it was impossible to detect if the tested transcription and translation factors were binding to the ribosome or RNAP•ribosome complexes. Furthermore, RNAP has a tendency to get stuck within the well of the SDS polyacrylamide gel. With this in mind, I decided to optimize the SDS polyacrylamide gel further.

I adapted the existing protocol of preparing continuous gradient gels to preparing discontinuous gradient gels, introducing a 4% stacking gel on top of the gradient gel. This provided a two-fold benefit, sharpening up the bands, enabling lower quantities of material to be visualized, as well as lowering the initial percentage of gel, facilitating the passage of RNAP into the gel matrix. The results of this change had dramatic effects on the quality of the results, allowing us to resolve the size differences between the β and β' bands as well as easily distinguish ribosomal proteins. (Figure 2.3)

Lastly, the gel loading buffer had to be adjusted to accommodate RNAP, changing from a typical SDS-PAGE loading buffer to one including more denaturing agents in the 2x loading buffer, i.e., 8 M urea, 2 M thiourea, and 1.4 M β-mercaptoethanol. By providing a more denaturing loading buffer, I found RNAP to more easily entered the gel matrix, increasing the reliability of our analysis even further.

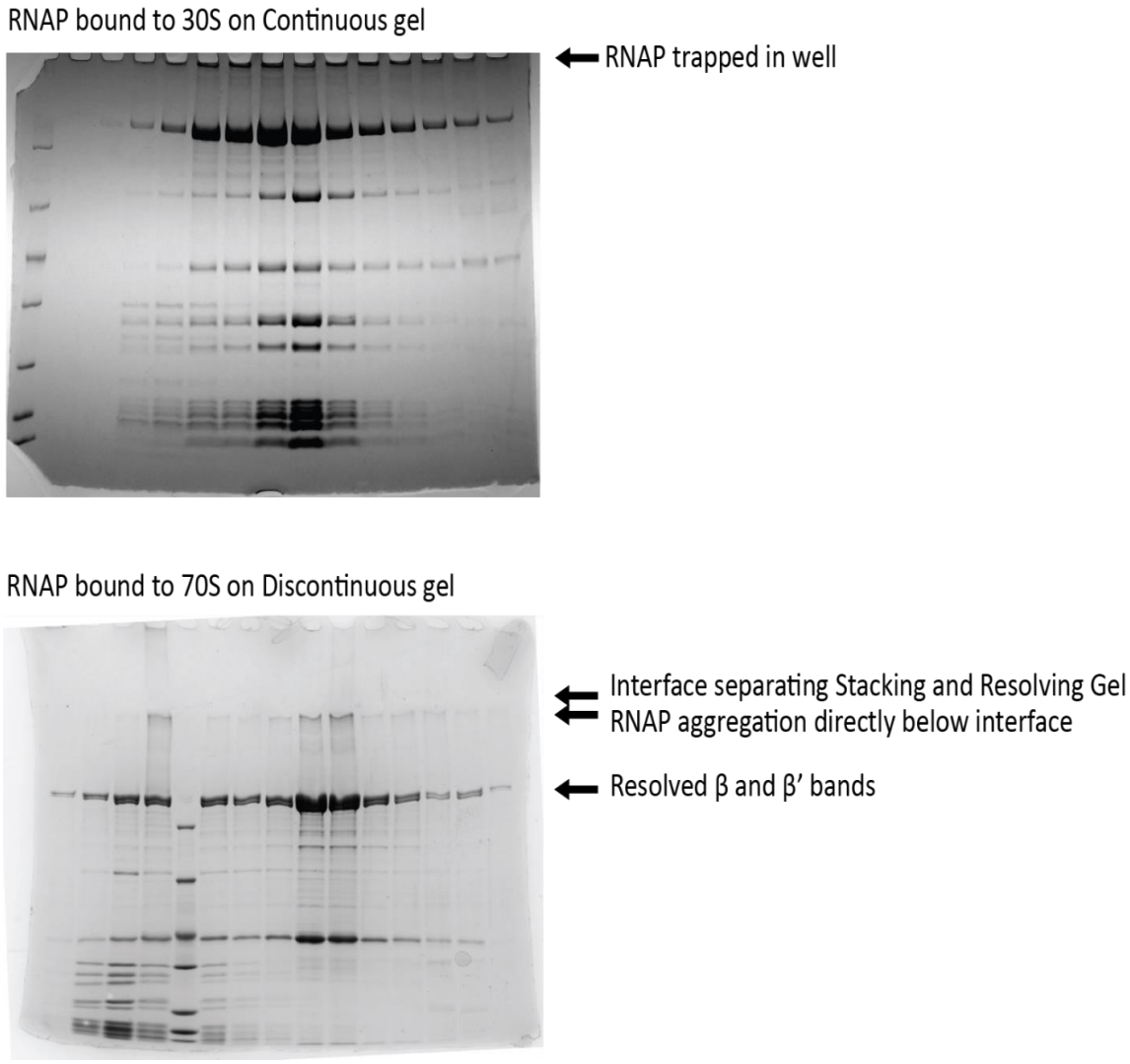

Figure 2.3: Comparison of Continuous vs. Discontinuous Gradient Gels. Introduction of a 4% stacking gel improved incorporation of RNAP into the gel as well as sharpened bands which became important for distinguishing 10-30 kDa factors in experiments with ribosomes. Though there is clearly some RNAP trapped at the interface between stacking and resolving gels, the quantity is less than the amount trapped in the continuous gel wells. Furthermore, the RNAP trapped at this interface is able to be quantified through ImageJ and included in the analysis.

Improving the SDS Polyacrylamide Gel Staining Procedure.

Coomassie Blue R-250 stain tends to not destain fully and in some cases, leave blotches on the gel itself. These results were at best, an uneven background that ImageJ would not effectively subtract from the densitometry measurements and were at worst completely unusable because the stains were interpreted as bands themselves. In order to rectify this, I decided to investigate alternative staining methods that were described as more applicable for quantitative analysis of polyacrylamide gels (Westermeier 2006), eventually deciding on colloidal Coomassie staining. Colloidal Coomassie staining makes use of Coomassie G-250, a minor variation on the R-250 structure with an extra pair of methyl groups attached to two of its three central rings. Additionally, the staining buffer changed significantly with the inclusion of 16% (w/v) ammonium sulfate which provided a means to aggregate the stain particles, increasing the sensitivity of the stain while also making the destaining process more effective (Neuhoff, Arold et al, 1988 Electrophoresis). The destaining procedure consisted of 3 hours of rocking the gel in de-ionized water followed by a two to three additional rinses with de-ionized water resulting in a consistent, nearly clear background (Figure 2.7).

Standardizing SDS Polyacrylamide Gel Quantification

ImageJ was used previously by our lab for lane/band identification as well as quantification. Within the software there are tools included to identify individual lanes and then once identified, the program can integrate the lanes to produce an intensity profile for each. The intensity profile corresponds to the density of Coomassie stain along

the length of each lane, resulting in 14 profiles per imaged gel from which the β/β' band would need to be extracted to determine bound versus unbound RNAP. The processing of the profiles was time consuming, required a lot of handling, and generated much more information than was required for quantification, often leading to ambiguity in the assignment of the protein to the integrated density. In order to resolve these issues, I forwent the use of the integrated tool and instead designed by own macro using the ImageJ macro language to address the following main concerns:

1) *Limit the area of the gel integration to only the specified band*- By removing all non-β/β' bands, there was less data interfering with the analysis, thus reducing the time spent on each gel to yield quantifiable data.
2) *Standardizing and automation of background subtraction*- Be it the gel, the lighting, or the tray the gel was imaged on, background subtraction still needed to be performed. Since I was using a macro to speed up image processing, the other integrated tools of ImageJ would have to be abandoned. As an added benefit though, there was no confusion as to how the program was performing the background subtraction since I wrote the code to do so.
3) *Produce a single profile and output file rather than 14 separate profiles and output files for each gel*- Multiple images/profiles for one gel was functional, but difficult to display the raw data cleanly and effectively. By combining all data onto one image, the entire scope of the individual gel/experiment could be easily recorded, catalogued, and referenced for later use. Given the volume of

quantification required for the successful completion of the projects described in this thesis, this point proved essential.

The finished macro is called “background_subtract.ijm” and can simply be run in ImageJ through the ‘Plugins’ menu option. After clicking on the Plugins option, click on ‘Macros’, followed by ‘Edit’ to open the macro file. Afterwards, the file can be run by pressing ‘Ctrl’ + ‘r’ and then follow the prompts as they appear (The full macro file is included in Appendix).

Limit the area of the gel integration to only the specified band

The code in Figure 2.4 allows the user to mouse over an image loaded into ImageJ, then define a rectangular region by using the ‘shift’ and ‘alt’ keys to display an overlay of the top left and bottom right corners of the selection. This method is much smaller in scope than ImageJ or any other competing lane identification software when it comes to a singular selection, which for my project was sufficient.

However, there are strict limitations with this simple design, chiefly that any lanes running faster than other lanes due to poor gel polymerization or inconsistent buffer conditions will increase the selection area, which near densely packed bands could make the selection infeasible. Given our selected band was the β/β' band with a molecular weight of ~155 kDa, it was separated clearly from all the other RNAP subunits, ribosomal proteins, and transcription and translation factors, meaning no further refinement of the code was necessary.

```
a = newArray(0,0,0,0);//defines the highlighted area

//define top left corner of ROI-region of interest
if (isKeyDown("shift")) {
 a[0] =x;
 a[1]=y;
 Overlay.remove;
 Overlay.drawLine(a[0],a[1],a[0]+800,a[1]);
 Overlay.drawLine(a[0],a[1],a[0],a[1]+40);
 Overlay.show;}

//define bottom right corner of ROI
if (isKeyDown("alt")) {
 a[2] =x-a[0];
 a[3] =y-a[1];
 Overlay.remove;
 if (a[0]!=0) {
     Overlay.drawLine(a[0],a[1],a[0]+800,a[1]);
     Overlay.drawLine(a[0],a[1],a[0],a[1]+40);}
     Overlay.drawLine(a[0]+a[2],a[1]+a[3],a[0]+a[2]-800,a[1]+a[3]);
     Overlay.drawLine(a[0]+a[2],a[1]+a[3],a[0]+a[2],a[1]+a[3]-40);
     Overlay.show;}
```

Figure 2.4: Selecting the area of interest, written in the macro language of ImageJ. '//' indicates the beginning of comment lines which are included in the code as documentation and ease of use.

Standardizing and automation of background subtraction

Figure 2.5 displays the process of defining a one-dimensional pixel matrix from the overlay described previously. This matrix stores the pixel intensity of every point within the selected overlay, then runs a straightforward method of background subtraction. Simply, the background is defined as the closest pixels above and below the selection, averaged across a length of 'background' (defaulted to ten pixels). The rationale was that the majority of the background remaining in the gel after my other optimizations would result not from the staining or destaining procedure, but rather from smearing within the lane itself. To account for this, every lane (or in this case, every column of pixels in every lane), would have the averaged background removed from every pixel intensity prior to profiling and quantification. Post-background subtraction, the image is updated to display the effects of the subtraction on the overlay selection to ensure proper functioning of the program and for documentation (Figure 2.7)

```
background = 10; //number of pixels height background defined as

//start body of background subtraction program
      if (isKeyDown("space")) {
      SafetyLock= 1;
      }

//define background pixels as average of ten pixels above and below column
//saves values into a_background
      if (SafetyLock==1) {

      makeRectangle(a[0], a[1], a[2], a[3]);
            print ("success!");
            for (i=0;i<(a[2]);i++) {
                  for (j=0;j<background;j++) {
                        a_temp[j] = getPixel(a[0]+i, a[1]+j-background);
//records values above ROI-region of interest
                        a_temp[j+background] = getPixel(a[0]+i, a[1]+a[3]+j);
//records below ROI
                        if (j==(background-1)) {     // way to determine
average and load in a_background
                              average =0;
                              for (k=0; k<(background*2);k++) {
                                    average = average + a_temp[k];
                                    if (k==background*2-1) {
                                          average = average/(background*2);
                                          a_background[i]= average;}}}}}

//calls each pixel intensity around ROI, then stores in 1d array
//subtracts background from sample columns

            for (i=0;i<(a[2]);i++) {
                  for (j=0;j<(a[3]);j++) {
                        a1[(j+a[3]*i)] = getPixel(a[0]+i, a[1]+j);
                        a1_backsub[(j+a[3]*i)] = a1[(j+a[3]*i)]-
a_background[i]; //creates updated matrix with background subtraction
                        if (a1_backsub[(j+a[3]*i)] <0) {
                              a1_backsub[(j+a[3]*i)]= 0;
                        }
                        setPixel(a[0]+i, a[1]+j,a1_backsub[(j+a[3]*i)]);
                        updateDisplay();
```

Figure 2.5: Code of the automated background selection and subtraction, written ImageJ macro language.

Produce a single profile and output file rather than 14 separate profiles and output files for each gel

By redefining our selection as a ‘lane’, (the horizontal selection encompassing every lane’s β/β' band), I produced a single output file containing all the data of interest by simply using the integrated call features in ImageJ’s macro language (Figure 2.6). Our overlay selection qualifies as ‘First Lane’ and since there is only one lane, the plot only displays a single image, each intensity corresponding to the β/β' band in each lane integrated across the entire gel. (Figure 2.7).

```
//displays and plots background subtraction

           run("Select First Lane");
           run("Plot Lanes");
```

Figure 2.6: Code for writing a single profile in a single output file, written the ImageJ macro language.

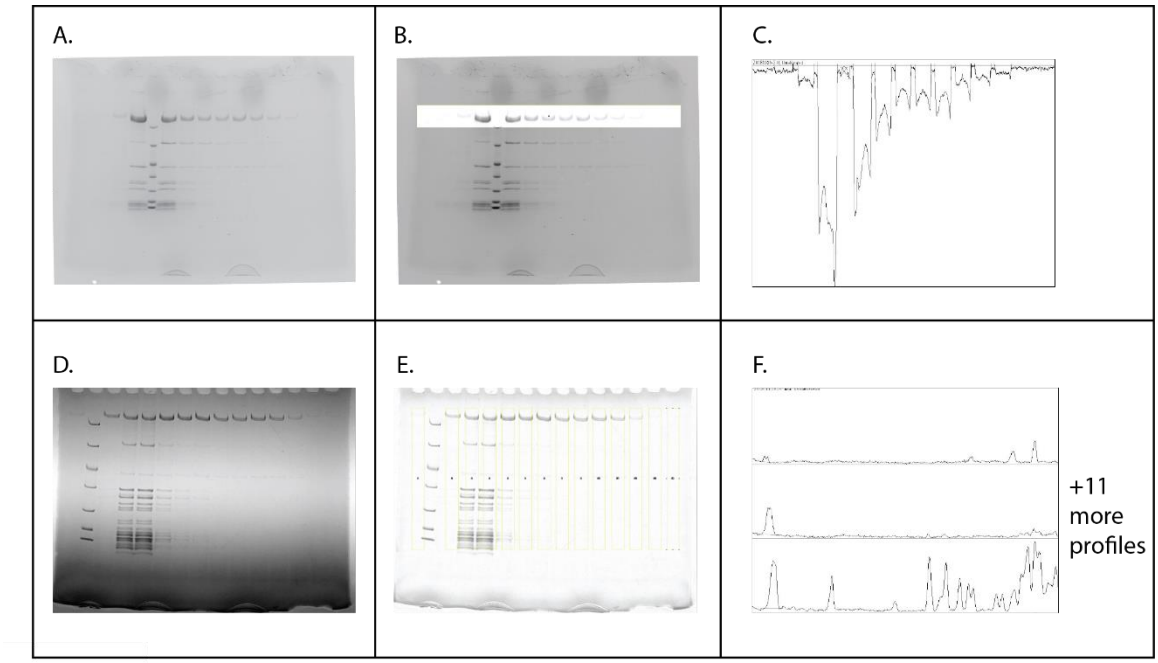

Figure 2.7: Comparison between new (A, B and C) and old (D, E, and F) methods of image quantification. **A)** SDS polyacrylamide gel post sucrose gradient centrifugation and fractionation of 30S bound to RNAP. **B)** Macro-based background subtraction output file, showing the β/β' bands subtraction. **C)** Pixel intensity of selected region from Panel B. Each peak includes an upside-down U-shaped pattern that was integrated to determine each band's quantity of β/β' relative to the remainder of the gel. **D)** SDS-PAGE gel post sucrose gradient centrifugation and fractionation of 70S bound to RNAP. **E)** ImageJ integrated method of background subtraction and lane identification/integration. Each lane is individually boxed (in yellow) and replicated, then resized to fit over each lane's profile. **F)** Pixel intensity of the first 3 entire lanes of the SDS polyacrylamide gel. In each profile, the β/β' must be identified based on distance traveled in the gel and then integrated before repeating the process for the next profile. Given that a gel has 14 lanes, 14 output files are produced, which amounts to much larger and more cumbersome workload compared to my optimized macro-based single image file per gel approach.

Optimization and Standardization of the Analysis of Free and RNAP-bound 30S subunits by Native Gel Electrophoresis:

While working on ribosomal subunit-RNAP interactions, our group became more interested in investigating weaker interactions. This required us to use more concentrated RNAP and ribosomes, depleting our preparations at a much faster rate. This forced us to use several ribosomes and RNAP preparations to accumulate sufficient data, resulting in larger variability between replicates. In order to find a method that required less input material than sucrose gradient centrifugation, I explored the use of electrophoretic mobility shift assays (EMSAs, aka Native Gels).

By the time I joined these efforts, the outline for native gel system was partially established, i.e., vertical gel format, low percentage agarose gel, and electrophoresis conditions. However, this outline required significant fleshing out in order to produce a reproducible and reliable protocol that allowed quantification of the RNAP-ribosome interactions.

Similar to our SDS gel issues, RNAP clogged in the native gel wells, resulting in smearing of RNAP from the well downwards. Interestingly, complex formation with the ribosomal subunits seemed to reduce the amount of smearing, distinct bands forming more regularly than in the control's case. Regardless, in order to establish a method that would yield more convincing native gel data, we had to optimize the running conditions to reduce the smearing of RNAP.

Building upon my strategy I used to solve the smearing problem in our SDS gels, I incorporated a 1.5% low-melting agarose on top of a higher percentage standard agarose gel to facilitate RNAP mobility. Low-melting agarose seems to have more vacuous pores than standard agarose at a similar percentage, but also tends to be more brittle, and when combined with a lower overall percentage of agarose makes for an extremely fragile and tear-prone product. At the established percentage, even comb removal became a struggle. I needed to reduce the size of the wells to about one quarter their traditional depth by attaching stoppers to the combs, preventing them from sinking too far into the vertical gel cassette during pouring.

The structural integrity was improved by first pouring high percentage agarose "frame" into which the low-percentage low-melting agarose gel was cast. To reduce the likelihood of tearing when the sample comb was removed from the gel, the thickness of the native gel was increased from 1.0 mm to 1.5 mm. By increasing the gel thickness, the walls between the sample wells of the low-melting agarose gel were thicker and significantly more structurally sound. With all changes in place, I was able to cast the gels more reliably and the RNAP was able enter the gel more effectively during electrophoresis (Figure 2.8).

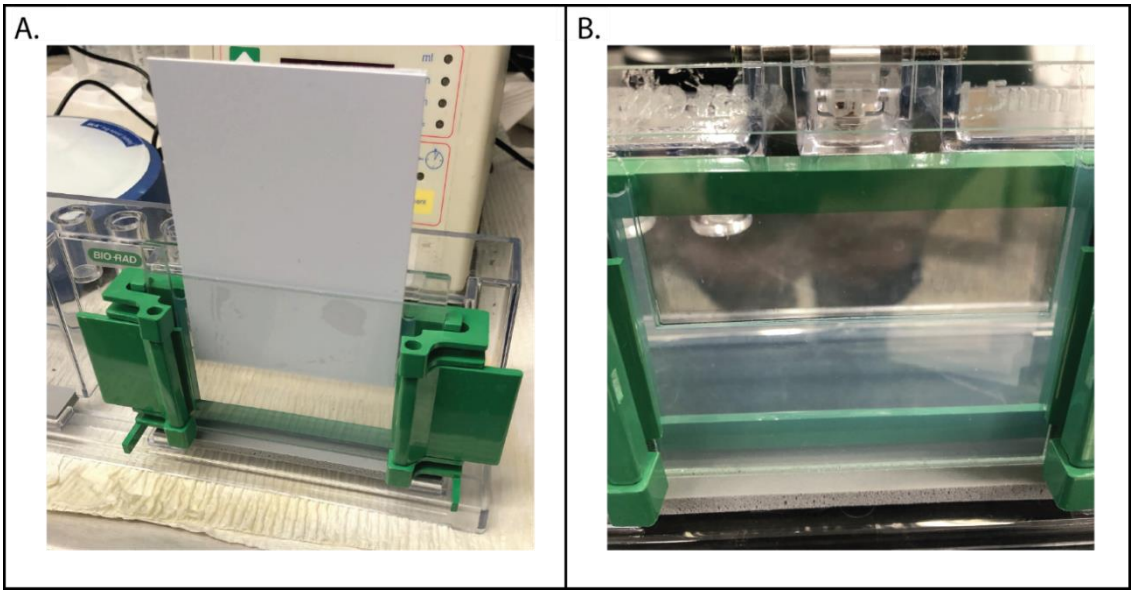

Figure 2.8: Casting the Native gel. **A)** Composing the higher concentration agarose 'frame' gel. Two 0.75 mm nylon sheets on top of each other are inserted between the gel cassette consisting of a short plate and spacer plate (larger plate behind the nylon sheets in the left image), leaving gaps on both sides of the casting matrix. Molten native gel agarose solution is pipetted through one of the side gaps until the chamber is filled. In our case, I did so within an oven set to 45°C to keep the plates warm enough to avoid premature gelling of the agarose. Once the structural frame gel is poured, the casting system was moved from 45°C to 4°C. After 20 minutes incubation at 4°C, I removed the nylon sheets one by one from the gel without tearing it. **B)** Poured structural frame gel. Once the structural frame gel has set at 4°C, the gel is returned to the 45°C oven, to warm the glass plates of the gel cassette without melting the agarose. The molten low percentage, low-melting agarose solution is filled into the gap of the structural frame gel and then the comb is inserted only a few millimeters into the gel. The gel is transferred to 4°C to gel before carefully removing the sample comb.

Quantification of Native Gels

Given the separation of the bound and unbound RNAP even after 4 hours of electrophoresis was not large enough to unequivocally distinguish both (longer run times led to more smearing and thus lower resolution), the question of how to quantify the results became the next concern. Luckily, the free ribosomal subunit band was far enough away from all other bands to be easily distinguished and quantified. Instead of measuring the increasing intensity of the bound band as I did for the SDS gels, I decided to measure the amount of free ribosomal subunit. The disappearance of the free ribosomal subunit as a result of increasing RNAP concentrations was used to estimate the subunit's fractional saturation for RNAP (Figure 2.9).

Due to the thickness and brittleness of the gel, post-processing also became a challenge. Upon removing the front plate of the gel cassette, any attempt at sliding the gel into staining solution was met with the gel tearing into pieces. Further attempts at recovery caused the gel to break more aggressively until the entire experiment was non-recoverable. In order to avoid rips, the cassette was submerged in water into a clear bottom tray slightly larger in dimension than the gel. After allowing the gel to rest for a minute, the gel could be slid off of the spacer plate and into the tray. The agarose adhered tightly to the bottom of the tray, allowing me to easily pour off the water and future stain/rinses. The gel was stained overnight with colloidal Coomassie Brilliant Blue G-250 as with the SDS gels, but without agitation as rocking tore the gels.

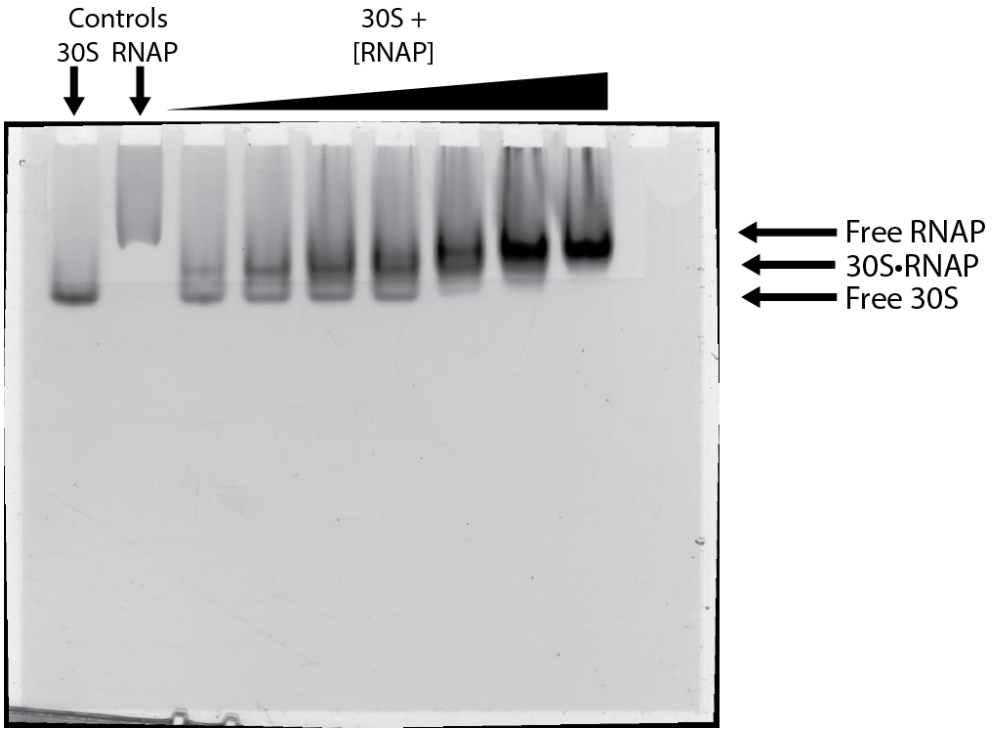

Figure 2.9: Native gel titration series of 30S subunit with RNAP (1.25, 2.5, 3.75, 5, 7.5, 12.5, 21.6 μM). As the concentration of RNAP increases from left to right, the free 30S subunit band becomes fainter and travels less through the gel until fully bound by RNAP. The bound 30•RNAP band migrates less into the gel as the concentration of RNAP increases.

A similar process was used for destaining. The gel was left within the tray, pouring off the stain and destaining with water while avoiding moving the gel as much as possible. The gels were imaged using a ChemiDoc Touch, but since they were too fragile to be transferred onto the loading tray of the imaging unit without breaking, they were left within the vessel they stained in. After imaging, the gel was quantified by running the same ImageJ macro as used for the SDS-PAGE analysis, but instead of quantifying the amount of RNAP I measured the amount of free 30S subunit.

Analyzing Native Gel bands using SDS-PAGE

What I have shown so far with regard to native gels is built on the assumption that the bands appearing in the native gel unseen in either ribosomal subunit or RNAP control must be a product of the complex. For distinct bands this might be considered acceptable, but it starts to become a concern when more factors are bound to the complex. The native gel does not solely provide information on what components are bound to the complex. Were the effects caused by introduction of a specific factor, or did the component never actually bind into the complex?

I had decided introducing a second dimension to the native gel, a simple SDS polyacrylamide gel would be an effective means of determining which factors were bound to the native complexes. Unfortunately, loading the sample onto the SDS gel turned out to be much more challenging than expected. The given model for loading proteins onto an SDS gel derived from agarose gels typically make use of either direct loading of the native gel matrix into the well of the SDS gel, soaking the protein out, or

some combination of soaking and trichloroacetic acid (TCA) precipitation. None of these methods yielded very promising results, the SDS gels either showing no proteins whatsoever, or the lane was a smeary, uninterpretable mess. In some cases, ribosomal proteins could partially be distinguished, but the RNAP once again was an issue, never leaving the agarose gel once it had entered.

Since the RNAP would not be removed from the gel, I decided to remove the gel as an obstacle. The simplest method of re-melting the gel matrix to segregate RNAP from agarose proved ineffective; nor did TCA precipitation assist in crashing the proteins out any better. Even when protein was recovered, the SDS gel was extremely smeary, which defeated the entire purpose. So instead of melting the gel to remove the RNAP, I decided to digest the gel matrix instead, using commercially available agarase to break down the polysaccharide matrix.

By incubating excised, molten bands from the native gel with agarase overnight at 42°C, the gel became degraded enough to release the captured proteins into solution, which could be concentrated afterwards by using TCA before loading onto the SDS gel. What resulted was evidence that the complex we reported seeing in the native gel system between ribosomal subunits and RNAP was legitimate (Figure 2.10).

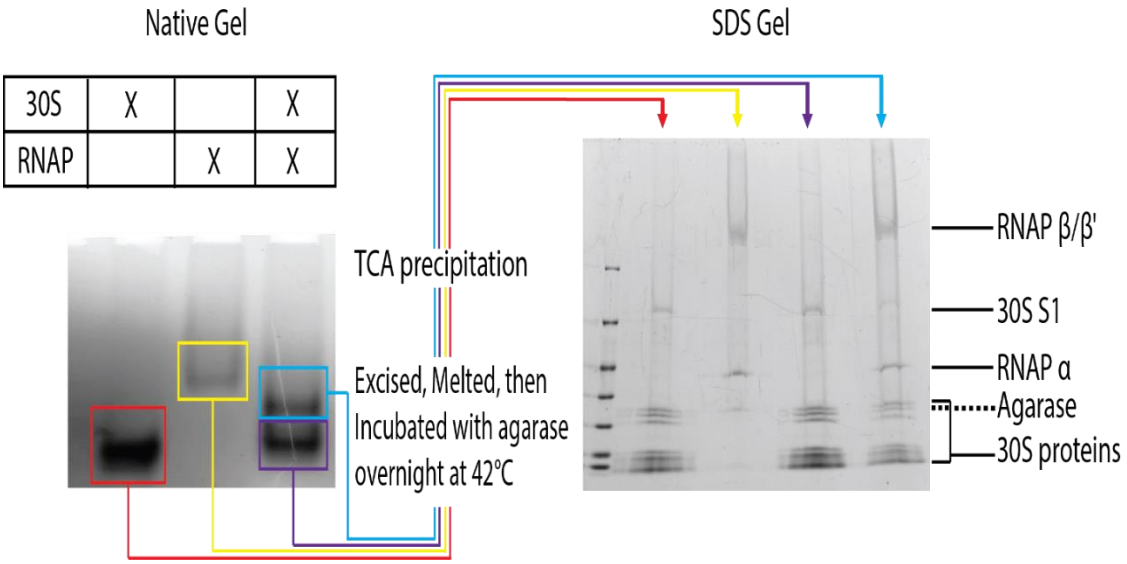

Figure 2.10: Analysis of individual native gel bands by SDS-PAGE. Samples of 30S and RNAP were incubated at 37°C for 15 min before being loaded onto a native gel at 90V/0.05Amp for 3 hours at 4°C. Afterwards, samples were colloidally stained overnight, followed by destaining with water until the bands were clear. Each of the bands was excised and melted to a molten state in a 70°C heat block, before the temperature was lowered to 42°C with agarase added. Molten bands with agarase were incubated overnight, then TCA precipitated and loaded onto an SDS polyacrylamide gel at 120V for 60 minutes. The SDS gel was colloidally stained overnight then destained with water. The lower native gel bands in both 30S and 30S/RNAP mixes corresponded to exclusively ribosomal proteins, and the RNAP control as exclusively RNAP. However, the upper band of the 30S/RNAP mix included both RNAP and ribosomal proteins, indicating binding.

Chapter 3*:*

***E. coli* Ribosomal Direct Coupling to RNAP**

Publication:

Fan, H., Conn, A. B., Williams, P. B., Diggs, S., Hahm, J., Gamper, H. B., Jr, Hou, Y. M., O'Leary, S. E., Wang, Y., Blaha, G. M. (2017) "Transcription-Translation Coupling: Direct Interactions of RNA Polymerase with Ribosomes and Ribosomal Subunits." Nucleic Acids Res., **45**(19):11043-11055.

[PMID**:** 28977553].

-
- With copyright permission from Oxford University Press

Abstract:

In prokaryotes, RNA polymerase and ribosomes can bind concurrently to the same RNA transcript, leading to the functional coupling of transcription and translation. The interactions between RNA polymerase and ribosomes are crucial for the coordination of transcription with translation. Here, we report that RNA polymerase directly binds ribosomes and isolated large and small ribosomal subunits. RNA polymerase and ribosomes form a one-to-one complex with a micromolar dissociation constant. The formation of the complex is modulated by the conformational and functional states of RNA polymerase and the ribosome. The binding interface on the large ribosomal subunit is buried by the small subunit during protein synthesis, whereas that on the small subunit remains solvent-accessible. The RNA polymerase binding site on the ribosome includes that of the isolated small ribosomal subunit. This direct interaction between RNA polymerase and ribosomes may contribute to the coupling of transcription to translation.

Introduction:

In eubacteria, transcription and translation occur in close spatial and temporal proximity, allowing the processes to couple. In *E. coli*, most proteins are translated while their genes are still being transcribed (Bakshi, Choi et al. 2015). The inhibition of translation results in the genome-wide stalling of transcription (Zhang, Mooney et al. 2014). Stalled RNA polymerases act as a barrier for the DNA replication machinery, jeopardizing the processivity of replication, and with it, the integrity of the genome (Mirkin and Mirkin 2007, Dutta, Shatalin et al. 2011).

Functional interactions between RNA polymerase and the ribosome have been demonstrated for polycistronic operons (Yanofsky and Ito 1966, Landick, Carey et al. 1985, Yanofsky 1999). For example, a nonsense mutation in an upstream gene attenuates the transcription of downstream genes (Franklin and Luria 1961, Jacob and Monod 1961). Premature translation termination causes ribosomes to dissociate from nascent RNA (Kaempfer 1974, Baggett, Zhang et al. 2017). Unhindered by ribosomes, transcription termination factor rho proceeds along the nascent RNA to RNA polymerase, where it induces transcription termination (Richardson, Grimley et al. 1975, Adhya, Gottesman et al. 1976, Adhya and Gottesman 1978).

The functional interaction between ribosomes and RNA polymerase is also exploited in the regulation of gene expression, as exemplified by the regulation of the *trp* operon. During tryptophan starvation, ribosomes translating the operon's leader peptide stall at the two consecutive tryptophan codons. This stalling prevents the nascent RNA from forming a short stem-loop that acts as an intrinsic transcription termination signal;

without the stem-loop, RNA polymerase transcribes the downstream genes of the operon, which are necessary for tryptophan synthesis (Yanofsky and Ito 1966, Landick, Carey et al. 1985, Yanofsky 1999).

In some cases, the functional coupling of transcription and translation is thought to be promoted by physically connecting the ribosome to RNA polymerase via a small protein, such as transcription factor NusG or its paralog, RfaH (Burmann, Schweimer et al. 2010, Burmann, Knauer et al. 2012). Both factors consist of two domains, the N- and C-terminal domains. The N-terminal domain binds directly to RNA polymerase (Belogurov, Sevostyanova et al. 2010, Drogemuller, Strauss et al. 2015), while the C-terminal domain binds to ribosomal protein S10 on a surface accessible on the ribosome (Burmann, Schweimer et al. 2010, Burmann, Knauer et al. 2012). These results point to NusG and RfaH as a physical link between RNA polymerase and ribosomes (Burmann, Schweimer et al. 2010, Burmann, Knauer et al. 2012).

However, biophysical considerations of NusG's interactions with RNA polymerase and ribosomes point to a significant contribution of factor-independent interactions in the physical linking of RNA polymerase and ribosomes. Because the two domains of NusG are structurally independent of each other (Mooney, Schweimer et al. 2009), formation of the NusG-link between RNA polymerase and ribosome can be broken down into two thermodynamically separate events: the binding of NusG's N-terminal domain to the RNA polymerase and the binding of NusG's C-terminal domain to the ribosome. During exponential growth, the segregation of the nucleoid from the cytoplasm (Bratton, Mooney et al. 2011, Bakshi, Siryaporn et al. 2012, Endesfelder,

Finan et al. 2013) increases the local concentration of RNA polymerase and NusG in the nucleoid (1–2 μM (Mooney, Davis et al. 2009, Bratton, Mooney et al. 2011, Endesfelder, Finan et al. 2013)) beyond the NusG dissociation constant for RNA polymerase (0.15 μM (Turtola and Belogurov 2016)), resulting in near-saturation of the NusG binding to RNA polymerase. On the other hand, the same segregation also limits the local concentration of ribosomes in the nucleoid (2–8 μM (Bakshi, Siryaporn et al. 2012, Sanamrad, Persson et al. 2014)) to as much as an order of magnitude below NusG's dissociation constant for ribosomes (50 μM (Burmann, Schweimer et al. 2010)), implying that only a small fraction of ribosomes is engaged by NusG. These data suggest that only a modest amount of the ternary complex of RNA polymerase, NusG, and ribosomes accumulates under conditions of transcription-translation coupling, raising the question of whether additional mechanisms of coupling ribosomes to RNA polymerase exist.

We hypothesize that direct interactions between RNA polymerase and ribosome may contribute to the coupling of RNA polymerase and ribosomes during transcription-translation coupling. Early electron microscopy as well as recent functional studies demonstrate that ribosomes can directly contact RNA polymerase by translating all of the nascent mRNA being synthesized (Miller, Hamkalo et al. 1970, Proshkin, Rahmouni et al. 2010). Such proximity may be stabilized by one of several ribosomal proteins that directly bind to RNA polymerase and moonlight as transcription factors (*e.g.*, ribosomal protein S4, which binds to RNA polymerase and inhibits the premature termination of ribosomal RNA transcription (Torres, Condon et al. 2001)).

The present work tests the hypothesis of direct physical interactions between RNA polymerase and the ribosome. By applying biophysical methods and chemical crosslinking in combination with mass spectrometry, we demonstrate that these interactions occur. We expect that these direct interactions between RNA polymerase and the ribosome play an important role in the coupling of translation to transcription.

Materials and Methods:

Bacterial strains and plasmids.

E. coli MRE 600.rif was a kind gift from Dr. Knud Nierhaus, and pVS10 (T7P–α–β–β'-His_6–ω), pIA900 (T7P-α-β-β'-TEV-His10-ω), and pIA1127 (T7P-His6-TEV-σ^{70}[1-613]) were from Dr. Irina Artismovitch. Chemically competent T7 Express and BL21(DE3) *E. coli* were from New England Biolabs (Ipswich, MA, USA).

RNA polymerase and ribosome preparation.

The purification of *E. coli* RNA polymerase and ribosomes followed published protocols (Blaha, Stelzl et al. 2000, Artsimovitch, Svetlov et al. 2003, Fong, Gillies et al. 2010, Nedialkov, Opron et al. 2013) with minor modifications that were designed to reduce the co-purification of RNAs and other factors. Briefly, RNA polymerase captured on a Ni^{2+} affinity column was washed with two column volumes of 1.8 M NaCl before elution (Martin, Gillette et al. 2002); ribosomes from the lysate were pelleted through a high-salt sucrose cushion (Robertson, Paulsen et al. 1988). To remove ribosome-bound mRNAs, ribosomes were dissociated into subunits, and the purified subunits were re-

associated into vacant ribosomes following a published protocol (Blaha, Stelzl et al. 2000).

RNA polymerase•ribosome complex formation.

In a standard reaction, 2.5 µM RNA polymerase and 2.5 µM ribosomes were incubated for 15 min at 37 °C in buffer A (20 mM HEPES-KOH pH 7.5, 20 mM $Mg(OAc)_2$, and 30 mM KCl), followed by 5 min of incubation at 4 °C and a 10-min centrifugation at 19,000 × *g* at 4 °C.

Separation of free RNA polymerase from ribosome-bound RNA polymerase.

Mixtures of RNA polymerase and ribosomes were analyzed by rate zonal centrifugation or by gel filtration. For rate zonal centrifugation, samples were loaded on a 10 – 40 % sucrose or 10 – 40 % glycerol gradient in buffer A and centrifuged in an SW32.1 Ti rotor for 18 hours at 24,000 rpm at 4 °C. After centrifugation, the gradients were collected in 13 fractions starting from the bottom. The protein content of each fraction was precipitated with trichloroacetic acid (TCA) and analyzed by SDS-polyacrylamide gel electrophoresis (SDS-PAGE).

For gel filtration, samples were loaded onto a Superdex 200 10/300 GL column (GE Healthcare) equilibrated in buffer A with the KCl concentrations indicated in the text. The collected elution fractions were TCA-precipitated and analyzed by SDS-PAGE.

To probe the interactions between RNA polymerase and ribosomes, complex formation was performed in the presence of 20 µM bovine serum albumin (BSA), a 14-nucleotide-long RNA (rGrArGrUrCrUrGrCrGrGrCrGrArU) at a 5 µM concentration, 10 mM sodium phosphate pH 7.5, or additional KCl.

Separation of free ribosomes from RNA polymerase-bound ribosomes.

RNA polymerase, ribosomes, and mixtures of both were loaded onto Ni Sepharose High Performance spin columns and washed several times with increasing concentrations of imidazole before step-eluting the complex. Flowthrough, wash, and elution fractions were collected, TCA-precipitated, and analyzed by SDS-PAGE.

Capturing ribosomes with RNA polymerase immobilized on an affinity matrix.

A Ni Sepharose High Performance column was loaded with saturating amounts of His-tagged RNA polymerase before loading purified ribosomes. The column was washed with increasing concentrations of imidazole before step-eluting the complex. Fractions from all steps were TCA-precipitated and analyzed by SDS-PAGE.

Determining the RNA polymerase-ribosome binding curves.

To generate binding curves, various concentrations of ribosomes and RNA polymerase were incubated in buffer A with different concentration of KCl as indicated in the text. The content of each sample was analyzed by sucrose gradient centrifugation followed by SDS-PAGE and staining with colloidal Coomassie (Westermeier 2006). The stained gels were imaged with a ChemiDoc™ Touch Gel Imaging System (Bio-Rad), and the β/β' bands of each digital gel image were quantified using ImageJ 1.46 (Schneider, Rasband et al. 2012). The fraction of bound RNA polymerase was determined by subtracting the concentration-adjusted profile of the free RNA polymerase from that of the overall RNA polymerase profile.

The experimental data were modeled assuming that the RNA polymerase binds to one binding site on the ribosome in the presence of a dimer-monomer equilibrium of

RNA polymerase. The affinities of RNA polymerase for ribosomes were estimated by nonlinear least-square fitting of the partitioning function

$$Z=[RNAP]+[70S]+K_1[RNAP]^2+K_2[RNAP][70S]+\alpha K_1K_2[RNAP]^2[70S]+$$

$$RNAP_{total}\ln[RNAP]-70S_{total}\ln[70S]$$

to the experimentally determined fraction of bound RNA polymerase using the "Equilibrium Expert" add-in for Microsoft Excel® (Raguin, Gruaz-Guyon et al. 2002). $[RNAP]$ and $[70S]$ are the concentrations of free RNA polymerase and ribosomes, respectively; $RNAP_{total}$ and $70S_{total}$ represent the total concentrations of RNA polymerase and ribosomes, respectively; K_1 and K_2 are the association constants for RNA polymerase dimer formation and RNA polymerase•ribosome complex formation, respectively; and α is the cooperativity factor for the binding of an RNA polymerase dimer to a ribosome. An average core enzyme•ribosome dissociation constant and its pooled standard deviation were calculated from the dissociation constants determined at 55 mM and 250 mM KCl according to (Box, Hunter et al. 2005) and yielded ~0.93 ± 0.21 μM. To calculate the holoenzyme•ribosome dissociation constant in the presence of a dimer-monomer equilibrium of the holoenzyme, we assumed a dissociation constant of 10 μM (Berg and Chamberlin 1970, Shaner, Piatt et al. 1982) and a cooperativity factor (α) of one. To calculate the complex formation in the absence of RNA polymerase dimerization (*i.e.*, holoenzyme), K_1 was set to zero. The fraction of bound RNA polymerase was set to $f_{bound}=\frac{RNAP_{bound}}{RNAP_{total}}$ for titrating the complex with increasing amounts of ribosomes and $f_{bound}=\frac{RNAP_{bound}}{70S_{total}}$ for titration with increasing amounts of RNA polymerase.

Preparation of NusG and sigma factor σ^{70}.

C-terminally His_6-tagged NusG was purified by Ni^{2+} affinity chromatography. Sigma factor σ^{70} was purified using a protein construct with an N-terminal His_6 tag and TEV protease site. After the initial capture of the protein on a Ni-NTA column, the protein was washed with two column volumes of 1 M NaCl before eluting with an imidazole gradient. The purified His_6-tagged factor was digested with TEV protease, and the free sigma factor was then separated from its cleaved His-tag and the TEV protease by passing it over a Ni-NTA column.

Formation of functional RNA polymerase complexes.

For preparation of holoenzyme, stoichiometric amounts of σ^{70} and core RNA polymerase were incubated (Gill, Weitzel et al. 1991). The transcription elongation complex was prepared following (Kashkina, Anikin et al. 2005), in which first a 14-nucleotide oligoribonucleotide (rGrArGrUrCrUrGrCrGrGrCrGrArU) and non-template DNA (GCGATTCAGACAGG) are annealed to the template DNA strand (CCTGTCTGAATCGCTATCGCCGC) to form a DNA:RNA hybrid scaffold before incubating with core RNA polymerase.

Formation of tRNA-bound ribosome complexes.

For preparation of tRNA-bound ribosomes, vacant ribosomes were incubated with an mRNA containing a Shine-Dalgarno sequence and codons for Pro and Phe (rArArArGrGrArArArUrArArArArCrCrArUrUrC), followed by sequential incubation with *E. coli* UGG $tRNA^{Pro}$ isoacceptor and yeast $tRNA^{Phe}$ (Holschuh and Gassen 1982, Schilling-Bartetzko, Franceschi et al. 1992). The UGG $tRNA^{Pro}$ isoacceptor was

transcribed *in vitro*, purified by gel electrophoresis, and *N*1 methylated at G37 with TrmD and AdoMet (Christian, Evilia et al. 2004).

Chemical crosslinking of RNA polymerase•ribosome complexes.

The RNA polymerase•ribosome complexes from *E. coli* were incubated with 5 mM 1-ethyl-3-(3-dimethyl-aminopropyl) carbodiimide (EDC) and 5 mM sulfo-*N*-hydroxysuccinimide (sulfo-NHS) at room temperature for 30 min before quenching the crosslinking reaction with 50 mM Tris-HCl. The protein content of the crosslinked sample was analyzed by SDS-PAGE with either a discontinuous 6 – 10 % Tris-glycine or a 6 – 9 % Tris-acetate gradient gel. The compositions of the SDS gel bands that occurred only in the presence of RNA polymerase and ribosomes were further analyzed by Western blot or excised and stored at 4 °C for further analysis by liquid chromatography-tandem mass spectrometry (LC-MS/MS).

Sample preparation for LC-MS/MS.

Excised SDS-PAGE bands were washed overnight before reducing and alkylating the captured protein with dithiothreitol and iodoacetamide, respectively. The alkylated proteins were subjected to tryptic digestion, followed by the extraction and desalting of the peptide fragments. The lyophilized peptides were resuspended in 0.1 % formic acid and immediately analyzed by LC-MS/MS.

LC-MS/MS for protein identification and quantification.

On-line LC-MS/MS analysis was performed on an LTQ-Orbitrap Velos mass spectrometer coupled with an EASY-nLC II HPLC system and a nanoelectrospray

ionization source (Thermo, San Jose, CA, USA). Sample injection, enrichment, desalting, and HPLC separation were conducted automatically. The HPLC was equipped with an in-house-packed ReproSil-Pur C18-AQ column. The peptides were separated using a linear gradient of 2 – 40 % acetonitrile in 0.1 % formic acid at a flow rate of 230 nL/min and electrosprayed (spray voltage 1.8 kV) into the mass spectrometer operating in positive-ion mode. Data-dependent acquisition was enabled, and the twenty most abundant ions found in the full-scan (*m/z* 300 – 1500 at a resolution of 60,000 at *m/z* 400) MS exceeding a threshold of 1000 counts were selected for collision-induced dissociation to generate the MS/MS.

LC-MS/MS data analysis.

Proteins were identified and quantified using MaxQuant software (version 1.5.3.8) (Cox and Mann 2008) to search raw LC-MS/MS data against the *E. coli* database downloaded from Uniprot (Alpi, Griss et al. 2015), which contains 4306 protein entries and additional entries for known contaminants. The fixed modification option was set to include cysteine carboamidomethylation, and the maximum number of missed cleavages was set to two per peptide. The tolerance levels in mass accuracy for MS and MS/MS were set to 4.5 ppm and 0.6 Da, respectively. The false positive rate was set to 1 %. For each protein, the spectral index (SI) was calculated as the sum of the ion intensities of all the tryptic peptides detected throughout the LC-MS/MS analysis of a sample (Griffin, Yu et al. 2010):

$$SI = \sum_{k=1}^{pn} \left(\sum_{j=1}^{sc} i_j \right)_k$$

where i_j is the ion intensity of the *j*th spectrum of peptide fragment *k* summed over all spectra *sc* for all tryptic peptides of the protein of interest, *pn*. The SI of each protein was weighted based on the length of the amino acid sequence of the protein:

$$Weighted\ SI = \frac{SI}{Protein\ Length}$$

The weighted SI values for all identified proteins were normalized to the highest weighed SI value within the sample (Griffin, Yu et al. 2010). Proteins were only considered enriched in the crosslink if they were present in all three biological replicates of the crosslinked band. We excluded proteins as potential RNA polymerase-ribosome interaction partners when they were present at the same relative mobility of the crosslinked species in either the crosslinked RNA polymerase or crosslinked ribosome sample and their SIs exceeded two-thirds of the SI observed for the crosslinked RNA polymerase-ribosome sample. The SIs of the remaining proteins were normalized to that of the protein with the highest index in each replicate. The average normalized SI values were calculated. The mass spectrometry proteomics data have been deposited to the ProteomeXchange Consortium via the PRIDE17 partner repository (Vizcaino, Csordas et al. 2016) with the data set identifier PX006717.

Results:

E. coli RNA polymerase and ribosomes form a complex in vitro.

Eighty percent of RNA polymerase co-migrates with ribosomes when a micromolar mixture of stoichiometric amounts of RNA polymerase (core enzyme, consisting of $\alpha_2\beta\beta'\omega$ subunits) and vacant ribosomes (lacking bound mRNA and tRNAs) from *E. coli* are separated by sucrose density gradient centrifugation (Figure 3.1A). The presence of sucrose or glycerol in the density gradient does not influence the extent of complex formation (compare Figure 3.1A with 3.1B). Similar levels of complex formation are detected when the mixture is separated by size exclusion chromatography (Figure 3.1C). Density gradient centrifugation and size exclusion chromatography probe the hydrodynamic parameters of the complex, which are dominated by the sedimentation coefficient and the size of the ribosome, preventing the separation of free ribosomes from bound ribosomes.

To separate free ribosomes from bound ribosomes, we captured the complex on a Ni^{2+} affinity matrix via a C-terminal poly(His)-tag on the β' subunit of the RNA polymerase, either by pre-forming the RNA polymerase•ribosome complex or by first immobilizing the core enzyme on the matrix and then capturing vacant ribosomes from solution (Figure 3.1D). Although only an estimated 10 % of the applied RNA polymerase-ribosome complex is captured by the Ni^{2+} affinity matrix, none of the ribosomes are captured in the absence of RNA polymerase (compare 70S alone and RNAP + 70S in Figure 3.1E).

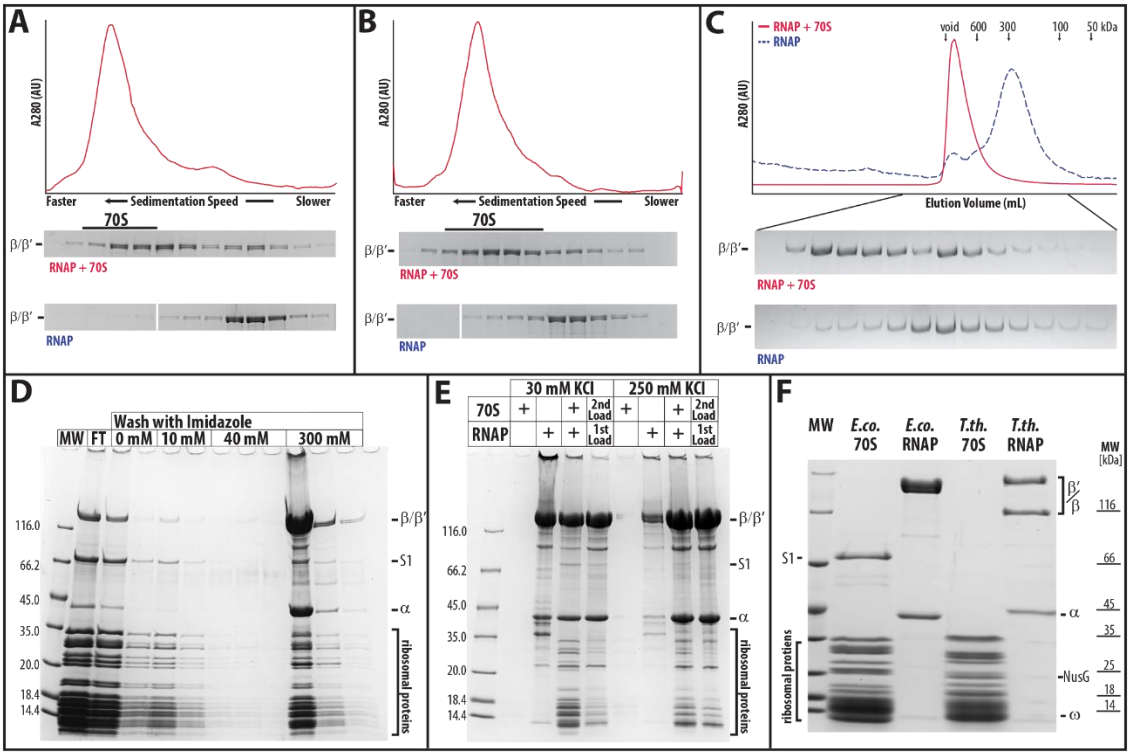

Figure 3.1: Isolating RNA polymerase•ribosome complexes using different methods: **A**) Sucrose gradient centrifugation. The top panel displays the sedimentation profiles of RNA polymerase alone (dashed blue line) and a stoichiometric mixture of RNA polymerase and ribosomes (solid red line) recorded at 280 nm. The two bottom panels display the SDS-polyacrylamide gel electrophoresis (SDS-PAGE) result of each of the sucrose gradient fractions. The top panel shows the β/β' region of the SDS-PAGE result of the gradient centrifugation of RNA polymerase (RNAP) alone, while the bottom presents the full gel of a mixture of RNA polymerase and ribosomes (RNAP + 70S, marker lane removed for clarity). **B**) Glycerol gradient centrifugation. The panels are the same as in **A**. During ultracentrifugation, the complex of RNA polymerase and ribosome constantly re-equilibrates, causing the bound RNA polymerase to trail the ribosome in **A** and **B**. **C**) Size exclusion chromatography. The top panel shows the elution profiles of a mixture of RNA polymerase and ribosomes (solid red line) and of RNA polymerase alone (dashed blue line; for comparison, the absorption is increased by 160-fold) from a 10/30 Superdex 200 column. **D-E**) Capturing His-tagged RNA polymerase•ribosome complexes on a Ni-sepharose spin column. **D**) SDS-PAGE results of all fractions, *i.e.*, flowthrough (FT), washes with 0, 10, and 40 mM imidazole and elution with 300 mM imidazole. **E**) SDS-PAGE results of the first 300 mM imidazole elution step from Ni^{2+} affinity binding experiments. Various amounts of RNA polymerase and ribosomes are either loaded together or sequentially – first RNA polymerase ("1st Load"), followed by a stoichiometric amount of ribosomes ("2nd Load"). These experiments are performed in the presence of 30 mM KCl and 250 mM KCl. **F**) RNA polymerase binding to ribosomes in the presence of 10 mM phosphate buffer (PO_4), 20 µM bovine serum albumin (BSA), a 14-nucleotide long RNA (RNA) at 5 µM, or 80 µg of poly(U)-RNA.

All employed methods exploit different molecular principles, yet they all consistently point to an upper limit of the apparent dissociation constant of the RNA polymerase•ribosome complex that is in the one to two micromolar range.

Non-specific competitors do not significantly impair complex formation.

While RNA polymerase consists only of protein subunits, two-thirds of the mass of the ribosome consists of RNA, implying that protein-protein and/or RNA-protein interactions may contribute to complex formation. To exclude non-specific interactions between RNA polymerase and ribosomes, we formed the complex in the presence of several potential non-specific competitors for RNA-protein and protein-protein interactions, such as phosphate buffer, a short RNA, random-sized poly(U) RNA, or BSA. The extent of complex formation is not significantly impaired by the presence of either an eight-fold excess of BSA or by 10 mM phosphate buffer at pH 7.4 (Figure 3.1F). At higher phosphate buffer concentrations, ribosomes dissociate into subunits, *i.e.*, in the presence of 10 mM phosphate buffer, none of the ribosomes dissociate, whereas with 100 mM phosphate buffer, approximately 40 % of the ribosomes dissociate into subunits. The presence of poly(U) RNA or a 14-nucleotide-long RNA reduces the extent of complex formation by approximately one-third. A fraction of RNA polymerase, ribosomes, and the RNA polymerase•ribosome complex appears to bind poly(U), causing it to sediment faster during sucrose gradient centrifugation. The nominal effect of these non-specific competitors for binding argues in favor of a specific interaction between the RNA polymerase core enzyme and the vacant ribosome. Thus, we hypothesize that the interactions between RNA polymerase and the ribosome are direct and specific.

Stoichiometry and dissociation constants of the RNA polymerase•ribosome complex.

Specific interactions between macromolecules cause the formation of defined stoichiometric complexes. Depending on the ionic conditions, the RNA polymerase core enzyme exists in an equilibrium of multiple oligomeric states (Stevens, Emery et al. 1966, Shaner, Piatt et al. 1982, Harris, Williams et al. 1995, Kansara and Sukhodolets 2011). To distinguish between the binding of an oligomer and the binding of multiple monomers, titration experiments were performed at salt concentrations that favor either the oligomeric or monomeric state of the RNA polymerase.

The titration of the core enzyme with vacant ribosomes in 55 mM KCl saturates at a one-to-one stoichiometry, while two equivalents of RNA polymerase bind to one equivalent of ribosomes under saturating conditions (Figure 3.2A and 3.2B, 55 mM KCl). At 250 mM KCl, a one-to-one complex is formed between the RNA polymerase and ribosomes at a saturating concentration of RNA polymerase (Figure 3.2B, 250 mM KCl). The similar sedimentation coefficients of ribosomes and of RNA polymerase•ribosome complexes indicate that only one ribosome is bound in each of the observed complexes. Ribosome dimers would sediment much faster than monomers, *i.e.*, 100 Svedbergs versus 70, respectively (Stoffler, Hasenbank et al. 1973, Morrison, Tischendorf et al. 1977, Kato, Yoshida et al. 2010).

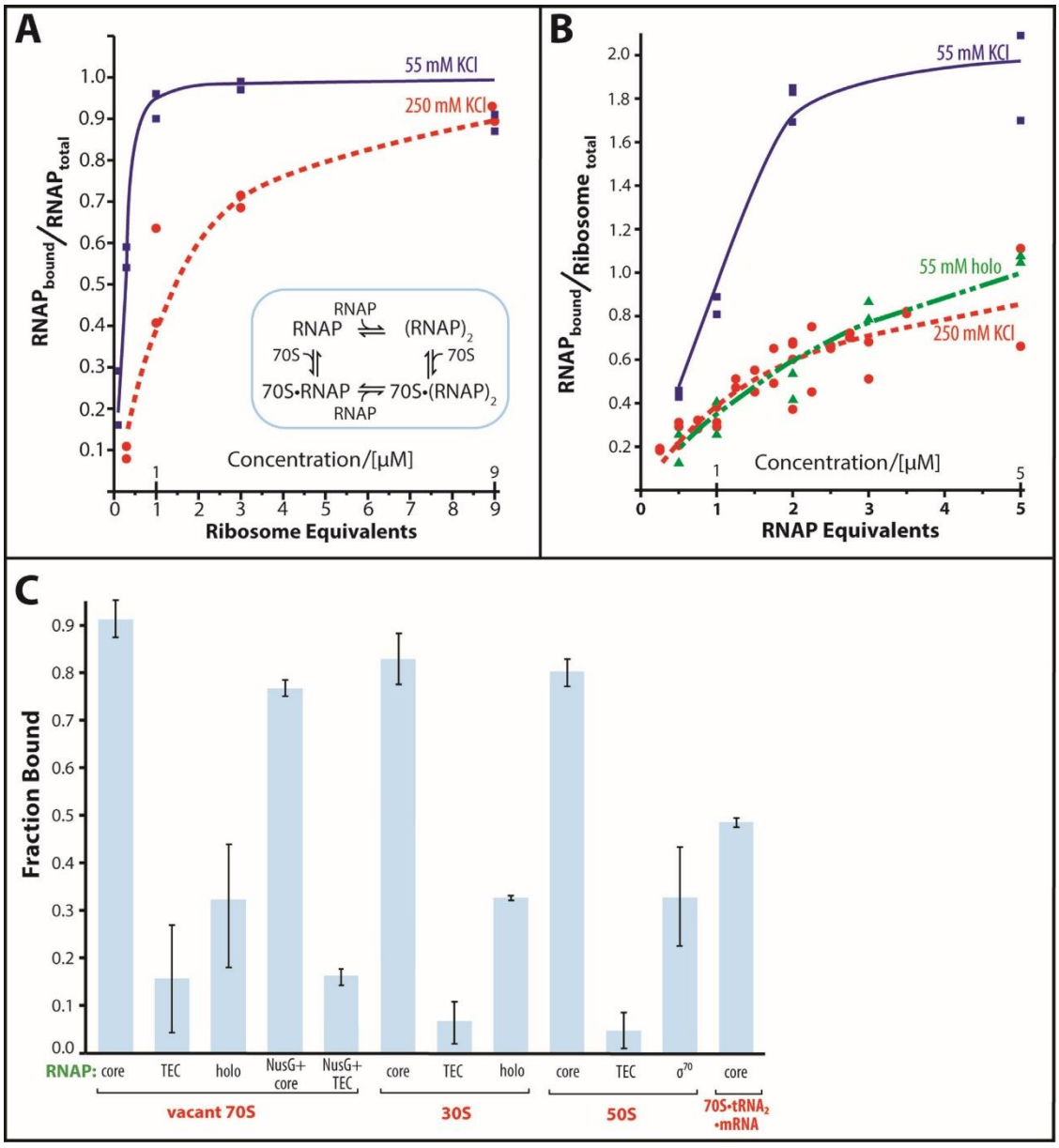
A
55 mM KCl
250 mM KCl
RNAP bound/RNAP total
RNAP
RNAP (RNAP)2
70S
70S
70S•RNAP
70S•(RNAP)2
RNAP
Concentration/[μM]
Ribosome Equivalents
B
55 mM KCl
55 mM holo
250 mM KCl
RNAP bound/Ribosome total
Concentration/[μM]
RNAP Equivalents
C
Fraction Bound
RNAP: core
TEC
holo
NusG+ core
NusG+ TEC
core
TEC
holo
core
TEC
σ70
core
vacant 70S
30S
50S
70S•tRNA2 •mRNA

Figure 3.2: Titration of RNA polymerase with ribosomes and vice versa. **A)** Binding of ribosomes to RNA polymerase. RNA polymerase (1 μM) is incubated with increasing concentrations of ribosomes in the presence of 55 mM KCl (blue squares) or 250 mM KCl (red circles). The inset displays the proposed binding model of complex formation. **B)** Binding of RNA polymerase to ribosomes. Ribosomes (1 μM) are incubated with increasing concentrations of RNA polymerase core enzyme (blue squares) or holoenzyme (green triangles) in the presence of 55 mM KCl or 250 mM KCl (red circles, core enzyme only). The lines connecting the data in **A** and **B** are the binding curves calculated as described in the Materials and Methods section of the text. For the holoenzyme, the simulated binding curve in the presence of dimer-monomer equilibrium is shown. **C**) Influence of the functional state of the RNA polymerase and of the ribosome on the RNA polymerase•ribosome complex formation. The complex formation of ribosomes (70S), small subunits (30S), large subunits (50S), and tRNA-bound ribosomes (70S•$tRNA_2$•mRNA) with RNA polymerase core enzyme (core), transcription elongation complex (TEC), holoenzyme (holo), core enzyme and transcription elongation complex in the presence of NusG (NusG + core and NusG + TEC) was analyzed by sucrose gradient centrifugation.

We were able to model the formation of the RNA polymerase•ribosome complex assuming the presence of one binding site on the vacant ribosome and a dimer-monomer equilibrium of the core enzyme (with estimated dissociation constants of 0.02 μM and 0.2 mM for 55 and 250 mM KCl, respectively, based on (Harris, Williams et al. 1995), inset in Figure 3.2A). This model yields a nearly identical RNA polymerase•ribosome dissociation constant of 0.93 ± 0.21 μM. However, upon transitioning from 55 to 250 mM KCl, the presence of ribosomes ceases to skew the RNA polymerase towards dimer formation, as reflected by a drop in the cooperativity factor, α, from 50 to 1. The significantly lower ratio of ribosomes to RNA polymerase captured on the Ni-affinity matrix at 250 mM KCl compared to 30 mM KCl supports the results from sucrose gradient centrifugation (compare experiments at 30 mM with 250 mM KCl in Figure 3.1E).

The observed dissociation constant for the RNA polymerase•ribosome complex constitutes an upper limit, as the presence of a nascent RNA that connects both interaction partners further reduces the dissociation constant. Despite being an upper limit, the one micromolar dissociation constant of the RNA polymerase•ribosome complex is by itself similar to those seen for other processes that regulate RNA polymerase or ribosome activity (*i.e.*, 0.9 μM for RNA polymerase binding to ribosomes versus 0.1 μM for transcription factor NusA binding to RNA polymerase (Gill, Weitzel et al. 1991) or 0.2 μM for EF-G (Katunin, Savelsbergh et al. 2002) and 0.5 μM for EF-Tu•GTP•Phe-tRNA^{Phe} (Maracci, Peske et al. 2014) binding to ribosomes.)

Characterization of the interaction between RNA polymerase and the ribosome.

The RNA polymerase adopts multiple functional states in the course of transcribing a gene. Therefore, in addition to testing the core enzyme, we also tested RNA polymerase with bound sigma factor σ^{70} (holoenzyme) and RNA polymerase with a bound DNA:RNA scaffold (transcription elongation complex, TEC) as examples of the initiation and elongation states, respectively. The sigma factor, as well as the radioactively labeled RNA of the DNA:RNA scaffold, co-migrates with the RNA polymerase-ribosome complex (Figure S3.2A and B), indicating that actively transcribing RNA polymerase may also participate in complex formation. Both states display reduced affinity for the ribosome, albeit to different extents – 31 % of the holoenzyme and 15 % of the TEC bind to the ribosome versus 90 % of the core enzyme (Figure 3.2C).

Nonlinear regression to best fit the measured binding data results in a computed dissociation constant of 1.4 ± 0.2 μM for the holoenzyme•ribosome complex when modeled for the dimer-monomer equilibrium, as predicted for our experimental conditions (Berg and Chamberlin 1970, Shaner, Piatt et al. 1982). An assumption of pure monomer reduces the quality of the fit but yields a dissociation constant of 1.2 ± 0.2 μM, which is still consistent with a weaker binding of the holoenzyme than of the core enzyme (K_d of core enzyme complex 0.9 ± 0.2 μM).

Like RNA polymerase, ribosomes adopt multiple functional states when translating a gene. Therefore, in addition to testing the vacant ribosomes, we tested tRNA-bound ribosomes. The tRNA-bound ribosomes display a weaker affinity for the core RNA polymerase (Figure 3.2C). The modulation of the dissociation constant by the

functional states of the RNA polymerase and ribosome may indicate that certain combinations of functional states permit tight binding, possibly synchronizing transcription and translation during transcription-translation coupling.

The ribosome consists of a small and a large ribosomal subunit. To identify the contribution of each subunit to the binding of the RNA polymerase, we investigated the interaction of the RNA polymerase with each subunit individually. The RNA polymerase core enzyme interacts with both subunits (Figure 3.2C), and the non-specific competitors have similar effects on the complex formation as on the RNA polymerase•ribosome complex formation (Figure S3.3). These results suggest that either each ribosomal subunit interacts with a different part of the RNA polymerase or that one RNA polymerase binding site is blocked upon subunit association. To distinguish between these two possibilities, we identified the RNA polymerase binding interfaces on the ribosome and on each of its subunits using chemical crosslinking.

Chemical crosslinking of RNA polymerase and ribosomes.

In the presence of sulfo-NHS, the zero crosslinker 1-ethyl-3-(3-dimethyl-aminopropyl) carbodiimide (EDC) produces a ribosome-dependent crosslink of the core enzyme (Figure 3.3A, 30 mM KCl). The effect of non-specific competitors on the crosslinking efficiency mirrors the effect of these competitors on RNA polymerase•ribosome complex formation (Figure S3.4A). In addition, the crosslinking efficiency correlates with the affinity of the RNA polymerase for the ribosome. The holoenzyme and TEC, which have lower affinity for ribosomes, display no increase in crosslink formation in the presence of ribosome (Figure S3.4A inset).

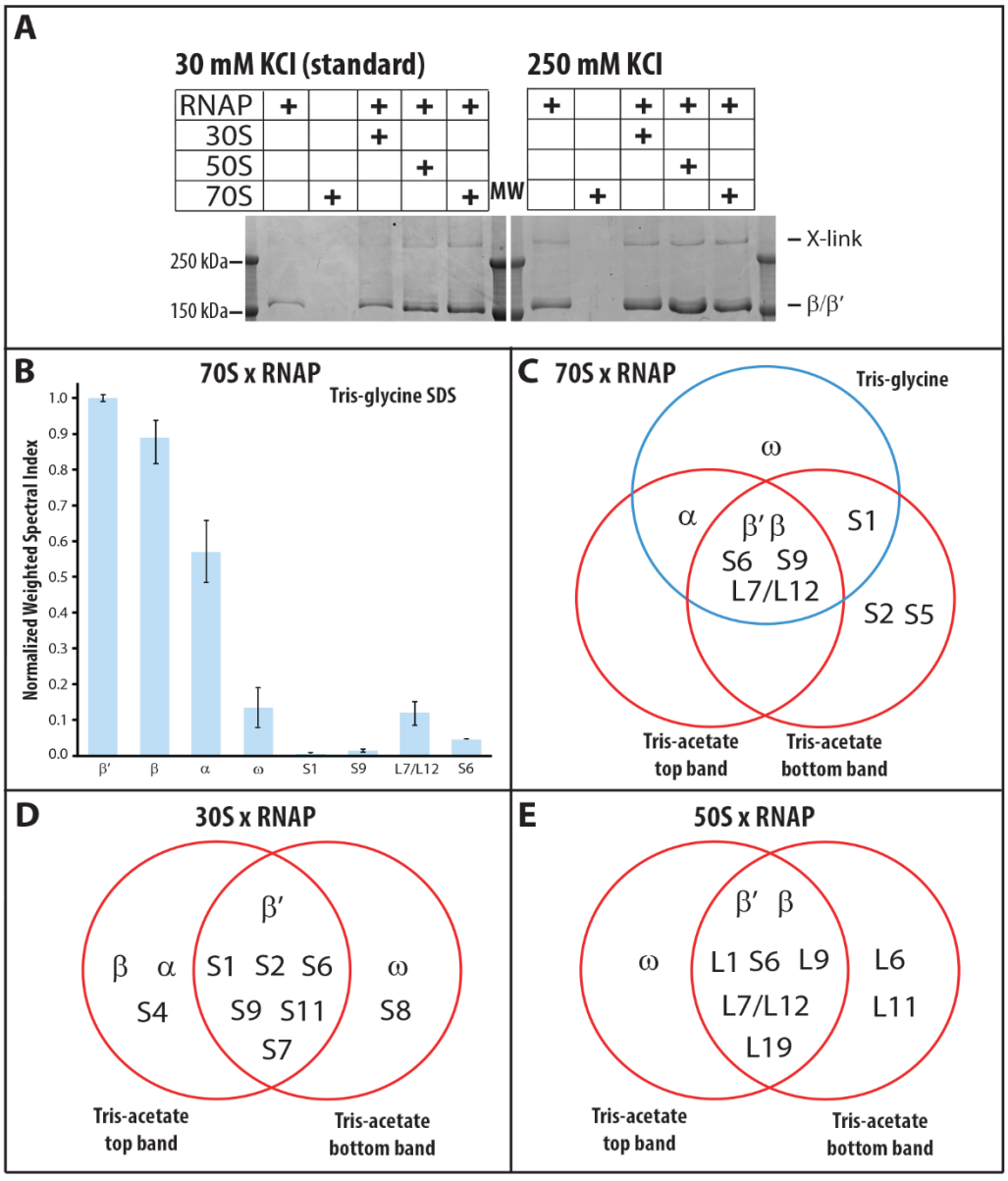
A
30 mM KCl (standard)
250 mM KCl
RNAP
30S
50S
70S
MW
250 kDa
150 kDa
X-link
β/β′
B
70S x RNAP
Tris-glycine SDS
Normalized Weighted Spectral Index
β′
β
α
ω
S1
S9
L7/L12
S6
C 70S x RNAP
Tris-glycine
ω
α
β′ β
S1
S6 S9
L7/L12
S2 S5
Tris-acetate top band
Tris-acetate bottom band
D
30S x RNAP
β′
β α
S1 S2 S6
ω
S4
S9 S11
S8
S7
Tris-acetate top band
Tris-acetate bottom band
E
50S x RNAP
β′ β
ω
L1 S6 L9
L6
L7/L12
L11
L19
Tris-acetate top band
Tris-acetate bottom band

Figure 3.3: EDC crosslinking of RNA polymerase-ribosome complexes. **A)** EDC crosslinking of RNA polymerase in the presence of the small ribosomal subunit (30S), large ribosomal subunit (50S), and ribosome (70S) with 30 mM and 250 mM KCl. **B**) Normalized weighted spectral index of LC-MS/MS analysis of the Tris-glycine SDS-PAGE purified RNA polymerase-ribosome crosslink. **C)** Venn diagram of crosslinked proteins after exposing a mixture of RNA polymerase and ribosomes to EDC and isolating the unique crosslinked species by 6 – 10 % Tris-glycine (single band) and by 6 – 9 % Tris-acetate SDS-PAGE (two bands). **D** and **E)** Venn diagram of the proteins in the two species isolated from 6 – 9 % Tris-acetate PAGE, which are specific to the EDC crosslinking of RNA polymerase in the presence of the small and the large ribosomal subunits.

However, an LC-MS/MS analysis of the SDS-PAGE-purified crosslink reveals a significant enrichment of the RNA polymerase subunits α, β, and β' in the crosslink (Figure 3.3A). The presence of the RNA polymerase subunits in the crosslink was confirmed by Western blot analysis (Figure S3.4B). Therefore, we conclude that upon ribosome binding, the core enzyme adopts a conformation that promotes EDC-induced crosslinking within the polymerase. A similar crosslink is produced with the core enzyme alone in the presence of 250 mM KCl (Figure 3.3A, 250 mM KCl). RNA polymerase can be coaxed into different functional states by manipulating the solvent conditions (Ruff, Kontur et al. 2015, Ruff, Record et al. 2015). The similarity of the two crosslinks may point to a similar conformation of the RNA polymerase when bound to the ribosome and in the presence of 250 mM KCl.

EDC induces a limited number of crosslinks between RNA polymerase and the ribosome.

MS analysis of the crosslink identified several ribosomal proteins that co-migrate with the intramolecularly crosslinked polymerase. These ribosomal proteins are less abundant than the α, β, or β' subunits in the crosslinked band (Figure 3.3B), implying that only a fraction experienced an additional crosslinking event to a ribosomal protein. Except for minuscule amounts of β and β' subunits, no other protein can be identified at the relative mobility of the crosslinked species in the absence of the chemical crosslinker (Table S1). The crosslinked species resolve into at least three bands on Tris-acetate SDS gels (Figure S3.5). LC-MS/MS analysis of two of these bands confirms that the single crosslinked species on our standard Tris-glycine gel indeed contains multiple components. Common to all three analyzed crosslinks are β, β', S6, S9, and L7/L12

(Figure 3.3C; L7 is the acetylated form of L12. The ratio of L7 to L12 varies with the cell's growth phase (Gordiyenko, Deroo et al. 2008)). The observed crosslinks place the ribosome-bound RNA polymerase on the cytosolic site of the small ribosomal subunit, covering the mRNA exit and entry sites (Figure 3.4C). The restricted number of ribosomal proteins in the crosslinks further hints at a defined arrangement between the RNA polymerase and the ribosome, which also supports our observation of a stoichiometric complex between RNA polymerase and ribosomes in solution.

Crosslinks between RNA polymerase and ribosomal subunits overlap with those between RNA polymerase and the ribosome.

The same crosslinked species are present on a Tris-acetate gel when the RNA polymerase is crosslinked to the small and to the large ribosomal subunits. LC-MS/MS analysis of two crosslinked species of the small and of the large ribosomal subunit indicates that the ribosomal proteins have a similar abundance relative to that of the RNA polymerase subunit, as they do when the RNA polymerase is crosslinked to the ribosome. Common to the two RNA polymerase-small subunit crosslinks are the RNA polymerase β' subunit and the small ribosomal subunit proteins S1, S2, S6, S9, S11, and S7 (Figure 3.3D). All of the identified ribosomal proteins cluster next to the mRNA exit site on the small ribosomal subunit (Figure 3.4A).

Common to the two RNA polymerase-large ribosomal subunit crosslinks are the β and β' RNA polymerase subunits and the ribosomal proteins L1, S6, L9, L7/L12, and L19 (Figure 3.3E). The proteins of the large ribosomal subunit are clustered at the tRNA entry (L7/L12) and exit sites (L1 and L9). L19 is the only ribosomal protein on the

interface between the small and large ribosomal subunits (Figure 3.4B), which, upon association of these subunits, is buried within the ribosome. These identified crosslinks position the RNA polymerase on the ribosomal subunit interface of the large subunit, indicating that only the RNA polymerase interface of the small ribosomal subunit contributes to RNA polymerase binding to the ribosome.

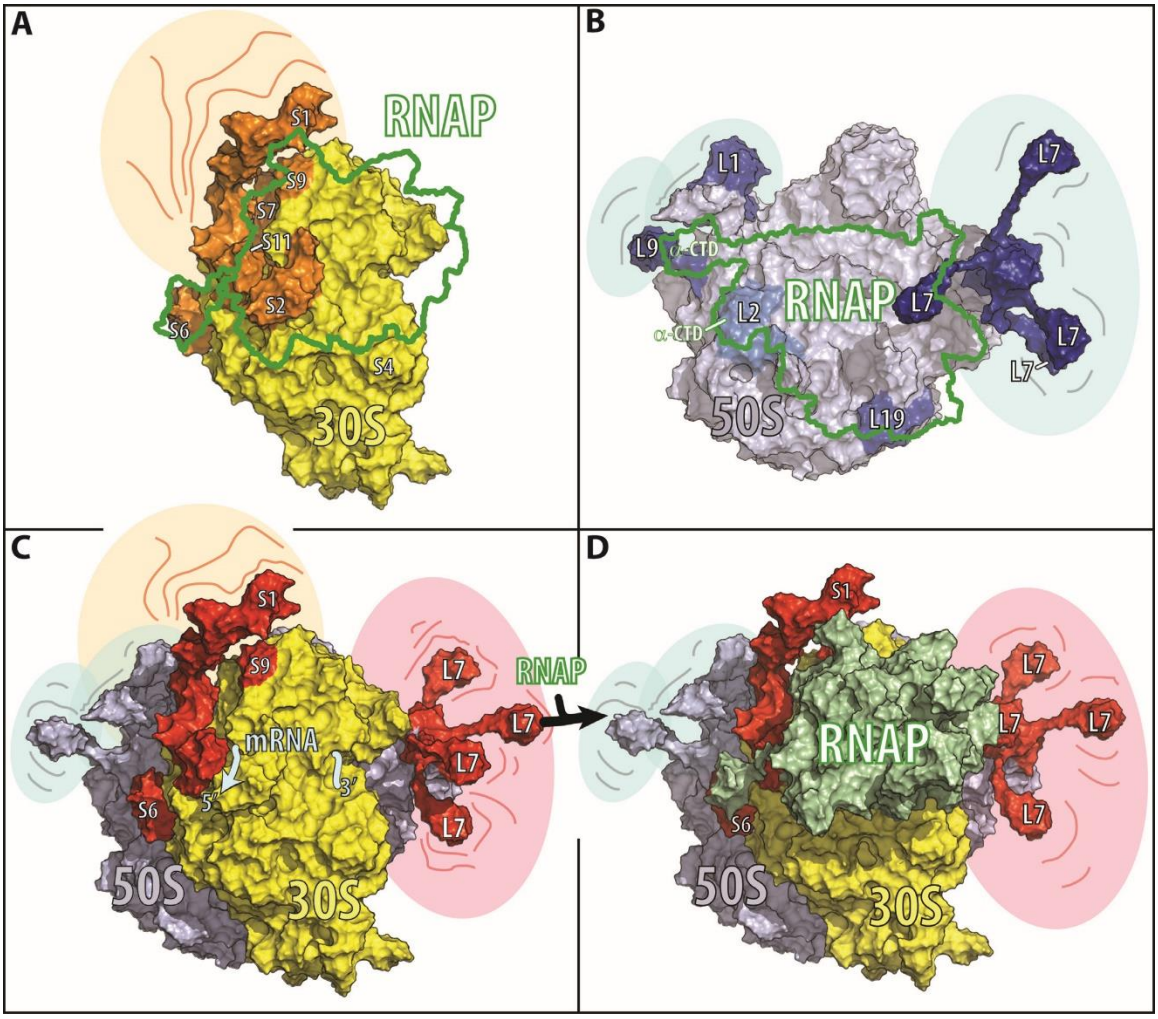
A
RNAP
S1
S9
S7
S11
S2
S6
S4
30S
B
L1
L7
L9
α-CTD
RNAP
L2
L7
α-CTD
L7
L7
50S
L19
C
S1
S9
L7
RNAP
L7
mRNA
L7
3'
5'
S6
L7
50S
30S
D
S1
L7
L7
RNAP
L7
S6
L7
50S
30S

Figure 3.4: Models for RNA polymerase binding to the small ribosomal subunit, the large ribosomal subunit, and the ribosome. Ribosomal proteins crosslinked to RNA polymerase (RNAP, in green) are indicated in orange for the small ribosomal subunit (30S, in yellow), in blue for the large ribosomal subunit (50S, in gray), and red for the whole ribosome (70S). The model of the full-length RNA polymerase is based on the cryo-EM structure of *E. coli* RNA polymerase (PDB: 5UPC (Kang, Olinares et al. 2017)) and the NMR structure of the C-terminal domain of the α subunit (PDB: 2MAX (Borin, Tang et al. 2014)). The models of the ribosome and its subunits are based on the cryo-EM structure of *E. coli* ribosomes (PDB: 4V6Q (Agirrezabala, Liao et al. 2012)). To complete the ribosome model, the L1 stalk is modeled based on the crystal structure of the L1 stalk (PDB: 1U63 (Nevskaya, Tishchenko et al. 2005)), the L7/L12 stalk is based on the NMR structure of L10•$(L7/L12)_4$ (PDB 1RQU (Bocharov, Sobol et al. 2004)), the C-terminal residues of ribosomal protein S6 are modeled according to the full-length S6 in the cryo-EM structure of the ribosome (PDB: 4V6P (Agirrezabala, Liao et al. 2012)), and ribosomal protein S1 is modeled based on the crystal structure of domain I in complex with ribosomal protein S2 (PDB 4TOI (Byrgazov, Manoharadas et al. 2012)) and the NMR structures of domains 4 and 6 (PDB 2KHI and 2KHJ (Salah, Bisaglia et al. 2009)). The relative position of the RNA polymerase on the small ribosomal subunit and ribosome is restrained by the identified crosslinks as well as by the assumption that the nascent RNA between the RNA polymerase and ribosome has the shortest length during transcription-translation coupling. The shaded areas surrounding different components of the ribosome in **A-D** indicate spatial flexibility. On the small ribosomal subunit the flexible region involves ribosomal protein S1; on the large ribosomal subunit it involves the L1 stalk, the L7 stalk, and of the ribosomal protein L9; and on the ribosome the L1 stalk, the L7 stalk, and the ribosomal proteins S1 and L9. **A)** The small ribosomal subunit viewed from the cytosolic site with crosslinked ribosomal proteins S6, S2, S11, S7, S9, and S1 in orange. The green boundary outlines the RNA polymerase position on the small ribosomal subunit. **B)** The large subunit viewed from the ribosomal subunit interface. In blue are the crosslinked proteins L1, L9, and L19, and in light blue is L2, a known binding partner of the RNA polymerase α-subunit. **C)** Ribosome with identified crosslinked proteins S6, S9, and L7 in red. **D)** Model of RNA polymerase-ribosome interactions based on the chemical crosslinks identified in this study. The figures were prepared in PyMOL (Schrödinger, LLC) using a solvent radius of 5 Ångstrom.

Discussion:

In *E. coli*, the translation rate is the same as the transcription rate (Proshkin, Rahmouni et al. 2010). The first ribosome trailing the transcribing RNA polymerase directly assists the polymerase during elongation (Proshkin, Rahmouni et al. 2010) and suppresses transcription termination within coding regions (Lesnik, Sampath et al. 2001, Li, Zhang et al. 2016). Recent ribosome profiling studies show that translational elongation speed is not uniform (Li, Oh et al. 2012, Mohammad, Woolstenhulme et al. 2016). Prolonged pausing of translation decouples RNA synthesis from protein synthesis, causing the premature termination of transcription (Elgamal, Artsimovitch et al. 2016). Prolonged pausing of transcription turns the RNA polymerase into a roadblock for the leading ribosome. Any barrier encountered by the translating ribosome promotes the loss of its reading frame (Caliskan, Katunin et al. 2014, Chen, Petrov et al. 2014, Kim, Liu et al. 2014, Yan, Wen et al. 2015), which, in turn, results in the premature termination of translation. Premature translation termination causes premature rho-dependent and rho-independent transcription termination (Adhya and Gottesman 1978, Elgamal, Artsimovitch et al. 2016, Li, Zhang et al. 2016). Consequently, the synchronization of transcription and translation is essential for gene expression in eubacteria.

The direct interaction between the RNA polymerase and the ribosome results in stoichiometric complex formation. The spatial arrangement of the polymerase and ribosome is reflected in the proteins that are crosslinked within the complex and allows us to triangulate the location of the RNA polymerase on the surface of the subunits and the ribosome. The interface between the polymerase and the large subunit is located on

the face that binds the small subunit, which, upon association with the small subunit, is buried within the ribosome (Figure 3.4B and 3.4C). Modeling the binding of RNA polymerase on the large ribosomal subunit places the RNA polymerase in close proximity to the ribosomal protein L2, which is known to bind the α subunit of RNA polymerase (Rippa, Cirulli et al. 2010). The set of proteins crosslinked in the complex with ribosomes overlaps with that of the small ribosomal subunit complex (Figure 3.3C and 3.3D), clustering around the mRNA exit site of the ribosome (Figure 3.4A and 3.4C), hinting at the possible coordination between the transcription and translation initiation of the nascent RNA.

During the initial phase of translation initiation, the mRNA binds to a ‘‘standby’’ site on the ribosome that encompasses the entire mRNA exit site (Yusupova, Jenner et al. 2006). The binding of translation initiation factors repositions the mRNA on the small ribosomal subunit, permitting translation initiation to progress (Gualerzi and Pon 2015). *In vivo*, transcription pauses near the promoter (Mooney, Davis et al. 2009, Larson, Mooney et al. 2014). This pausing of the RNA polymerase seems to allow the ribosome to initiate translation and catch up with the polymerase. The “standby” position of the mRNA may interfere with the interaction of the RNA polymerase with the mRNA exit site, thus coordinating the accommodation of the nascent RNA and the subsequent initiation of translation with the resumption of transcription. During eukaryotic translation initiation, initiation factor eIF3 also engages with the mRNA in the exit site while it is bound to both the mRNA entry and exit sites, thereby coordinating mRNA

accommodation with the downstream steps of translation initiation (Aylett, Boehringer et al. 2015, Aitken, Beznoskova et al. 2016).

Common to the identified RNA polymerase interfaces on the ribosome and small ribosomal subunit are ribosomal proteins S6 and S9; additionally, S1 is present in all but one of the identified crosslinked species (Figure 3.3C). Ribosomal protein S1 binds to RNA polymerase near the exit site of the nascent RNA (Sukhodolets and Garges 2003, Liu, Zuo et al. 2015) and promotes the recycling of the RNA polymerase after transcription termination (Sukhodolets, Garges et al. 2006). Similar to the C-terminal domains of ribosomal protein S1, the two to six glutamic acid residues of the C-terminal tail of S6 extend away from the ribosome, reaching into the surrounding solution. This local accumulation of glutamic acid residues may form the same salt bridges with the RNA polymerase as free glutamate at high cellular concentrations, when it releases the RNA polymerase stalled at the *osmY* promoter DNA (Lee and Gralla 2004). Although ribosomal protein S9 is farther from the mRNA exit site, its long C-terminal tail reaches through the head of the subunit to the mRNA channel. In the mRNA channel, the tail stabilizes the tRNA-mRNA interactions at the P-site (Selmer, Dunham et al. 2006), contributing to the fidelity of translation initiation and the maintenance of the reading frame (Arora, Bhamidimarri et al. 2013) (Figure 3.4A and 3.4D).

The potential mechanistic implications of the observed interaction of the RNA polymerase with the large ribosomal subunit are difficult to reconcile with our current understanding of the coupling of transcription and translation. However, this interaction might hint at the potential coordination of ribosomal RNA transcription and ribosome

assembly during ribosome biogenesis. Ribosome assembly factors can, like RNA polymerase, bind to mature ribosome particles *in vitro* and *in vivo* (Sharma, Barat et al. 2005, Qin, Polacek et al. 2006, Jain 2008, Gibbs, Moon et al. 2017).

In summary, our binding studies suggest that during transcription-translation coupling, the RNA polymerase binds to the cytosolic site of the small ribosomal subunit, extending from the mRNA exit to the mRNA entry site. This binding allows the polymerase to monitor the translation rate of the ribosome while providing it with more nascent RNA. The coordination of transcription and translation may be conferred via the interaction with ribosomal protein S9. The tightest interaction between RNA polymerase and the ribosome arises from an RNA polymerase conformation that is distinct from that of the TEC.

While revising our manuscript, Cramer, Landick, and colleagues published a 9 A cryo-EM structure of the RNA ˚ polymerase•ribosome complex (Kohler, Mooney et al 2017). Although the stoichiometry and the ribosomal interface components of our model agree well with that of the EM structure, the relative orientation of the polymerase and ribosome are distinct. The EM structure places the polymerase more towards the mRNA entry site of the ribosome, with the nascent RNA exit site of the polymerase in closer contact with the mRNA entry site of the ribosome and the RNA polymerase rotated more towards the cytosol. Further studies will be required to understand the origins of these differences.

Our biochemical study, as well as the recently published EM structure of the RNA polymerase•ribosome complex (Kohler, Mooney et al 2017), demonstrates the existence

of a direct interaction between RNA polymerase and ribosomes, and points to its functional relevance during transcription–translation coupling. However, the here determined equilibrium constants only reflect the strength of the interaction between two the molecules, but not the time that interaction will persist in a dynamic setting, such as during on-going transcription and translation. Consequently, detailed kinetic studies will be needed to fully understand the feedback between the RNA polymerase and ribosome during transcription–translation coupling. The mechanistic insights derived from such studies will add to this new paradigm of how gene expression is controlled.

Funding: National Institutes of Health [R21 ES025392 to Y.W.]; University of California, Riverside (to G.B. and Y.W.). Funding for open access charge: University of California, Riverside.

Conflict of interest statement. The authors declare that there are no conflicts of interest.

Acknowledgements: We thank Mr. Carlos Rodriguez and Ms. Gabriela Sanchez for technical assistance during sample preparation, Dr. Jacques Barbet for unwavering technical support with the "Equilibrium Expert" add-in for Microsoft Excel®, Dr. Whitney Yin for critical discussion, and Mr. Tim Rowsell, Mr. Timothy Tam and Ms. Kacey Kilpatrick for assisting in the preparation of the manuscript.

Supplementary Data:

Material & Methods:

Chemicals.

RNase-free sucrose and, ultra-pure Tris were from Amresco (Solon, OH, USA), HEPES and imidazole were from Calbiochem (San Diego, CA, USA), 1-ethyl-3-(3-dimethylaminopropyl) carbodiimide (EDC) was from Pierce (Waltham, MA, USA), sulfo Nhydroxysuccinimide (sulfo-NHS) was from Chem-Impex Int'l (Wood Dale, IL, USA), and βmercaptoethanol was from Bio-Rad (Hercules, CA, USA). Poly(U)-RNA and all other chemicals were purchased from Sigma Aldrich (St. Louis, MO, USA). The oligoribonucleotide and oligodeoxyribonucleotides were from IDT (Coralville, IA, USA). All buffers were prepared with DEPC-treated water. Polyvinylidene difluoride membranes, antibodies, and Western blot luminol reagent were from Santa Cruz Biotechnology (Santa Cruz, CA, USA). The ReproSil C18-AQ resins (300 Å pore size) with 3-μm and 5-μm particle sizes used to pack the LC-MS/MS separation and trapping columns, respectively, were purchased from Dr. Maisch HPLC GmbH, Germany.

Quality assessment of purified ribosomes.

The amount of NusG present in our ribosome preparations was assessed by tandem mass spectrometry analysis. As internal standards for our assessment, ribosome samples were spiked with one-tenth or with equimolar amounts of NusG. Samples were loaded onto a 6 % SDS-polyacrylamide gel and run a few millimeters into the gel. The band containing all of the ribosomal proteins was excised from the gel. The proteins captured in the excised gel band were reduced, alkylated, and in-gel digested with

trypsin. The resulting peptide mixture was extracted and subjected to liquid chromatography-tandem mass spectrometry (LC-MS/MS) analysis as described below.

Ribosomal RNA from purified and crude ribosomes was extracted using an E.Z.N.A. Bacterial RNA kit (Omega Bio-tek, Norcross, GA, USA) according to the protocol provided by the manufacturer. The quality of the extracted ribosomal RNA was assessed after separation by microfluidic chip gel-electrophoresis with an RNA 6000 Nano kit (Agilent, Santa Clara, CA, USA).

Preparative isolation of the RNA polymerase•ribosome complex.

One milliliter of 10 µM RNA polymerase and 2.5 µM ribosomes were incubated for 15 min at 37 °C in buffer A (20 mM HEPES-KOH pH 7.5, 20 mM Mg(OAc)2, and 30 mM KCl). The mixture was loaded onto a 36- mL 10 – 40 % sucrose gradient prepared in buffer A and centrifuged in a SW32 Ti rotor for 16 hours at 24,000 rpm and 4 °C. After centrifugation, the gradient was collected in 1.8-mL fractions. The protein content of each fraction was determined by SDS-polyacrylamide gel electrophoresis. Fractions containing ribosomes with co-migrated RNA polymerase were pooled, concentrated, and buffer-exchanged into buffer A. The concentrated complex was aliquoted, flash frozen in liquid nitrogen, and stored at -80 °C until further use.

To test the stability of the complex, a frozen aliquot of the complex was diluted with buffer to a final concentration of 1 µM and incubated for 15 min at 37 °C, before analyzing the RNA polymerase-ribosome content by sucrose gradient centrifugation as described in “Separation of free RNA polymerase from ribosome-bound RNA polymerase.” To determine the quality of the ribosomal RNA, we extracted ribosomal

RNA from the purified complex and, as a positive control, from crude ribosomes, both of which were analyzed using an RNA 6000 Nano kit (Agilent).

Western blot analysis.

Proteins were electro-blotted onto a polyvinylidene difluoride membrane, probed with mouse antibodies against individual RNA polymerase subunits, incubated with horseradish peroxidase-conjugated goat anti-mouse antibodies, and visualized via a chemiluminescence reaction, which was documented with the ChemiDoc™ Touch Gel Imaging System (Bio-Rad).

Results:

*Establishing conditions for the analysis of RNA polymerase-ribosome interaction*s.

The effect of different cations and anions on ribosomes and RNA polymerase has been extensively documented (Miskin, Zamir et. Al 1970, Zamir, Miskin et al 1971, Suh, Leirmo et al 1992, Shaner, Piatt et al 1982)). We chose to perform our studies with KCl in the presence of magnesium ions either as chloride or acetate, as these ions are compatible with both transcription (So, Davie et al 1967) and translation (Zamir, Miskin et al 1974).

The stability of the RNA polymerase-ribosome complex decreases with increasing concentrations of potassium chloride. Compared to 30 mM KCl in the sucrose gradient, only half the amount of the complex is detected with 125 mM KCl, and none was detected with 250 mM KCl (Figure S3.1A). RNA polymerase-ribosome complexes appear to be more stable at low salt conditions during sucrose gradient centrifugation. To prevent the dissociation of RNA polymerase-ribosome complexes during sucrose

gradient centrifugation, all analyses of complex formation were performed with sucrose gradients under low-salt conditions of 30 mM KCl and 20 mM magnesium acetate or chloride.

Supplemental Figures:

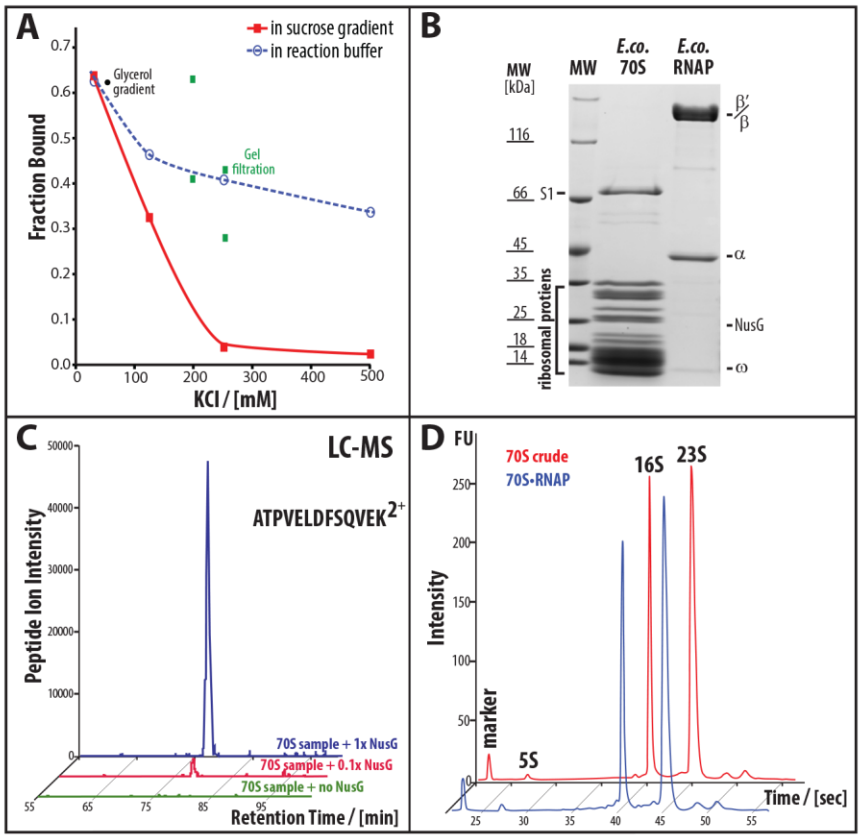

Figure S3.1: Characterization of the RNA polymerase, ribosomes and complexes thereof. **A)** Establishing experimental conditions for analysis of the complex formation. Titration of RNA polymerase-ribosome mixtures with KCl during the reaction (blue) and during sucrose gradient centrifugation (red). In black is the fraction of bound RNA polymerase as determined by glycerol gradient centrifugation at a low salt concentration. In green are the fractions of bound RNA polymerase as determined by gel filtration. **B)** SDS-polyacrylamide gel electrophoresis (SDS-PAGE) analysis of purified RNA polymerase (RNAP) and ribosome (70S) samples from Escherichia coli (E.co.). The positions of ribosomal protein S1 and additional ribosomal proteins are indicated on the left of the gel image, and RNA polymerase subunits α, β, β', and ω and the expected position of NusG are indicated on the right. The molecular weights of the protein ladder are to the left side of the gel. **C)** Determination of the amount of NusG contamination of E. coli ribosomes by LC-MS/MS. Ion intensity of one tryptic-digest peptide fragment of NusG (ATPVELDFSQVEK2+). The blue and red traces are ribosome samples with NusG added in stoichiometric and sub-stoichiometric amounts. The green trace is the ribosome sample alone. **D)** Ribosomal RNA quality determined by micro-chip capillary electrophoresis. The red trace is ribosomal RNA extracted from ribosomes from cell lysates that were pelleted through a high-salt sucrose cushion. The blue trace is ribosomal RNA extracted from the purified RNA polymerase ribosome complex.

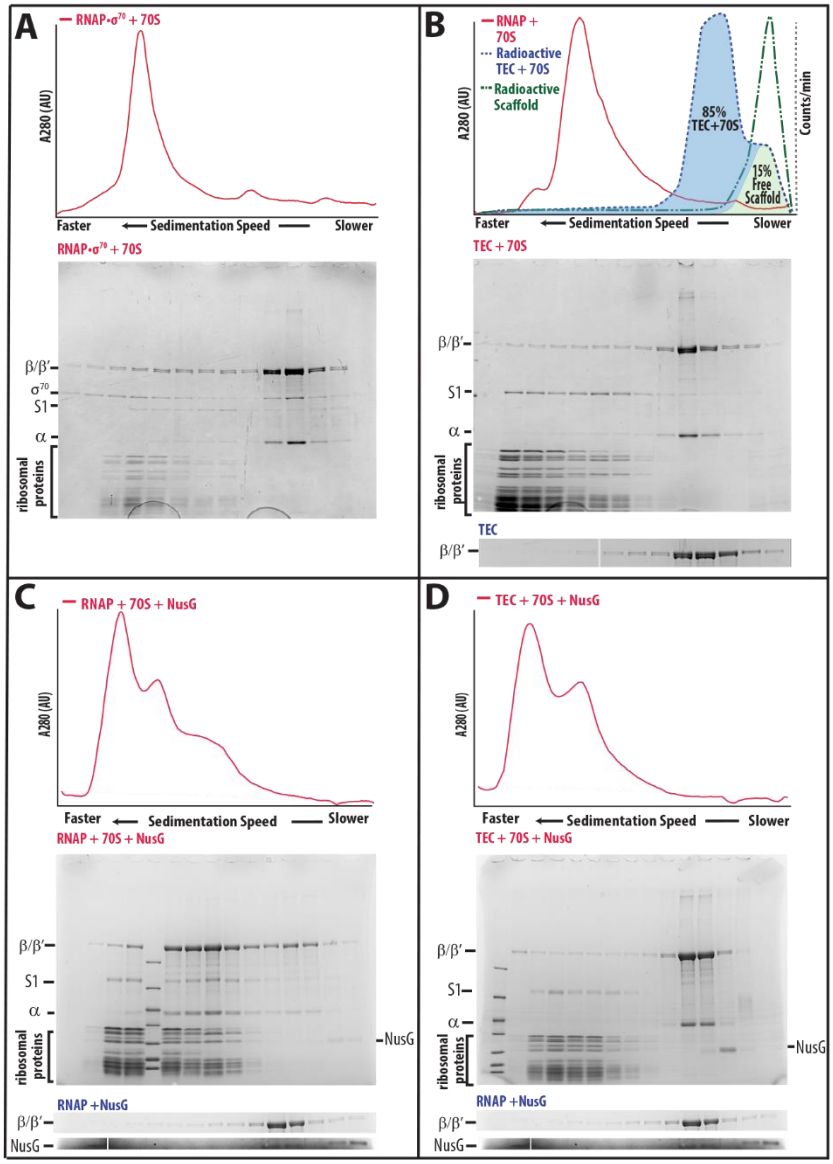
A
RNAP•σ70 + 70S
A280 (AU)
Faster
Sedimentation Speed
Slower
RNAP•σ70 + 70S
β/β′
σ70
S1
α
ribosomal proteins
B
RNAP + 70S
Radioactive TEC + 70S
Radioactive Scaffold
A280 (AU)
Counts/min
85% TEC+70S
15% Free Scaffold
Faster
Sedimentation Speed
Slower
TEC + 70S
β/β′
S1
α
ribosomal proteins
TEC
β/β′
C
RNAP + 70S + NusG
A280 (AU)
Faster
Sedimentation Speed
Slower
RNAP + 70S + NusG
β/β′
S1
α
ribosomal proteins
NusG
RNAP +NusG
β/β′
NusG
D
TEC + 70S + NusG
A280 (AU)
Faster
Sedimentation Speed
Slower
TEC + 70S + NusG
β/β′
S1
α
ribosomal proteins
NusG
RNAP +NusG
β/β′
NusG

Figure S3.2: Sucrose gradient analysis of the interactions of the vacant ribosome (70S) with A) the holoenzyme (RNAP•σ70), B) transcription elongation complex (TEC), C) the core enzyme in the presence of NusG, and D) the TEC in the presence of NusG. **A)** Analysis of the interactions between ribosome with the holoenzyme. The top panel displays the sedimentation profile of the complex recorded at 280 nm. The bottom panel displays the SDS-PAGE gel of the sucrose gradient fractions. **B)** Analysis of the interactions between the ribosome and TEC. The top panel displays the sedimentation profiles of the RNA polymerase-ribosome complex recorded at 280 nm (shown as a red solid line, left ordinate axis) and of the radioactively labeled DNA:RNA hybrid scaffold in the presence of ribosomes and alone (shown as a dashed blue line and dashdotted green line, respectively, right ordinate axis). The center panel displays the SDS-PAGE gel of the sucrose gradient analysis of the RNA polymerase•TEC complex formation. The bottom panel displays the SDS-PAGE gel of sucrose gradient analysis of the TEC alone, covering the β/β' molecular weight range. **C)** Analysis of the interactions between the ribosome, RNA polymerase, and NusG. The top panel displays the sedimentation profile of the complex recorded at 280 nm. The center panel presents the SDS-PAGE gel of the sucrose gradient fractions. The bottom panels show the SDS-PAGE gel of the sucrose gradient analysis of a mixture of RNA polymerase and NusG displaying only the regions covering β/β' and the NusG molecular weight ranges. The contrast of the NusG region has been enhanced to better visualize the NusG band. **D)** Analysis of the interactions between the ribosome, TEC, and NusG. Panels are the same for C).

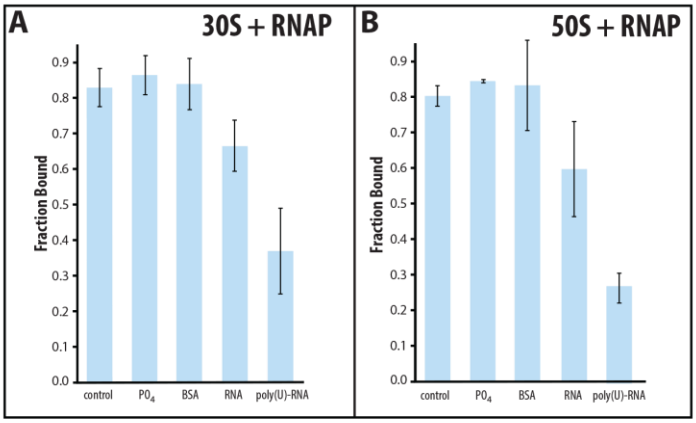

Figure S3.3: Characterizing the interactions between RNA polymerase and ribosomal subunits from E. coli. A and B) RNA polymerase binding to small ribosomal subunit (30S) and large ribosomal subunit (50S) in the presence of 10 mM phosphate buffer (PO4), 20 μM bovine serum albumin (BSA), a 14-nucleotide long RNA (RNA) at a 5 μM concentration, and 80 μg of poly(U)-RNA.

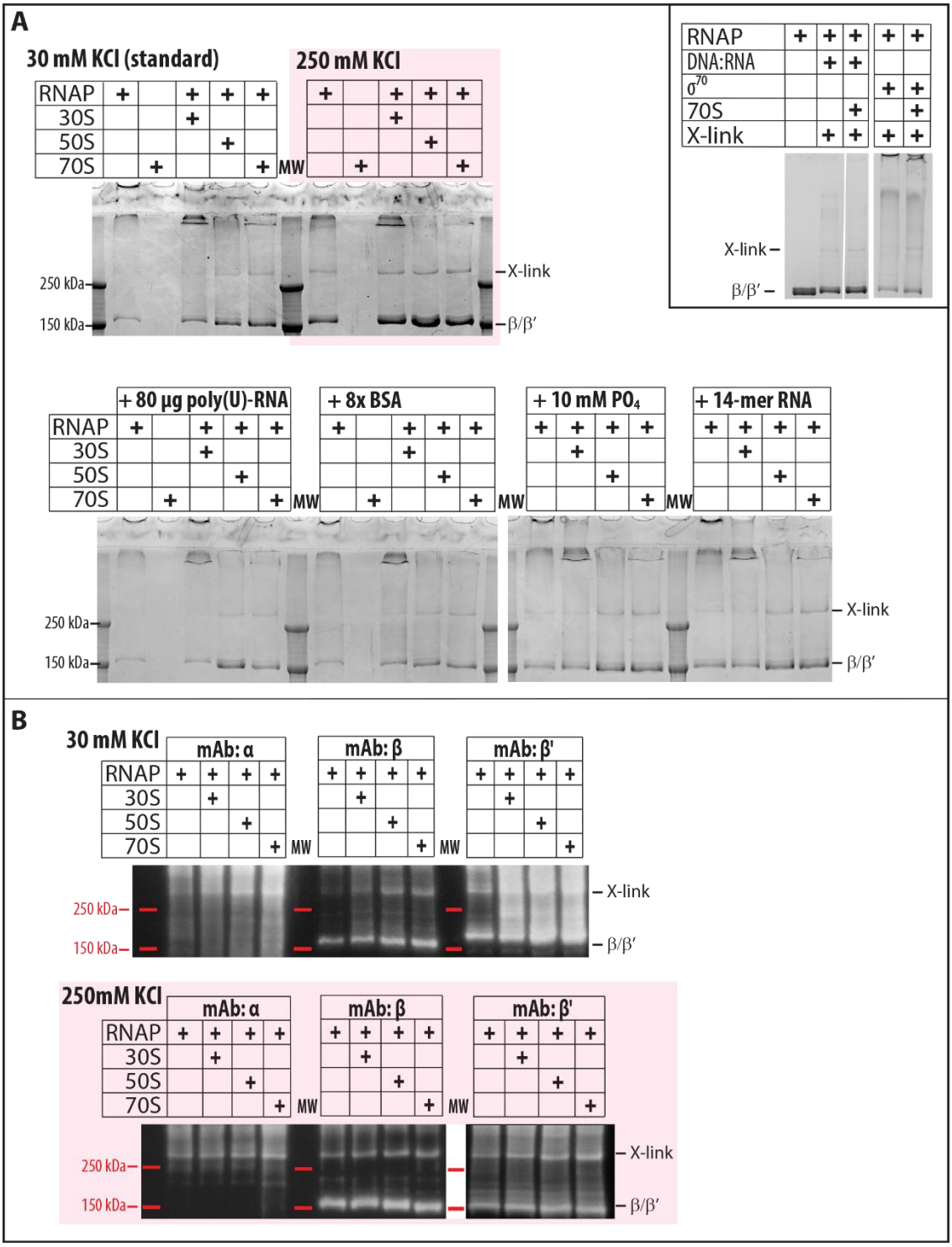
A
30 mM KCl (standard)
250 mM KCl
RNAP
30S
50S
70S
MW
250 kDa
150 kDa
X-link
β/β′
DNA:RNA
σ70
+ 80 µg poly(U)-RNA
+ 8x BSA
+ 10 mM PO4
+ 14-mer RNA
B
30 mM KCl
250mM KCl
mAb: α
mAb: β
mAb: β'

Figure S3.4: EDC crosslinking of RNA polymerase-ribosome complexes. **A)** EDC crosslinking of RNA polymerase in the presence of small ribosomal subunits (30S), large ribosomal subunits (50S), and ribosomes (70S) in 30 mM and 250 mM KCl buffer (light red background). Crosslinking experiments at 30 mM KCl were also performed in the presence of 80 μg of poly(U)-RNA, 40 μM bovine serum albumin (BSA), 10 mM phosphate buffer (PO4), and a 14-nucleotide long RNA (RNA) at a concentration of 10 μM. Inset in A) EDC crosslinking of holoenzyme and transcription elongation complex in the absence and presence of ribosomes. **B)** Western blot analysis of EDC crosslinked RNA polymerase in the presence of 30 mM KCl and 250 mM KCl (light red background) probed with monoclonal antibodies against α, β, and β'.

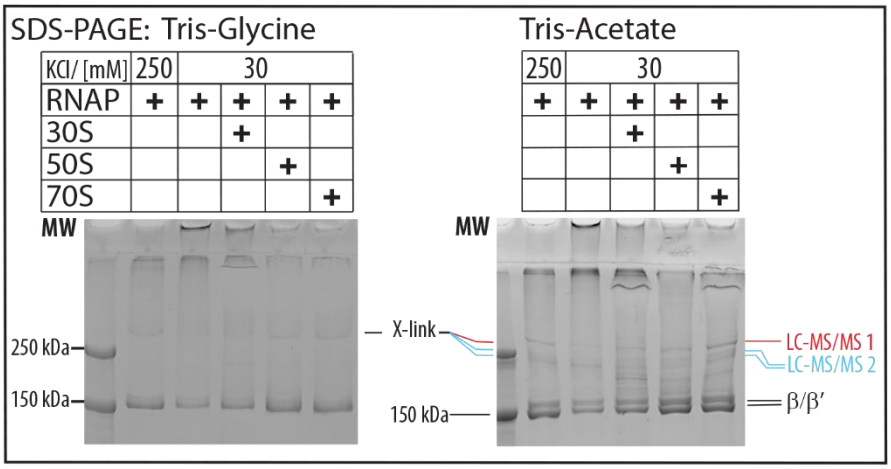

Figure S3.5: EDC crosslinking of RNA polymerase-ribosome complexes analyzed by Tris-glycine and Tris-acetate SDS-PAGE. Indicated on the right of the Tris-acetate SDS-PAGE are the bands which were extracted from the gel for further analysis by LC-MS/MS. The two bands indicated in blue were extracted as one sample for further LC-MS/MS analyses.

Protein Name - Purity of RNA polymerase

RNA polymerase, alpha subunit
RNA polymerase, beta subunit
RNA polymerase, beta prime subunit
RNA polymerase, omega subunit
predicted methltransferase, enzyme of biotin synthesis gb|ACB01978.1
hydrogenase 4, membrane subunit gb|ACB03634.1|
DNA-binding transcriptional dual regulator gb|ACB04972.1|
S-adenosyl-dependent methyltransferase activity on membrane-located substrates gb|ACB01263.1|
transcription elongation factor pTEF-b gb|ACB04465.1|
RNA polymerase, sigma 70 (sigma D) factor gb|ACB04152.1|
CPZ-55 prophage; predicted integrase gb|ACB03593.1|
predicted pilus assembly protein gb|ACB04454.1|
DNA helicase IV gb|ACB02162.1|
UDP-N-acetyl-D-mannosaminuronic acid (ManNAcA) transferase gb|ACB04824.1|
murein lipoprotein gb|ACB02879.1|

Table S3.1.1: LC-MS/MS analyses of the protein composition of purified RNA polymerase

Protein Name - Purity of 70S
50S ribosomal subunit protein L1
30S ribosomal subunit protein S5
50S ribosomal subunit protein L7/L12
50S ribosomal subunit protein L10
50S ribosomal subunit protein L2
50S ribosomal subunit protein L6
50S ribosomal subunit protein L14
50S ribosomal subunit protein L9
30S ribosomal subunit protein S4
50S ribosomal subunit protein L15
50S ribosomal subunit protein L3
30S ribosomal subunit protein S7
50S ribosomal subunit protein L11
50S ribosomal subunit protein L4
30S ribosomal subunit protein S13
50S ribosomal subunit protein L13
50S ribosomal subunit protein L22
30S ribosomal subunit protein S6
50S ribosomal subunit protein L19
30S ribosomal subunit protein S9
50S ribosomal subunit protein L16
50S ribosomal subunit protein L5
50S ribosomal subunit protein L18
30S ribosomal subunit protein S10
50S ribosomal subunit protein L17
30S ribosomal subunit protein S11
30S ribosomal subunit protein S20
50S ribosomal subunit protein L21
30S ribosomal subunit protein S8
30S ribosomal subunit protein S2
50S ribosomal subunit protein L31
30S ribosomal subunit protein S15
30S ribosomal subunit protein S18
50S ribosomal subunit protein L33
50S ribosomal subunit protein L24
30S ribosomal subunit protein S21
30S ribosomal subunit protein S19
50S ribosomal subunit protein L29
50S ribosomal subunit protein L20
30S ribosomal subunit protein S16
50S ribosomal subunit protein L25
50S ribosomal subunit protein L28
30S ribosomal subunit protein S14
30S ribosomal subunit protein S1
50S ribosomal subunit protein L30
50S ribosomal subunit protein L27
50S ribosomal subunit protein L23
50S ribosomal subunit protein L34
50S ribosomal subunit protein L32
membrane anchored protein involved in growth of wall at septum gb|ACB01274.1
30S ribosomal subunit protein S17
peptidyl-tRNA hydrolase gb|ACB02374.1|
RNA polymerase, alpha subunit
50S ribosomal subunit protein L35
RNA polymerase, beta subunit
RNA polymerase, beta prime subunit
ribose 1,5-bisphosphokinase gb|ACB05090.1|
gb|ACB04341.1| predicted amino-acid transporter subunit; ATP-binding component of ABC superfamily
gb|ACB04257.1| predicted RNA-binding protein
exonuclease
murein lipoprotein

Table S3.1.2: LC-MS/MS analyses of the protein composition of purified ribosome

	RNAP-70S_Glycine_Control_No X-Link			RNAP-70S_X-linked_Glycine		
Protein Name	Spectral Index - Trial 1	Spectral Index - Trial 2	Spectral Index - Trial 3	Spectral Index - Trial 1	Spectral Index - Trial 2	Spectral Index - Trial 3
RNA polymerase, beta subunit	72.67	112.66	71.44	56620.47	235181.24	37973.7
RNA polymerase, beta prime subunit	4.34	65.75	51.99	46463.49	225156.48	33893.44

	RNAP-70S_X-linked_AcOH_top_band			RNAP-70S_X-linked_AcOH_bottom		
Protein Name	Spectral Index - Trial 1	Spectral Index - Trial 1	Spectral Index - Trial 1	Spectral Index - Trial 1	Spectral Index - Trial 2	Spectral Index - Trial 3
RNA polymerase, beta subunit	78002.98	41994.78	41994.78	41994.78	35043.22	35257.82
RNA polymerase, beta prime subunit	109090.26	79303.48	79303.48	79303.48	43685.15	39953.09

	RNAP-50S_X-linked_AcOH_top			RNAP-50S_X-linked_AcOH_bottom		
Protein Name	Spectral Index - Trial 1	Spectral Index - Trial 2	Spectral Index - Trial 3	Spectral Index - Trial 1	Spectral Index - Trial 2	Spectral Index - Trial 3
RNA polymerase, beta subunit	17992.55	35043.22	35257.82	32234.72	35587.06	13090.16
RNA polymerase, beta prime subunit	32036.25	43685.15	39953.09	72885.57	35297.32	18090.26

	RNAP-30S_X-linked_AcOH_top			RNAP-30S_X-linked_AcOH_bottom		
Protein Name	Spectral Index - Trial 1	Spectral Index - Trial 2	Spectral Index - Trial 3	Spectral Index - Trial 1	Spectral Index - Trial 2	Spectral Index - Trial 3
RNA polymerase, beta subunit	10108.05	16827.87	20774.96	N/A	11634.13	20929.21
RNA polymerase, beta prime subunit	8850.75	20453.45	27675.2	10285	9342.57	23164.18

Table S3.1.3: LC-MS/MS analyses of the background at the relative mobility of the crosslinked band in Tris-glycine SDS PAGE (RNAP-70S_Glycine_Control), and the different crosslinked species isolated using Tris-glycine and Tris-acetate SDS-PAGE.

Protein Name - RNAP-70S_X-linked_Glycine	Average Normalized Spectral Index	Standard Deviation
RNA polymerase, beta prime subunit	1.0000	0.0000
RNA polymerase, beta subunit	0.8902	0.0684
RNA polymerase, alpha subunit	0.5693	0.1082
RNA polymerase, omega subunit	0.1346	0.0474
30S ribosomal subunit protein S1	0.0049	0.0039
30S ribosomal subunit protein S9	0.0145	0.0033
50S ribosomal subunit protein L7/L12	0.1203	0.0303
30S ribosomal subunit protein S6	0.0442	0.0060

Table S3.1.4: Average normalized Spectral index of crosslinked RNA polymerase and ribosomal proteins.

Chapter 4:

E. coli Small Ribosomal Subunit Interactions to RNAP

Unpublished work.

Abstract:

Direct interactions between RNA polymerase (RNAP) and the small ribosomal subunit (30S subunit) has been demonstrated recently. The effects of this interaction on transcription and translation, however, remain elusive. Here I present a study in progress on the thermodynamic and kinetic parameters that dictate the interactions between RNAP and the 30S subunit in isolation and in the presence of transcription and translation factors.

My equilibrium data indicate that RNAP has one binding site on the 30S subunit and can accommodate a single RNAP monomer or dimer, depending on the oligomeric state of RNAP. The micromolar dissociation constant of the RNAP binding is within the physiological concentration range of RNAP and the small ribosomal subunit, implying that these interactions may occur under cellular conditions. In addition, I could demonstrate that translation initiation factors (IF1, IF2•GTP, and IF3), mRNAs, and fMet-tRNA$_i$ affect, independently and in combination, the 30S subunit's affinity for RNAP. Based on these observations, we hypothesize that similar to the 3′ end of a structured mRNA, the RNAP relocates from the mRNA exit site to the mRNA entry site of the 30S subunit during translation initiation. This moves the RNAP more than 75 Å on the 30S subunit, explaining the apparent contradictory RNAP binding sites observed in the cryo-EM structures of RNAP bound to the 30S subunit and those of the RNAP in complex with 70S ribosome. Currently, we are in the process of determining the kinetic parameters of the RNA polymerase – ribosomal subunit interaction to gain a more complete picture.

Introduction:

In bacteria, translation initiation ensues when the 30S subunit, initiator tRNA fMet-tRNA$_i$, initiation factors IF1, IF2•GTP, and IF3 assemble on the start codon of the mRNA to form the 30S initiation complex. Upon binding of the 50S subunit to the 30S initiation complex, IF2 hydrolyzes its bound GTP and dissociates with IF1 and IF3, completing the association of subunits to form a 70S ribosome with bound mRNA and fMet-tRNA$_i$ (70S•mRNA•fMet-tRNA$_i$). This 70S initiation complex is ready to accept the first aminoacylated tRNA. With the binding of the first aminoacylated tRNA, translation progresses from translation initiation to translation elongation during which the remainder of the protein is synthesized (Simonetti, Marzi et al., 2009, Gualerzi, Pon, 2015).

Translation can also occur while an mRNA is actively being transcribed, a process referred to as transcription-translation coupling (Das, Goldstein et al., 1967, French, Santangelo et al., 2007). The simultaneous binding of RNA polymerase (RNAP) and ribosomes to the same mRNA brings both macromolecules physically close to each other (Miller, Hamkalo et al., 1970, Klaholz, 2017). This proximity of the RNAP and ribosome is thought to hamper premature transcription termination (Adhya, Gottesman, 1978, Stanssens, Remaut et al., 1986, de Smit, Verlaan et al., 2009, Elgamal, Artsimovitch et al., 2016, Li, Zhang et al., 2016) and match the rates of transcription and translation of mRNAs (Vogel, Jensen, 1994, Proshkin, Rahmouni et al., 2010, Iyer, Le et al., 2018). In addition, the distance between the RNAP and the first, trailing ribosome on a nascent mRNA affects folding of the intervening RNA, which in turn determines the

expression of downstream genes (Yanofsky, Ito, 1966, Landick, Carey et al., 1985, Landick, Turnbough et al., 1996, Yanofsky, 1999).

Our recent biochemical work and several independent cryo-EM structure studies demonstrated the existence of direct interactions between RNAP and the ribosome, with many key interactions clustering on the small ribosomal subunit (30S subunit) (Demo, Rasouly et al., 2017, Fan, Conn et al., 2017, Kohler, Mooney et al., 2017, Wang, Molodtsov et al., 2020, Webster, Takacs et al., 2020). However, depending on the complex being studied, three distinct binding locations of the RNAP on the 30S subunit are observed: 1) In the complex formed by directly binding the RNAP to the 30S subunit (30S•RNAP) (Demo, Rasouly et al., 2017). The RNAP and 30S subunit are arranged such that a nascent RNA extruded from the polymerase is directly fed into the 30S subunit, but at the site through which the mRNA exits the ribosome during protein translation. 2) While in the complex formed by having the ribosome translate all of the nascent RNA, the polymerase is placed at the 30S subunit's mRNA entry site (Kohler, Mooney et al., 2017). 3) In complexes formed with different length of intermittent RNAs between RNAP and the ribosome, the polymerase contacts the 30S subunits at multiples sites between mRNA entry and exit sites (Wang, Molodtsov et al., 2020, Webster, Takacs et al., 2020). In the complexes of transcribing and translating RNAP and ribosome, the nascent RNA exiting the polymerase is fed into the ribosome through the mRNA entry site of the 30S subunit.

Since all the direct interactions between RNAP and the ribosome were described only recently, their effects on transcription, translation, and the coordination of both

processes during coupling currently remains unknown. We hypothesize that the different observed arrangements of RNAP and ribosome may reflect different stages of transcription-translation coupling. By studying the interaction between RNAP and the 30S subunit, we expect to gain insights into the steps of transcription-translation coupling in which this interaction partakes.

My current data attempts to elucidate the cooperation between the polymerase and the ribosome, focusing on intermolecular interaction studies between RNAP and the 30S subunit. By measuring the binding affinities of different functional states of the polymerase and 30S subunit as well as of different species of RNAP, I aim to show how direct the interaction between polymerase and ribosome is dependent on the functional states of both, suggesting that the difference in observed structures are due to different states of the coupling.

Here I show that the 30S subunit has one binding site for a single RNAP in either its monomeric or dimeric form. The complex also extends cross species to *Thermus thermophilus* while being completely absent in viral T7 RNAP, suggesting an evolutionary role and perhaps a broader effect seen across eubacteria. The affinity of this site is reduced by the presence of mRNA and fMet-tRNA$_i$ and is most impaired when all factors required for translation initiation are present. Furthermore, mRNAs with a Shine-Dalgarno (SD) element inhibit complex formation to a greater extent than mRNAs absent the SD element, a factor consistent with the idea of nascent mRNA loading into the 30S subunit exit site to bind the anti-Shine-Dalgarno sequence located on the 3′ end of the 16S rRNA. The data suggest a model in which the interactions between RNAP and

ribosome are modulated by the formation of the translation initiation complex on the nascent mRNA, thus allowing the polymerase to migrate from its initial binding site on the 30S subunit at the mRNA exit site to its binding site during active transcription and translation at the mRNA entry site.

Materials and Methods:

Bacterial strains, plasmids, and oligonucleotides.

Chemically competent *E. coli* cells T7 Express and BL21(DE3) were from New England Biolabs (Ipswich, MA, USA), *E. coli* MRE 600.rif used for ribosomal subunit isolation was a kind gift from Dr. Knud Nierhaus, and pVS10 (T7P-α-β-β'-His_6-ω) and pIA1127 (T7P-His6-TEV-σ^{70}) expression vectors used for RNA polymerase and σ^{70} were kind gifts from Dr. Irina Artsimovitch. RNA, DNA, and 3'-biotinylated DNA oligos were from IDT (Coralville, IA).

Preparation of Ribosomes and RNA Polymerase.

E. coli ribosomal subunits and RNA polymerase were purified following established protocols (Blaha, Stelzl et al., 2000, Artsimovitch, Svetlov et al., 2003, Fong, Gillies et al., 2010, Nedialkov, Opron et al., 2013) with minor modifications as detailed in Fan et al. (Fan, Conn et al., 2017).

Purification of initiation factors IF2 and IF3.

For IF2 and IF3, *inf*B and *inf*C genes from MG1655 were cloned into pET28 to contain an N-terminal His-tag followed by a SUMO-tag. The tagged proteins were

overexpressed in T7 Express cells grown in TB media and induced with 0.5 mM IPTG at mid-log phase. Cells were harvested after 4 hours of overexpression, flash frozen in liquid nitrogen, and stored at -80°C until further use.

Cells were resuspended in 20 mM Tris HCl pH 8.0, 100 mM NaCl. PMSF was added to a final concentration 0.1 mM right before lysis. The resuspended cells were lysed by passing five times through an Emulsi Flex C3 cell disruptor at 5,000-10,000 psi. The lysate was clarified for two hours at 100,000 g and 4°C. The clarified supernatant was loaded onto Ni-NTA sepharose column (GE Health Science), washed with 2 column volumes of lysis buffer, washed with two column volumes 20 mM Tris HCl pH 8.0, 500 mM NaCl, and 20 mM Imidazole-HCl pH 8.0, before eluting the His-Sumo-tagged protein of the column with an Imidazole gradient from 0-300 mM in 20 mM Tris HCl pH 8.0, 100 mM NaCl over 10 column volumes. Fractions containing the tagged protein were pooled and incubated with Sumo protease (1 mg Sumo protease/100 mg His-sumo-protein) overnight at 4°C. The next day, the cleavage reaction was dialyzed twice for 3 hours against 20-100 volumes of 20 mM Tris HCl pH 8.0 containing 100 mM NaCl. Precipitated SUMO protease was removed by centrifugation at 100,000 g for 1 hour at 4°C, before loading onto a Ni-Sepharose column and collecting the flow through. After concentrating the sample in Amicon 15 filters with 3 kDa molecular weight cut off, it was dialyzed twice against 20 mM Tris HCl pH 7.5, 200 mM NaCl, 1 mM EDTA pH 8.0, 6 mM BME with 10% Glycerol. After the final dialysis, the protein was aliquoted, flash frozen in liquid nitrogen, and stored at -80°C until further use.

Purification of initiation factor IF1.

For IF1, the *infA* gene was cloned into the pET28 vector. T7 Express cells transformed with pET28-*infA* vector were grown in TB media, and IF1 expression was induced with 0.5 mM IPTG at mid-log phase. After 4 hours of induction, cells were harvested, flash frozen in liquid nitrogen, and stored at -80°C until further use.

Frozen cells were resuspended in 20 mM Tris-HCl pH 7.5, 60 mM NH_4Cl, 10 mM $MgCl_2$, and 1 mM Benzamidine-HCl. Cells were lysed by passing 5 times through an Emulsi Flex C3 cell disruptor at 5,000-10,000 psi. The lysate was clarified at 30,000 g, before adjusting the NH_4Cl concentration to 1 M NH_4Cl. Ribosomes were pelleted by ultracentrifugation for 16-18 hours at 143,000 g at 4°C. Solid $(NH_4)_2SO_4$ was added to the supernatant to yield 60% saturation. After 1 hour stirring at 4°C, the $(NH_4)_2SO_4$ precipitation was collected for 1 hour at 30,000 g at 4°C. The $(NH_4)_2SO_4$ pellet was resuspended in 20 mM Tris HCl pH 7.5, 1 mM EDTA pH 8.0 and filtered through a 0.45 μm filter and loaded onto a Resource Q column. The flowthrough of the Resource Q column was dialyzed into 20 mM Tris HCl pH 7.5, 100 mM NH_4Cl, 1 mM EDTA pH 8.0, 6 mM BME, 10% Glycerol. The dialysate was loaded onto a SP sepharose column washed with 1 column volume of dialysis buffer and eluted with an NH_4Cl gradient to 500 mM over 10 column volumes. Fractions containing pure IF1 were combined, concentrated, and dialyzed into 20 mM Tris HCl pH 7.5, 100 mM NH_4Cl, 1 mM EDTA pH 8.0, 6 mM BME, and 10% Glycerol, before flash freezing in liquid nitrogen and storing at -80°C until further use.

Purification of MetRS and MTF.

Methionine-tRNA ligase, MetRS, and methionyl-tRNA formyltransferase, MTF genes (*metG* and *fmt*, respectively) were cloned into pET23b between the BamHI and XhoI restriction sites. These constructs were transformed into BL21(DE3) cells, and cells were grown in LB to mid-log phase before inducing protein expression with 1 mM IPTG. After 4 hours of induction, cells were harvested, flash frozen in liquid nitrogen, and stored at -80°C until further use.

Frozen cells were resuspended in 20 mM Tris-HCl pH 7.5, 100 mM NaCl, and 1 mM Benzamidine-HCl. The resuspended cells were lysed by passing 5 times through an Emulsi Flex C3 cell disruptor set at 5,000-10,000 psi. The lysate was clarified for two hours at 100,000 g at 4°C. The clarified supernatant was loaded onto a Ni-NTA sepharose column (GE Health Science), washed with two column volumes of lysis buffer, washed with two column volumes 20 mM Tris HCl pH 8.0, 500 mM NaCl, and 20 mM Imidazole-HCl pH 8.0, before eluting the His-tagged protein off the column with a Imidazole gradient from 0-300 mM in 20 mM Tris HCl pH 8.0, 100 mM NaCl over 10 column volumes. Fractions containing the tagged protein were pooled, concentrated, and buffer exchanged into 20 mM Tris-HCl pH 8.0. MetRS was further purified over a Resource Q column and MTF over a SP sepharose column with a NaCl gradient from 0-500 mM in Tris HCl pH 8.0. The fractions containing pure protein were combined, concentrated, and dialyzed into 20 mM Tris HCl pH 8.0, 100 mM NaCl, before flash freezing in liquid nitrogen and storing at -80°C until further use.

Purification of $tRNA_i$ and preparation of fMet-tRNAi.

Native $tRNA_i$ was overexpressed in *E. coli* and affinity purified from total tRNA using biotinylated oligonucleotide probe (5'-TTATGAGCCCGACGAGCTACCAGGCT-Biotin-3') immobilized to streptavidin Sepharose (Yokogawa, Kitamura et al., 2010).

Formation of functional RNA polymerase complexes.

For preparation of holoenzyme, a 2.5-fold excess of σ^{70} was incubated with core RNA polymerase. The transcription elongation complex was prepared by incubating a template DNA strand (CCTGTCTGAATCGCTATCGCCGC) with a non-template DNA strand (GCGATTCAGACAGG) and a 14-nucleotide oligoribonucleotide (rGrArGrUrCrUrGrCrGrGrCrGrArU) which both anneal to the template strand to form a DNA:RNA hybrid scaffold prior to incubating with core RNA polymerase (Fan, Conn et al., 2017).

Formation and analysis of RNA polymerase and ribosomal subunit complexes

In a standard binding assay, 2.5 µM RNAP was incubated with 2.5 µM of 30S subunits in buffer A (20 mM Tris-HCl pH 7.6, 20 mM $MgCl_2$, 55 mM KCl) for 15 min at 37°C, briefly spun at 19,000 g at 4°C, and further analyzed with either sucrose gradient centrifugation or native gel electrophoresis.

Analysis of the RNA polymerase-ribosome complex formation by sucrose gradient centrifugation followed by SDS-PAGE.

Preformed RNA polymerase-ribosomal subunit complexes were loaded onto a 10-40 % sucrose gradient in Buffer B (20 mM Tris-HCl pH 7.6, 20 mM $MgCl_2$, 30 mM KCl) and spun in a SW 32.1 Ti rotor for 18 hours at 29,000 rpm at 4°C. After centrifugation, gradients were collected in 13 fractions and the potential ribosome pellet was resuspended in water. Each fraction, including the resuspended ribosome pellet was precipitated with a final volume of 10 % trichloroacetic acid, and washed with acetone, before resuspending in 60 μL SDS loading buffer containing 4 M urea and 1 M thiourea. The protein content of each SDS sample was separated on a Tris-Glycine SDS polyacrylamide gel with a 4 % stacking gel and a 4–20 % resolving gel at 120 V for 90 min. The SDS polyacrylamide gels were visualized by staining with colloidal Coomassie Brilliant Blue G-250 (Westermeier, 2006). The stained gels were documented using a ChemiDoc™ Touch Gel Imaging System (Bio-Rad). β/β' bands in each lane were quantified using ImageJ 1.46 (Schneider, Rasband et al., 2012). The fraction of bound RNAP was determined by subtracting the concentration adjusted profile of the free RNA polymerase control from bound complexes (Fan, Conn et al., 2017).

Analysis of the RNA polymerase-ribosome complex formation by native gel electrophoresis.

Preformed RNA polymerase – ribosomal subunit complexes were mixed with sucrose to a final concentration of 15% sucrose (w/v) and loaded onto a freshly prepared 1.5 mm thick composite native agarose gel in buffer C (34 mM Tris-base, 54 mM HEPES-free acid, 0.1 mM EDTA, 10 mM $Mg(acetate)_2$, 30 mM K acetate, and 1 mM DTT and adjusted to pH 8 with acetic acid). The free RNA polymerase was separated from bound RNAP during the 3-hour electrophoresis at 90V/0.05A at 4°C using a field inverter that continuously switched the field direction between forward and reverse. The duration of the forward field direction was 0.2 sec and for the reverse direction 0.1 sec. During the full duration of the electrophoresis, buffer C was cycled to maintain the pH of anode and cathode buffer within 0.2 pH units and a temperature below 10°C. After electrophoresis, the gels were stained overnight with 5-10-fold gel volumes of colloidal Coomassie G-250 without rocking or shaking. The next day, the stained gels were rinsed with water and then imaged with a ChemiDoc™ Touch Gel Imaging System (Bio-Rad). The band of free 30S subunit in each lane was quantified using ImageJ 1.46 (Schneider, Rasband et al., 2012). The fraction of free 30S subunit was ascertained by determining the ratio of the measured intensity of free 30S subunits in presence and absence of RNAP, both run on the same gel.

The protocol for agarase treatment – to analyze the composition of different bands of the native gel:

Excised agarose bands from the native gel were incubated at 65°C until molten, and then cooled to 42°C. The samples were mixed with 1 unit of β-agarase and incubated overnight at 42°C to break down the agarose gel matrix. The following day, samples were centrifuged for 10 min at 19,000 *g* at 4°C. Supernatant was collected and then precipitated with trichloroacetic acid at final concentration 10% [w/v] at 4°C for one hour. The precipitated protein was collected by a 10 min centrifugation at 19,000 *g* at 4°C. In order to remove excess salt, samples were suspended in 2-fold 95% acetone, vortexed for 15 minutes, and then spun for 15 min at 19,000 *g* at 4°C, discarding the supernatant. This process was repeated once more before drying the samples at 72°C and resuspending in 2x SDS loading buffer (120 mM Tris-HCl pH 6.8, 1.4M β-mercaptoethanol, 8M urea, 2M thiourea, 4% [w/v] sodium dodecylsulfate, 0.2% [w/v] bromophenol blue). Samples were loaded onto an 4-20% discontinuous SDS polyacrylamide gel and run at 120 V/60 minutes before being stained overnight with colloidal Coomassie G-250. The gel was destained with water and imaged using a ChemiDoc Touch™.

Estimating the RNA polymerase-ribosome dissociation constant.

The apparent binding affinity was estimated from the RNAP and ribosomal subunit titration experiments by nonlinear least-square fitting of the following Delaage's partitioning function:

$$Z=[RNAP] + [30S] + K_1[RNAP]^2 + K_2[RNAP][30S] + \alpha K_1K_2[RNAP]^2[30S] - RNAP_{total} \ln[RNAP] - 30S_{total} \ln[30S]$$

[RNAP] and [30S] are the concentrations of free RNAP and free 30S subunit; $RNAP_{total}$ and $30S_{total}$ represent the total concentrations of RNAP and of 30S subunit; K_1 and K_2 are the association constants for RNAP dimer formation and for RNA polymerase•30S subunit complex formation; and α is the cooperativity factor for the binding of an RNA polymerase dimer to the 30S subunit.

For our estimation of the association constant of 30S subunit for RNA polymerase, K_2, we assumed that: *i*) RNAP dimerizes ($K_d(RNAP_2)$ of 0.2 μM at low salt and of 0.2 mM at high salt conditions (Shaner, Piatt et al., 1982, Kansara, Sukhodolets, 2011)); *ii*) only one RNAP binding site exists on the 30S subunit; and, *iii*) 30S subunit binds RNAP dimers 10x tighter than monomers. All calculations were performed using the "Equilibrium Expert" add-in for Microsoft Excel® (Raguin, Gruaz-Guyon et al., 2002).

Results:

The 30S subunit performs multiple critical functions during translation, either as part of the 70S ribosome or on its own. By itself, the 30S subunit recruits the mRNA and determines with the help of the translation initiation factors and fMet-$tRNA_i$ the translation start site on the mRNA before associating with the 50S subunit to form a 70S ribosome which translates the bound mRNA (Caban, Gonzalez, 2015, Gualerzi, Pon, 2015). In the 70S ribosome, the 30S subunit ensures the proper decoding of the incoming amino acylated tRNA (Ogle, Ramakrishnan, 2005, Rodnina, 2018) and maintains the

reading frame of ribosome along the mRNA (Ratje, Loerke et al., 2010, Rodnina, 2018). The binding of different translation factors to the ribosome and the 30S subunit bestows different conformations onto the 30S subunit. These conformational changes often also affect the RNAP interfaces seen in various cryo-EM structures. Before determining the effects that the mRNA, fMet-tRNA$_i$, and initiation factors exert on the RNAP-30S subunit interaction, we characterized the interactions between RNAP and 30S subunit by itself.

Stoichiometry of the RNAP•30S subunit complex.

When RNAP is titrated with increasing concentrations of 30S subunits, the binding of 30S subunits saturates at a one-to-one ratio of 30S subunits to RNAP (Figure 4.1A, low salt). However, when 30S subunits are titrated with increasing concentrations of RNAP, the binding of RNAP saturates at two molecules of RNAP bound per 30S subunit (Figure 4.1B, low salt). This result is due to the oligomerization of RNAP under low salt conditions, such as the 55 mM KCl concentration used in our experiments (Shaner, Piatt et al., 1982, Kansara, Sukhodolets, 2011). By repeating the titrations under high salt conditions, i.e., 250 mM KCl, the RNAP binding to 30S subunits saturates at a one-to-one ratio (Figure 4.1C, high salt). The similar sedimentation coefficients of RNAP•30S subunit complexes compared to 30S subunits alone suggest that RNAP is bound to only one 30S subunit in each of the observed complexes. Taken together, these results point to a single RNAP binding site on the 30S subunit which can accommodate an RNAP dimer at low salt conditions and a monomer at high salt conditions. A mixture of RNAP monomers and dimers bound to the same binding site on the 30S subunit has

been observed in the cryo-EM work of the 30S•RNAP complex (Demo, Rasouly et al., 2017).

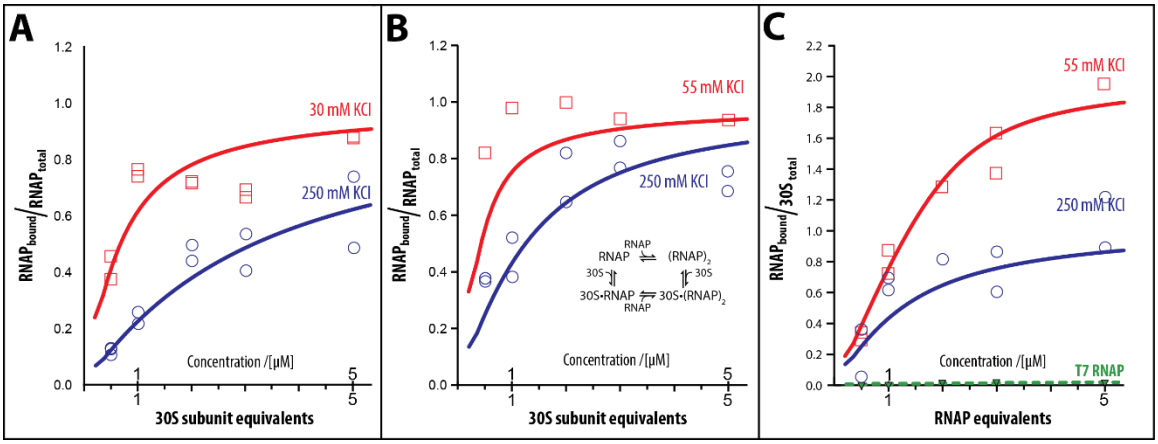

Figure 4.1: RNA polymerase affinity for 30S subunits and its dependence on heat activation of the 30S subunit. **A**) RNAP titrated with increasing concentration of 30S subunits. **B** and **C**) Titration curves of RNAP and heat activated 30S subunits. Inset in B displays the model used to determine the binding affinity of the RNAP for 30S subunit. Also shown in C is a titration of the 30S subunit with RNAP from bacteriophage T7.

Heat-activation of 30S subunit affects the RNAP•30S subunit affinity.

In the process of isolating ribosomal subunits, ribosomes are exposed to high monovalent and low magnesium concentrations. This treatment not only reduces the affinity of the subunits for each other, but also affects their competency to perform critical steps of protein synthesis (Zamir, Miskin et al., 1969). In the case of the 30S subunits, its ability to bind amino acylated tRNA is impaired which is correlated to detectable conformational change of the decoding center of 30S subunit (Zamir, Miskin et al., 1971, Moazed, Van Stolk et al., 1986). These changes are, however, reversible;

returning the subunits back to higher magnesium and reduced monovalent concentrations will allow the subunits to reactivate, a process facilitated by a 15 min incubation at 40°C.

Also, in the case of the binding of the RNAP to the 30S subunit, we see the same trend as reported previously for the binding of tRNAs. 30S subunits isolated without any heat activation show a binding affinity of 3.7 ± 0.5 μM at low salt and 2.7 ± 0.2 μM at high salt conditions that favor the formation for monomeric RNAP to the 30S subunit, while heat-activated 30S subunits show a binding affinity of 1.1 ± 0.3 μM at low salt and 0.75 ± 0.15 μM at high salt (compare Figure 4.1 A with B). In the case of tRNA, this suggests that the affinity of the RNAP is dependent on the conformation of the 30S subunits. All further studies were performed with heat-activated 30S subunits.

The single binding site for RNAP on the 30S subunit suggests that the interactions between polymerase and the ribosomal subunit are specific, potentially dependent on the polymerase functional state or limited to the endogenous RNAP only.

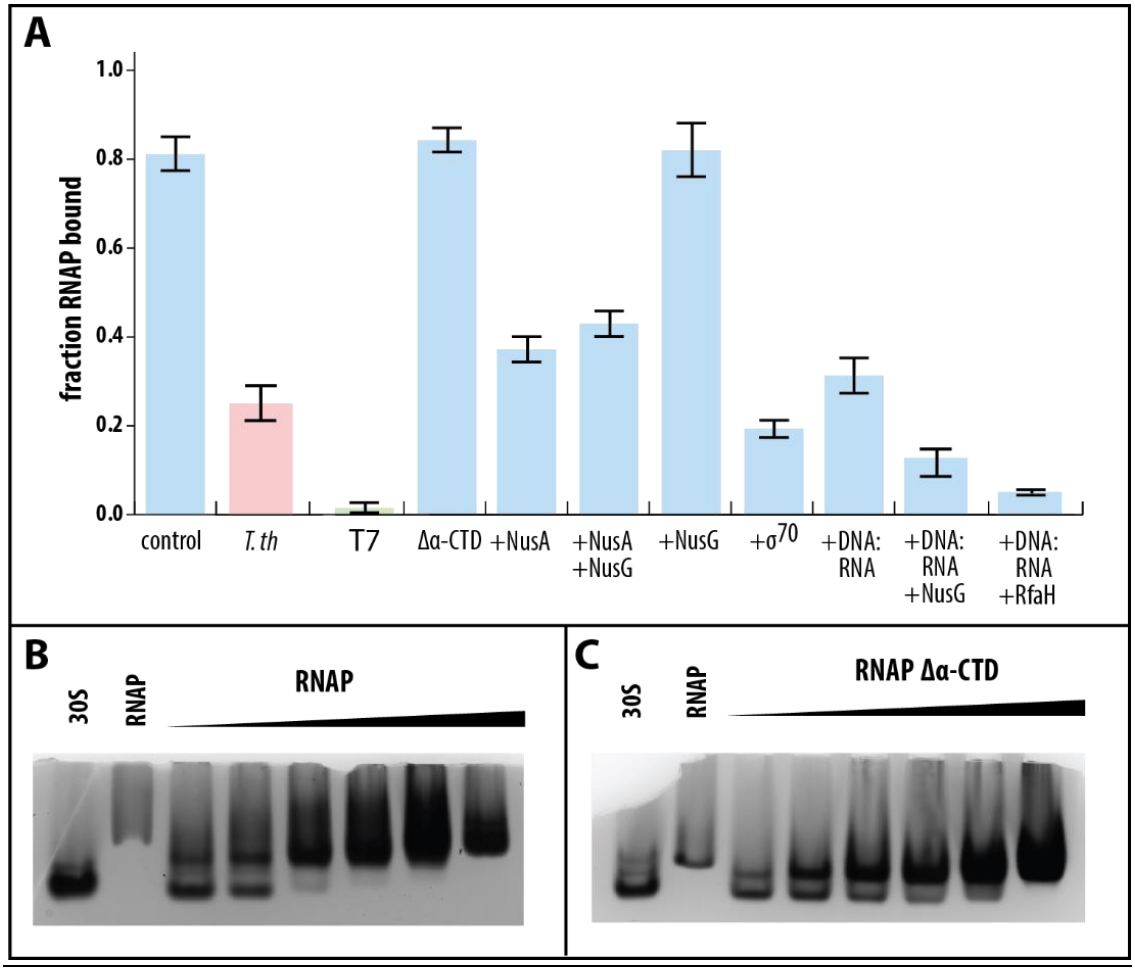

Figure 4.2: Probing the interaction between RNA polymerase and the 30S subunit. **A**) Fraction of RNAP bound to 30S subunits as determined by sucrose gradient centrifugation. All experiments were performed in 20 mM Hepes-KOH pH 7.5, 30 mM KCl, and 20 mM $MgCl_2$ with 2.5 μM 30S subunits and RNAP. DNA:RNA hybrid scaffold, and transcription factors, NusA, NusG, RfaH, and σ-factor and were pre-bound to RNAP before addition of 30S subunits. Histogram labelled with *T. th*, T7, and Δα-CTD indicate the fractional binding of *T. thermophilus* RNA polymerase, T7 bacteriophage RNA polymerase, and *E. coli* RNA polymerase with C-terminal domain of both α subunits deleted to *E. coli* 30S subunits. **B**) and **C**) Displays titration of 30S subunits with increasing concentration of *E. coli* RNA polymerase, B) with full-length α subunit (1.25, 2.5, 5, 7.5, 12.5, 21.6 μM titration) and C) with deleted C-terminal domain (1.25, 2.5, 5, 7.15, 12.5, 30.75 μM titration).

RNAP-30S subunit interaction specific to endogenous RNAP

The specificity of the RNAP binding-site on *E. coli* 30S subunits was determined by comparing its affinity from different sources, i.e., endogenous *E. coli* RNAP versus RNAPs from *Thermus thermophilus* and from T7 bacteriophage (Figure 4.1C and 4.2A). To this end, stoichiometric amounts of 30S subunits and RNAP were incubated at a final concentration of 2.5 μM, before analyzing the complex formation by sucrose gradient centrifugation and determining protein content of each gradient fraction by SDS-PAGE. Our data indicate that *E. coli* 30S subunits prefer *E. coli* RNAP four-times more than *T. thermophilus* RNAP while discriminating against T7 bacteriophage RNAP, suggesting a possible preference of 30S subunits for bacterial over bacteriophage RNAP. This discrimination of 30S subunits against the T7 RNAP concurs with the decoupling of transcription and translation observed in T7 RNAP-driven protein expression (Bhattacharyya, Jacobs et al., 2018).

Probing the 30S subunit interface of RNAP.

In the RNAP•30S subunit complex and in the translational run-on complex of the transcribing, translating RNAP•ribosome, the β flap-tip of the RNAP reaches across the binding interface and is buried within the 30S subunit (Demo, Rasouly et al., 2017, Kohler, Mooney et al., 2017, Conn, Diggs et al., 2019). The same β flap-tip also tightly binds NusA (Ma, Mobli et al., 2015), thus allowing us to probe the 30S subunit interface on the RNAP of the 30S-RNAP complex. The structure of the expressome indicates that the C-terminal domain of one of the two α subunits of the RNAP provides additional

interactions between RNAP and the 30S subunit. To determine the impact of both structural elements of RNAP on 30S subunit affinity, we repeated our binding assays with RNAP with deleted C-terminal domain as well as with full-length polymerase in the presence of excess of transcription factor NusA.

The deletion of the α subunit C-terminal domain has no effect on the RNAP affinity of 30S subunits under our *in vitro* conditions as determined by sucrose gradient centrifugation (Figure 4.2A). However, using native gel electrophoresis, a reduction of the 30S subunit affinity for RNAP with C-terminal deleted α subunit compared to full-length polymerase can be discerned, i.e. the half saturation of 30S subunit increases from 4.5 μM for full-length polymerase to 17 μM for polymerase with C-terminal deleted α subunits (see Figure 4.2B).

NusA not only binds the flap tip, but also abolishes the dimeric form of RNAP. Eliminating the RNAP-dimer formation in our model of RNAP-30S subunit interactions (i.e., K_{ass} ($RNAP_2$) = 0 [l mol^{-1}]) reduces the RNAP binding to 30S subunits from 82 % to 51 %. We experimentally observe a larger drop of RNAP binding to the 30S subunit in the presence of NusA (82% to 37% binding of both complexes, see Figure 4.2A), suggesting that NusA interferes with the binding of 30S subunits as predicted by RNAP•30S subunit complex and the translational run-on complex of the transcribing, translating RNAP•ribosome complex.

NusG and RfaH are implicated in mediating the interaction between RNAP and ribosomes during translation. RfaH is a paralog of NusG and competes with NusG for

binding to RNAP. Whenever the RNAP encounters the *ops*-sequence during transcription, it pauses and recruits RfaH, which in turn recruits the ribosome. RfaH-mediated interactions appear to affect, in addition to elongation, the initiation of translation of the nascent RNA, presumably by tethering the 30S subunits to the RNAP, thus increasing its local concentration at the nascent RNA (Burmann, Schweimer et al., 2010, Burmann, Knauer et al., 2012, Saxena, Myka et al., 2018, Artsimovitch, Knauer, 2019). Therefore, we determined the effects that NusG and RfaH exert on the RNAP binding to 30S subunits.

NusG by itself does not affect the 30S subunit's affinity for RNAP. On the other hand, RfaH decreased the affinity of 30S subunits for RNAP significantly in the presence of the *ops* sequence (Figure 4.2A). In neither the structure of RNAP•30S subunit complex or the run-on RNAP•ribosome complex are the NusG and RfaH binding sites on RNAP and the 30S subunit close enough to allow a single NusG or RfaH molecule to bridge both at the same time.

As NusA interferes with the RNAP flap tip binding to the 30S subunit, other RNAP-ribosome arrangements should become more preferable. Indeed, NusG appears to partially stabilize RNAP-30S subunit complex formation in the presence of NusA (Figure 4.2A), possibly indicating the presence of the recently observed factor-mediated transcription-translation coupling complexes seen for *E. coli* and *Mycoplasma pneumonia* (Wang, Molodtsov et al., 2020, O'Reilly, Xue et al., 2020).

The effect of functional states of RNAP on the complex formation.

The binding of σ^{70} and of DNA:RNA hybrid to RNAP converts the free RNAP into a holoenzyme and a transcription elongation complex, respectively. The holoenzyme enables the RNAP to initiate transcription, while the transcription elongation complex allows the RNAP to elongate the bound RNA. Our data suggest that the formation of the holoenzyme and the transcription elongation complex not only favors the monomeric over dimeric form but also influences the 30S subunit affinity of RNAP (Figure 4.2A).

Effect of the functional states of 30S subunit on the RNAP-30S subunit interaction.

During translation initiation, the 30S subunit recruits an mRNA, fMet-$tRNA_i$, and initiation factors IF1, IF2•GTP, and IF3 to form the 30S initiation complex. The binding of each component induces a different conformation of the 30S subunit (Carter, Clemons et al., 2001, Allen, Zavialov et al., 2005, Simonetti, Marzi et al., 2008, Julian, Milon et al., 2011, Hussain, Llacer et al., 2016). Several of these conformations affect the currently known RNAP binding interfaces on the 30S subunit. To identify the influence translation initiation has on RNAP-ribosome interactions, we determined the effects that different components of translation initiation exert on the 30S subunit's affinity for RNAP.

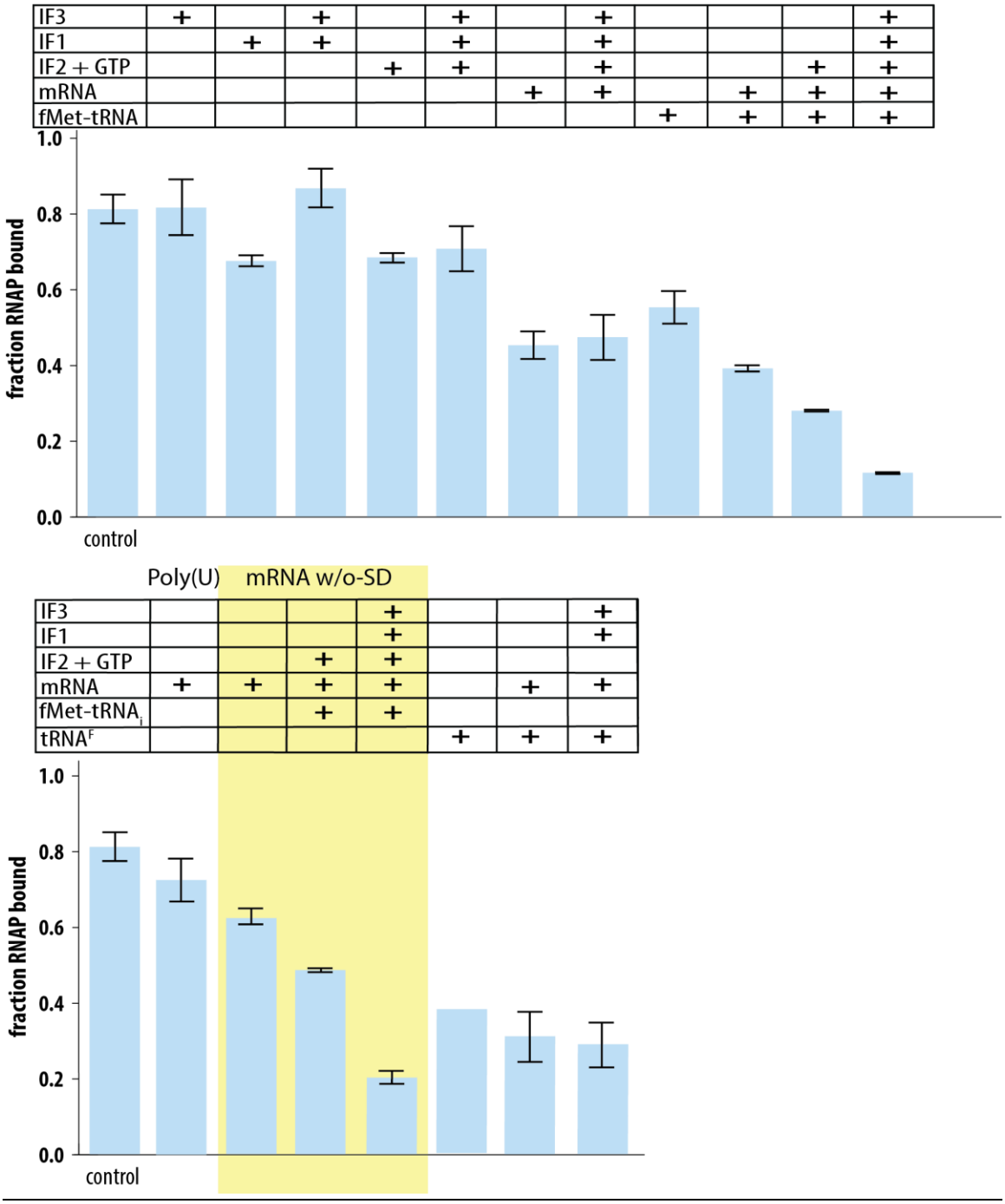

Figure 4.3: The effect of 30S subunit functional states on the RNA polymerase-ribosome interaction. Shown are the fractional binding of RNAP to 30S subunit both at 2.5 μM concentration. Initiation factors, tRNAs, and mRNAs with and without Shine Dalgarno (second row, yellow background) were pre-bound to the 30S subunit before its effect on the RNAP binding was determined by sucrose gradient centrifugation and SDS PAGE analysis.

mRNA recruitment.

Many bacterial mRNAs have upstream of their translation start site a ribosomal binding site, aka a Shine Dalgarno sequence (SD sequence). The SD sequence is complementary to the 3' end of the 30S subunit's ribosomal RNA, aka the anti-Shine Dalgarno sequence (anti-SD sequence). The base pairing between SD and anti-SD sequences recruits the mRNA to the 30S subunit, thereby placing the AUG start codon in proximity to the ribosomal binding site of fMet-tRNA$_i$ (Calogero, Pon et al., 1988). The base pairing of the SD and anti-SD sequence occurs in the mRNA exit site, resulting in an RNA helix that overlaps with β flap-tip binding site of the RNAP•30S subunit complex. The placement of the RNA helix within the mRNA exit site of the 30S subunit brings the helix also in proximity to the ribosomal RNA region that confers much of the conformational flexibility of the 30S subunit (i.e., ribosomal RNA helix 28 (Korostelev, Trakhanov et al., 2006, Korostelev, Trakhanov et al., 2007, Mohan, Donohue et al., 2014)).

Our results show that indeed the formation of the SD:anti-SD double helix interferes with the RNAP-30S subunit interaction, while the recruitment of mRNA by itself affects the RNAP•30S subunit complex formation to a much lesser extent (Figure 4.3A). In the absence of an SD sequence, the mRNA appears to have minimal effect on the RNAP-30S subunit interactions, possibly because of minimal interactions with the 30S subunit. The binding of an mRNA to the 30S subunit alone does not cause the same effect as the SD:anti-SD helix formation as seen by the smaller effects polyuridylic acid exerts on the 30S-RNAP interaction. Polyuridylic acid is recruited to the 30S subunit by

binding to ribosomal protein bS1 without the formation of an SD:anti-SD helix (Yokota, Arai et al., 1977, Komarova, Tchufistova et al., 2005, Studer, Joseph, 2006). This effect of the SD:anti SD interaction discerned here based on sucrose gradient centrifugation has been confirmed by native gel electrophoresis. The concentration of RNAP required to shift half of the 30S subunits under our standard conditions increases from 4.5 μM to 12.5 μM due to the presence of the mRNA with Shine-Dalgarno sequence (Figure 4.4A).

Therefore, the SD:anti-SD interaction appears to diminish the 30S subunit's affinity for RNAP by either preventing the binding of the RNAP β flap tip or by hampering the conformational adjustment of 30S subunit to maximizes the interactions with the RNAP or a combination of both.

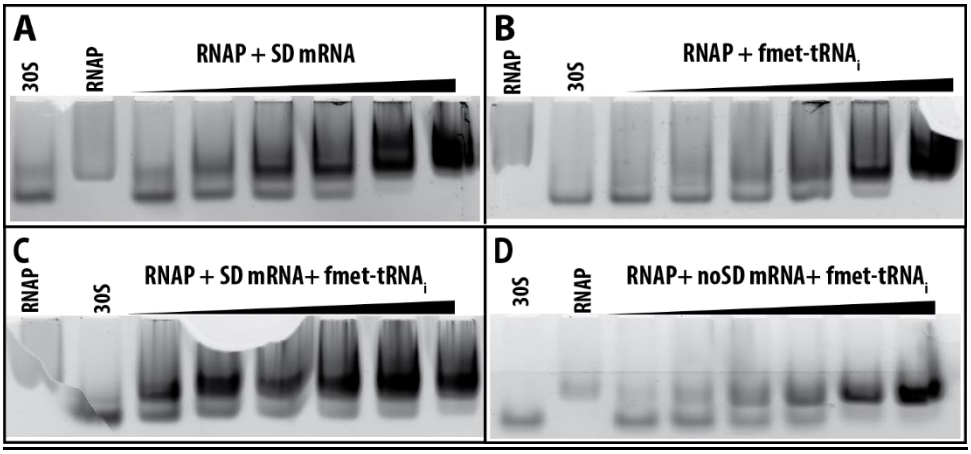

Figure 4.4: The effect of 30S subunit functional states on the RNA polymerase-ribosome interaction as observed by native gel electrophoresis. Representative native gels of RNAP titrations of 30S subunits with bound **A**) mRNA containing a SD sequence (half saturation ~12.5 μM as determined from four replicates), **B)** fMet-tRNAi (half saturation ~10 μM, two replicates), **C)** fMet tRNAi and mRNA containing a SD sequence (half saturation ~ 14 μM, four replicates), and **D)** fMet tRNAi and mRNA without a SD sequence (half saturation ~ 12 μM, two replicates). 2.5 μM 30S subunits are titrated with increasing concentration of RNAP: 1.25, 2.5, 5, 7.5, 12.5, and 21.6 μM.

Initiator tRNA recruitment.

The binding of fMet-tRNA$_i$ to 30S subunits with bound initiation factors and mRNA occurs in at least two steps: an initial fast binding of the tRNA to the 30S subunit is followed by a slow step during which the tRNA rearranges to form anticodon-codon interactions with the bound mRNA (Wintermeyer, Gualerzi, 1983). The slow step may be explained by the conformational change the 30S subunit undergoes from an unlocked to locked 30S initiation complex (Lopez-Alonso, Fabbretti et al., 2017). In the absence of the initiation factors, only a slow binding step of the tRNA is observed (Wintermeyer, Gualerzi, 1983, Antoun, Pavlov et al., 2006). This conformational change of the 30S subunit to 30S initiation complex may affect the 30S subunit's affinity for RNAP.

Here we show that the 30S subunit's affinity for RNAP is already affected by the mere binding of the initiator tRNA which is further decreased by the presence of an mRNA. This reduction of RNAP affinity to the 30S subunit is even more pronounced with mRNAs that contain a SD sequence (Figure 4.3A/B). Our native gel analysis of the RNAP•30S subunit complex formation confirms the same synergistic effect seen by sucrose gradient centrifugation, i.e., the half-saturation for the binding of RNAP to 30S subunits shift from 4.5 μM to 10 μM due to fMet-tRNA$_i$ and even further increases to 12 μM in the presence of mRNA and to 14 μM with mRNAs with Shine Dalgarno sequence (Figure 4.4B, C, and D).

In the absence of initiation factors, elongator tRNAs can efficiently compete with fMet-tRNA$_i$ for binding to an mRNA-bound 30S subunit by forming a codon-anticodon

interactions with a non-start codon that is proximal to the start codon (Hartz, McPheeters et al., 1989). The binding of $tRNA^F$ to the mRNA bound 30S subunit similarly affects the 30S subunit's affinity for RNAP as does fMet-$tRNA_i$ (Figure 4.3) This suggests that the binding of $tRNA^F$ to the UUC immediately downstream of the AUG start codon induces similar conformational changes on the 30S subunit that the fMet-$tRNA_i$ binding to AUG does.

The here observed difference in the RNAP•30S subunit binding affinity in the presence of initiator tRNA by itself and in the presence of an mRNA hints at a two-step recruitment of the initiator tRNA to the RNAP-bound 30S subunit comparable to that of the free 30S subunit.

IF2•GTP binding.

IF2•GTP makes extensive contacts with both the 30S subunit and fMet-$tRNA_i$ (Simonetti, Marzi et al., 2008) and increases the binding affinity of fMet-$tRNA_i$ to the 30S subunit (Antoun, Pavlov et al., 2006). Also, IF2•GTP appears to stabilize the fMet-$tRNA_i$ binding to an mRNA-bound 30S subunit in the presence of RNAP, reflected in synergistic reduction of the 30S subunit's affinity for RNAP. The presence of a SD sequence is required for IF2•GTP to affect the 30S subunit's RNAP affinity in the presence of fMet-$tRNA_i$. The small effect IF2•GTP has in the presence of an mRNA without SD sequence may be rooted in the 30S subunit's ineptness in recruiting short mRNAs without SD sequence, thereby preventing the base pairing between the initiator tRNA and the mRNA to occur that IF2•GTP stabilizes (Figure 4.3).

IF1 and IF3 recruitment.

IF3 antagonizes the association of ribosomal subunits to 70S ribosomes by itself and more so in cooperation with IF1. IF1 on its own has only a limited effect on ribosome association (Grunberg-Manago, Dessen et al., 1975, Antoun, Pavlov et al., 2004). To test if these anti-association effect extends to the RNAP•30S subunit interaction, we determined the 30S subunit's affinity for RNAP in the presence of IF3 alone and with stoichiometric amounts of IF1. IF3 by itself or with IF1 have no effect on the 30S subunit's affinity for RNAP (Figure 4.2B), even when the concentration of IF3 and IF1 exceed their individual and cooperative dissociation constants for the 30S subunit by more than tenfold (Weiel, Hershey, 1981, Zucker, Hershey, 1986) (Figure 4.4).

Cooperative effect of translation initiation factors on the 30S subunit's binding affinity for RNAP.

Although the presence of all three initiation factors mostly affect the kinetics of initiation complex formation on mature mRNA (Antoun, Pavlov et al., 2006), it appears that the presence of all initiation factors also affect the apparent affinity of the 30S subunit for RNAP, resulting in less RNAP•30S subunit complex formation than seen in their absence. Interestingly, the absence of the SD sequence on the mRNA is partially overcome by the addition of IF1 and IF3, resulting in the reduction of the 30S subunit's affinity for RNAP to a similar level than for mRNAs with an SD sequence (Figure 4.3).

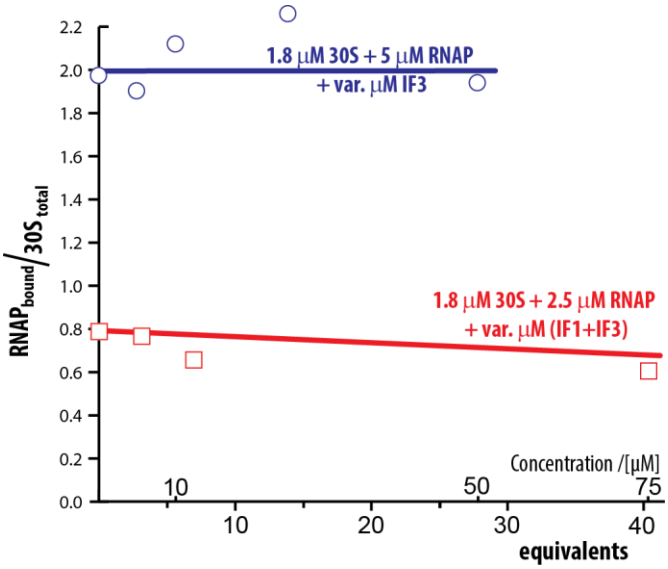

Figure 4.5: Effect of initiation factors IF1 and IF3 on the RNAP-30S subunit affinity. Increasing amount of IF3 by itself (blue line) or in combination with IF1 (red line) have no effect on the 30S subunit's affinity for RNAP. It should be noted that variations in bound RNAP-30S stoichiometry of complex formation is due to the concentration dependent dimerization of RNAP under low salt conditions (see text above and Fan, Conn 2017).

Presence of RNAP does not affect the association of 30S subunit and 50S subunit.

In one of the last steps of translation initiation, the 50S subunit associates with the 30S subunit initiation complex. In order to determine the effect of RNAP on this step of translation initiation, we investigated reassociation of 30S and 50S subunits into 70S ribosomes in the presence of RNAP via sucrose gradient centrifugation. Neither presence, nor pre-forming of the RNAP•30S subunit complex affected the reassociation. As expected, the presence of the RNAP also did not affect the 50S subunit association to the 30S subunit initiation complex (Figure 4.6).

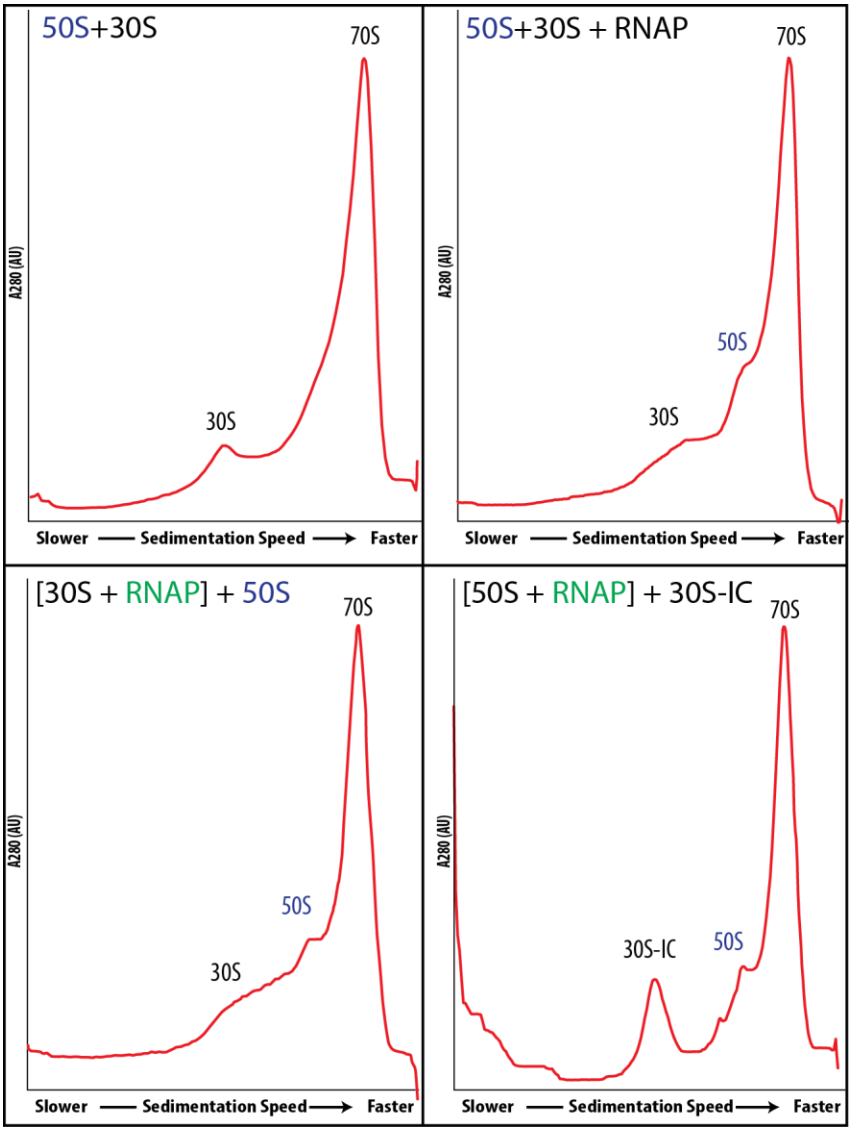

Figure 4.6: The effect of RNAP on reassociation of 30S and 50S subunit. **A)** Reassociation of 30S and 50S subunit by themselves, **B)** in the presence of RNAP, **C)** with 30S subunits pre-incubated with RNAP, and **D)** with 30S subunit initiation complex (30S-IC) and 50S subunit in the presence of RNAP.

Discussion:

Early EM studies demonstrated that ribosomes start translation of mRNA while they are being transcribed. In several EM images of these studies, the first ribosome trailing the RNAP appears to even contact the RNA polymerase (Miller, Hamkalo et al., 1970, Klaholz, 2017). Since then, additional evidence for direct interactions between RNAP and ribosomes has accumulated, such as RNAP co-purifying with ribosomes from cell lysate (Jiang, Sullivan et al., 2007), chemical crosslinking of RNAP and ribosome *in situ* (Tsai, Du et al., 2012), or visualization of direct contacts between polymerase and ribosomes within the cells by cryo Electron Tomography (O'Reilly, Xue et al., 2020). However, only recent structural and biochemical work directly demonstrated a physical interaction between RNAP and ribosomes (Demo, Rasouly et al., 2017, Fan, Conn et al., 2017, Kohler, Mooney et al., 2017, Wang, Molodtsov et al., 2020, Webster, Takacs et al., 2020). Considering the known genetic interaction between RNAP and the 30S subunit (Chakrabarti, Gorini, 1977), such direct interactions appear to play more than just a mere structural role, but perhaps a functional role as well.

The structures of RNAP bound to the ribosome and the 30S subunit identified three distinct locations the polymerase contacts on the ribosomal subunit: the mRNA entry site, the mRNA exit site, and the region between both mRNA sites (Demo, Rasouly et al., 2017, Kohler, Mooney et al., 2017, Wang, Molodtsov et al., 2020, Webster, Takacs et al., 2020). Contacts between the RNAP and the 30S subunit at the entry and between the entry and exit site are seen in the structures of the different transcribing, translating RNAP-ribosome complexes. Despite these different contact points, the nascent RNA

extruded from the polymerase is always fed to the ribosome through the mRNA entry site. This allows the ribosome to immediately translate the newly synthesized RNA and maintain close distance to the polymerase. These structures also show that only short regions of nascent RNA between the RNAP and ribosome are not in contact with either, rationalizing how transcription-translation coupling prevents RNAP pausing, backtracking, and rho-dependent transcription termination and thus synchronizes the rate of transcription and translation *in vivo* (Proshkin, Rahmouni et al., 2010, Elgamal, Artsimovitch et al., 2016, Eriksen, Sneppen et al., 2017, Stevenson-Jones, Woodgate et al., 2020).

Only in the structure of the RNAP•30S subunit does the polymerase contact the 30S subunit at the mRNA exit site. Here the polymerase faces with its mRNA exit site towards the mRNA exit site of the 30S subunit. This suggests that nascent RNA extruded from the polymerase would enter the ribosome where mRNAs exit the ribosome during protein translation. This seemingly counterintuitive RNAP binding site is however the location where structured mRNAs are initially recruited to and is also in close proximity to the binding site of mRNA's Shine Dalgarno sequence (SD sequence) (Marzi, Myasnikov et al., 2007). For structured mRNAs with a buried SD sequence, this binding site allows the 30S subunit's anti-SD sequence to capture the mRNAs' SD sequence during the short periods of exposure that are purely driven by Brownian motion. Once the SD region is captured, the mRNA is accommodated into the mRNA channel on the 30S subunit (de Smit, van Duin, 2003A, Studer, Joseph, 2006). This accommodation places

the 3′ end of the mRNAs into the mRNA entry site on the 30S subunit (Marzi, Myasnikov et al., 2007).

The fate of the nascent RNA during translation initiation may parallel that of structured mRNAs. As for many structured RNAs, the SD region of the nascent RNA is buried, not in a secondary structure, but in the polymerase (Larson, Mooney et al., 2014). Therefore, the binding of the polymerase to the exit site may enable the ribosomal anti-SD sequence to engage with the buried SD sequence of the nascent RNA. The nascent RNA exit channel can accommodate double-stranded RNA (Kang, Mishanina et al., 2018), and therefore the SD:anti-SD base pairing in- or out-side the polymerase may allow the polymerase to overcome its pausing over translation start sites (Larson, Mooney et al., 2014). The widened mRNA exit site of the 30S subunit appears to provide unrestricted access of the nascent RNA to the anti-SD sequence of the 30S subunit (Demo, Rasouly et al., 2017). The enlargement of the mRNA exit site is wider than seen in any other translation initiation complex (Simonetti, Marzi et al., 2009, Julian, Milon et al., 2011, Hussain, Llacer et al., 2016). Our data suggest that the formation of the SD:anti-SD double helix on the 30S subunit not only tethers the RNAP and ribosome, but also weakens the interaction of the RNAP with the mRNA exit site of the 30S subunit. The SD:anti-SD duplex forms in the neck region of the 30S subunit, which forms the hinge between the head and the body of the 30S subunit (Korostelev, Trakhanov et al., 2007), thus influencing the flexibility of the 30S subunit to accommodate the binding of RNAP. In addition, the SD:anti-SD base pairing establishes also the directionality of the nascent RNA's accommodation into the 30S subunit, i.e., toward the mRNA entry site.

As the nascent RNA extends, the more it resembles a mature mRNA and will be more efficiently accommodated by the 30S subunit. Our data further suggests that with the recruitment of the initiation components, the affinity of the polymerase for the mRNA exit site further decreases, thus enabling the repositioning of the 3′ end of the nascent RNA and with it that of the RNAP (see Figure 4.7). Our observation that RfaH reduces the affinity of RNAP for the mRNA exit site correlates well with the fact that RfaH enable the translation of genes that lack SD sequences in their 5′ untranslated region (Burmann, Knauer et al., 2012).

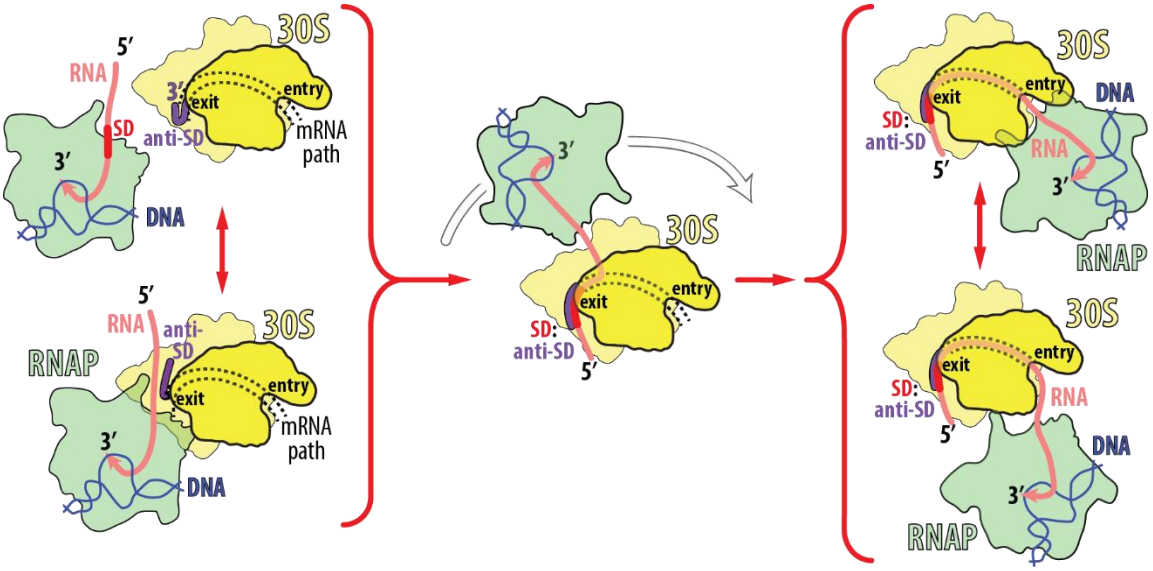

Figure 4.7: Model for translation initiation of nascent RNA. RNA polymerase (RNAP, green) is recruited to the 30S subunit (yellow) at its mRNA exit site. After the SD:anti-SD interaction has established (red and purple regions on the mRNA and 30S subunit, respectively), the initial interactions between RNAP and the 30S subunit are weakened sufficiently enough to allow the nascent RNA to be accommodated in the mRNA path of the 30S subunit (middle panel). With the accommodation of the nascent RNA, the RNAP transitions from the mRNA exit to mRNA entry site of the 30S subunit (right panels). The models of RNAP recruited to the 30S subunit (left panels) are based on the cryo-EM structure of RNAP•30S subunit complex (Demo, Rasouly et al., 2017) and the models of RNAP•30S subunit with accommodated nascent RNA (right panels) are based on the structures of transcribing, translating RNAP•ribosome complexes ((Kohler, Mooney et al., 2017) top right panel and (Wang, Molodtsov et al., 2020, Webster, Takacs et al., 2020) bottom right panel).

Chapter 5:

E. coli Large Ribosomal Subunit Interactions to RNAP

Unpublished work.

Introduction:

Although biochemical results indicate that RNAP interacts not only with the small but also with large ribosomal subunits (30S and 50S subunit) (Fan, Conn et al., 2017), only interactions between RNAP and the 30S subunit have been visualized by electron microscopy or have been further considered up to now (Demo, Rasouly et al., 2017, Fan, Conn et al., 2017, Kohler, Mooney et al., 2017, Wang, Molodtsov et al., 2020, Webster, Takacs et al., 2020). To uncover the functional significance of the reported RNAP-50S subunit interaction, we have decided to study this interaction in more detail.

Materials and Methods:

The materials and methods used in this chapter are well established in the Blaha laboratory and have been described in this thesis in 'Chapter 4: *E. coli* Small Ribosomal Subunit Interactions to RNAP' in detail (see pages 105-113), with minor changes. These changes include the collection of 50S instead of 30S subunits during the preparation of the ribosomal material and the use of 50S instead of 30S subunits in all experiments designed to determine the ribosome affinity to RNAP.

Results:

The 50S subunit houses the site of the peptidyl transferase reaction, the central enzymatic activity of protein synthesis. A coordination of this activity with RNA polymerase activity, either through regulating the abundance of either sites within the cell or by directly influencing each other's activity during transcription and translation are both enticing concepts worth exploring. To do so, we analyzed the thermodynamic

interactions between RNAP and the 50S subunit in the presence and absence of factors that regulate the activity of either. Before doing so, we had to establish a base line by determining the affinity and stoichiometry of the interaction between the 50S subunit and RNAP.

Binding affinity and stoichiometry of the RNAP•50S subunit complex.

The binding of 50S subunits to RNAP saturates at a one-to-one stoichiometry, while the binding of RNAP to the 50S subunit saturates at a two-to-one stoichiometry of RNAP to 50S subunits at low salt and at a one-to-one stoichiometry at high salt conditions (Figure 5.1A and 5.1B). The similarity of the sedimentation coefficients of the RNAP complexes and of the 50S subunits suggests the presence of a single 50S subunit in each of the observed complexes. Similar to the 30S subunit, the 50S subunit has one RNAP-binding site that can accommodate one RNAP dimer at low salt conditions and one RNAP monomer at high salt conditions. Using a model with a single RNAP binding site on the 50S subunit and accounting for the dimerization of the RNAP, we estimate an RNAP•50S subunit dissociation constant of 2.02 ± 0.67 μM and 1.12 ± 0.18 μM at 30 mM and 250 mM KCl, respectively.

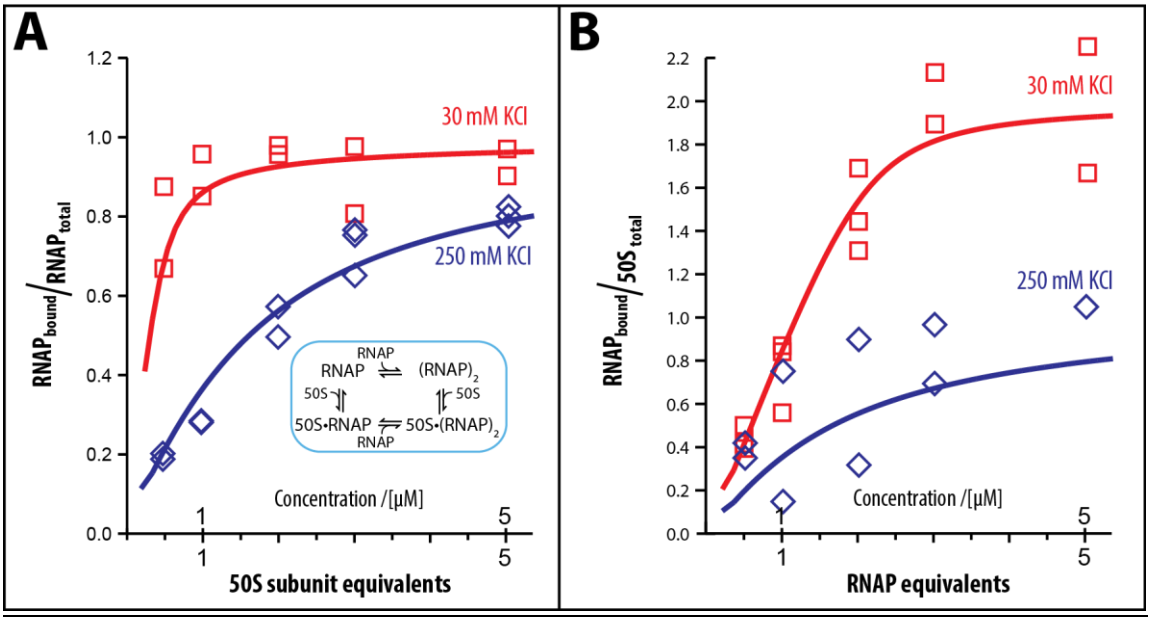

Figure 5.1: Titration curves of RNAP and 50S subunits. **A**) RNAP is titrated with increasing concentration of the 50S subunits and **B**) 50S subunits are titrated with increasing concentration of RNAP under low and high salt conditions.

Activation of the 50S subunit has not affect RNAP•50S subunit complex formation.

Although the ionic conditions for isolating subunits significantly impairs the 30S subunit's function, only local conformations of some regions of the 50S subunit appear to be affected, such as that of the peptidyl transferase center (Zamir, Miskin et al., 1974, Bayfield, Dahlberg et al., 2001). The conformation of the peptidyl transfer center can be converted to that of 70S ribosomes by heat activation. In addition the peptidyl transfer center can be enticed to perform a peptidyl transferase reactions with minimal substrates in the presence of aliphatic alcohols, such as methanol (Monro, Staehelin et al., 1969, Zamir, Miskin et al., 1974, Bayfield, Dahlberg et al., 2001). However, neither heat activation nor the presence of methanol affects the binding affinity of 50S subunits for RNAP (Figure 5.2).

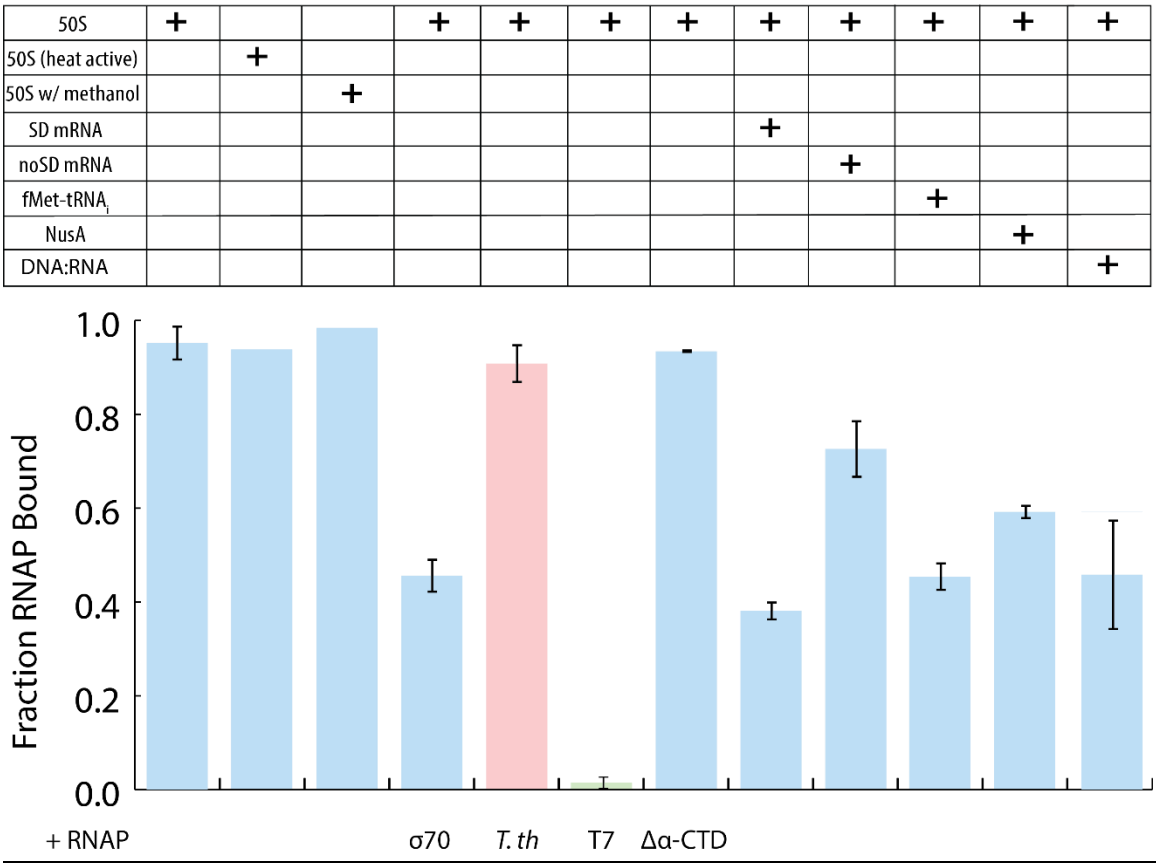

Figure 5.2: Probing the 50S binding interface on the RNAP. Shown are the fractional binding of RNAP to 50S subunit (both at 2.5 μM concentration) as determined by sucrose gradient centrifugation and following SDS-PAGE analysis.

Probing the RNAP-50S subunit interface.

The single RNAP-binding site on the 50S subunit suggests a specific interaction between RNAP and the 50S subunit. Therefore, we probed the specificity of the RNAP-site on the 50S subunit with RNAPs from different sources, with transcription factors, and with different functional states of the RNAP.

Our data indicates that the *E. coli* 50S subunits have similar preference for *E. coli* and *Thermus thermophilus* RNAPs but discriminate against T7 bacteriophage RNAP, thus displaying the same preferences as the 30S subunit (compare Figure 5.2 with Figure 4.2 of Chapter 4). The presence of NusA reduces the amount of RNAP engaged in a complex with the 50S subunit by less than half. Similar to NusA, the binding of σ^{70} to RNAP appears to mainly reduce the amount of RNAP dimers bound rather than interfering with the RNAP-50S subunit complex formation. However, the binding of the DNA:RNA hybrid weakens the interaction between RNAP and 50S subunits significantly, suggesting that the functional states of the RNAP affect the RNAP's affinity for 50S subunits differently than for 30S subunits (compare Figure 5.2 with Figure 4.2 of previous chapter). These variances hint at different binding interfaces on the RNAP for binding to the 50S and the 30S subunits.

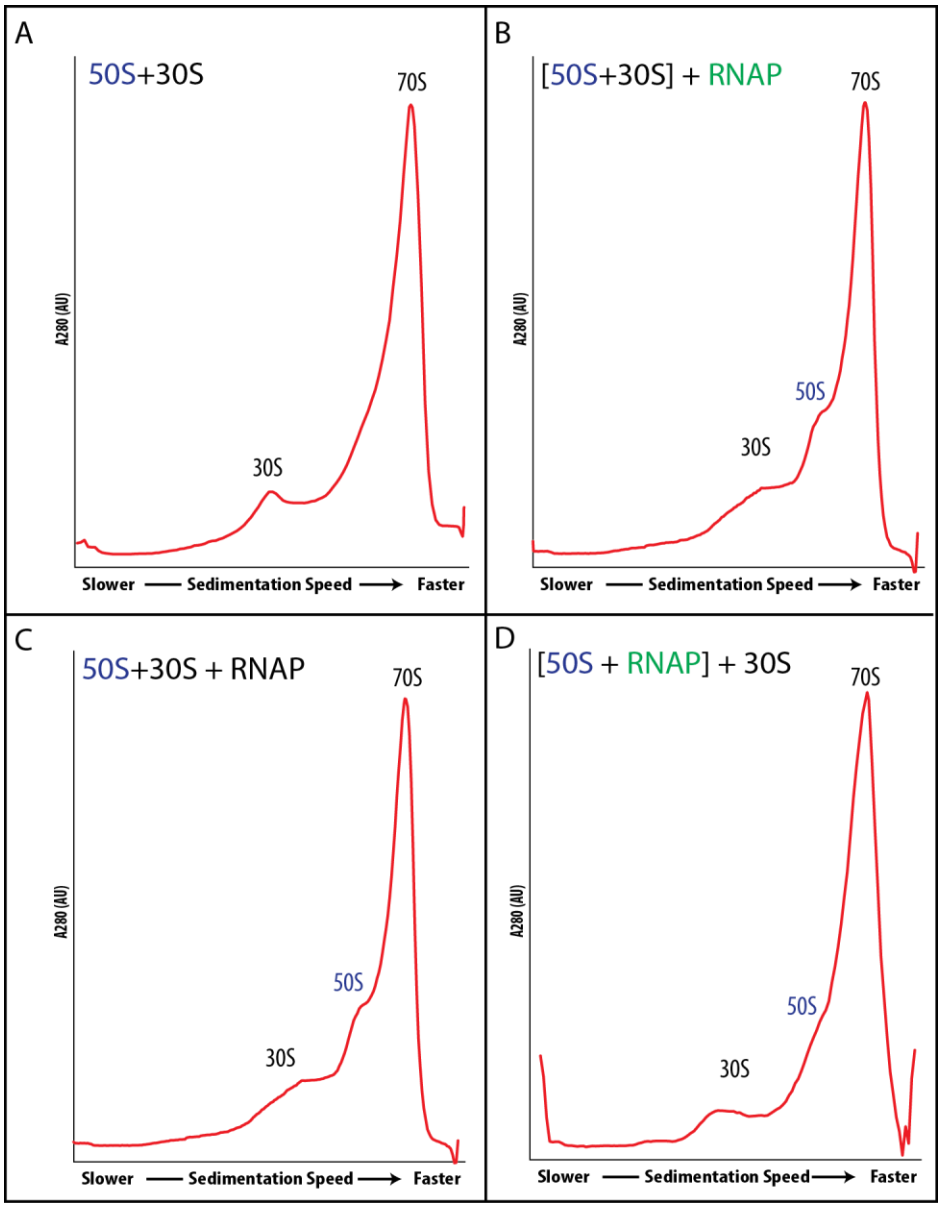

Figure 5.3: Reassociation of 50S subunits with 30S subunits. Panels **A**, **B**, and **C** are the same as in Figure 4.6 of the previous chapter. **D)** Preincubation of the 50S subunits with RNAP does not affect the 50S subunit reassociation with 30S subunit.

As RNAP binding to the 30S subunit induces a conformational change on the 30S subunit (Demo, Rasouly et al., 2017), similar conformational changes may occur upon RNAP binding to the 50S subunit, potentially affecting the 50S subunit's capability to associate with 30S subunits. The presence of excess RNAP neither dissociates ribosomes nor prevents the association of subunits to ribosomes (Figure 5.3).

Discussion:

Our current analysis of the interaction between RNAP and the 50S subunit suggests that the interaction seems not to contribute to translation or transcription, thus is less likely to play a role in transcription-translation coupling. The interwoven structure of the ribosomal RNA (Ban, Nissen et al., 2000), the existence of multiple assembly intermediates *in vivo* (Chen, Williamson, 2012), and the coordination transcription of the ribosomal RNA with their maturation (Lewicki, Margus et al., 1993) suggest a sophisticated mechanism for the assembly of the 50S subunit. We hypothesize that our here studied interaction between RNAP and 50S subunit may play a more significant role in the biogenesis of the 50S subunit than in the coupling of transcription and translation.

Chapter 6:

Modeling Factor-free and Factor-mediated Coupling of Transcription and Translation.

Publication:

Conn, A.B., Diggs, S., Tam, T.K., Blaha, G.M. (2019**)** "Two Old Dogs, One New Trick: A Review of RNA Polymerase and Ribosome Interactions during Transcription-Translation Coupling." Int. J. Mol. Sci., ***20*** 2595.

[PMID: 31137816]

Abstract:

The coupling of transcription and translation is more than mere translation of an mRNA that is still being transcribed. The discovery of physical interactions between RNA polymerase and ribosomes has spurred renewed interest into this long-standing paradigm of bacterial molecular biology. Here we provide a concise presentation of recent insights gained from super-resolution microscopy, biochemical, and structural work, including cryo-EM studies. Based on the presented data, we put forward a dynamic model for the interaction between RNA polymerase and ribosomes in which the interactions are repeatedly formed and broken. Furthermore, we propose that long intervening nascent RNA will loop out and away during the forming the interactions between RNAP and ribosomes. By comparing the effect of the direct interactions between RNA polymerase and ribosomes with those that transcription factors NusG and RfaH mediate, we submit that two distinct modes of coupling exist: factor-free and factor-mediated coupling. Finally, we provide a possible framework for transcription-translation coupling and elude to some open questions in the field.

Introduction:

In bacterial cells, the lack of a physical barrier allows transcription and translation machineries to mingle, thus enabling concurrent translation of an mRNA while it is being transcribed in a process known as transcription-translation coupling (French, Santangelo et al. 2007, McGary and Nudler 2013). Due to this coupling, ribosomes translating the nascent RNA trail the transcribing RNA polymerase (RNAP) (Das, Goldstein et al. 1967), bringing both physically close to each other (Miller, Hamkalo et al. 1970, Klaholz 2017). This proximity of transcribing RNAP and the first translating ribosome rationalizes long-standing observations, such as transcription polarity and transcription attenuation.

In transcription polarity, a premature stop codon curtails not only the expression of the mutated gene, but also that of all genes on the same polycistronic operon downstream of the mutation. The premature translation termination causes the ribosome to dissociate from the nascent mRNA, allowing transcription termination factor Rho to proceed along the nascent RNA all the way to the RNAP. At the RNAP, the Rho factor induces transcription termination, halting transcription of the downstream genes on the operon (Richardson, Grimley et al. 1975, Adhya, Gottesman et al. 1976, Adhya and Gottesman 1978) (Figure 6.1A). Premature transcription termination can occur by simply reducing the rate of translation. The slower speed of the first trailing ribosome will increase the length of the intervening nascent RNA between the ribosome and RNAP. This longer RNA gap between RNAP and leading ribosome allows the Rho factor to bind to the nascent RNA ahead of the ribosome in direct line to the RNAP (de Smit, Verlaan et

al. 2008). The longer intervening RNA also provides sufficient room for intrinsic terminator signals to fold and cause the termination of transcription (Elgamal, Artsimovitch et al. 2016). (Figure 6.1B).

The intrinsic transcription termination signal consists of a stable hairpin stem loop followed by a uridine-rich sequence (Ray-Soni, Bellecourt et al. 2016).

Programmed decoupling of transcription and translation is also exploited for gene regulation, *i.e.*, transcription attenuation. The most well-known example of transcription attenuation involves the cellular concentration of tryptophan regulating the expression of the *trp* operon. Starvation for tryptophan induces stalling of the first ribosome translating the leader sequence of the operon. The stalled ribosome prevents the formation of a transcription termination signal on the nascent RNA, allowing the RNAP to continue to transcribe downstream genes on the *trp* operon (Yanofsky and Ito 1966, Landick, Carey et al. 1985). In other instances of transcription attenuation, the stalled ribosome leads to transcription termination, thereby halting the expression of downstream genes (Turnbough, Hicks et al. 1983, Landick, Turnbough et al. 1996, Yanofsky 1999).

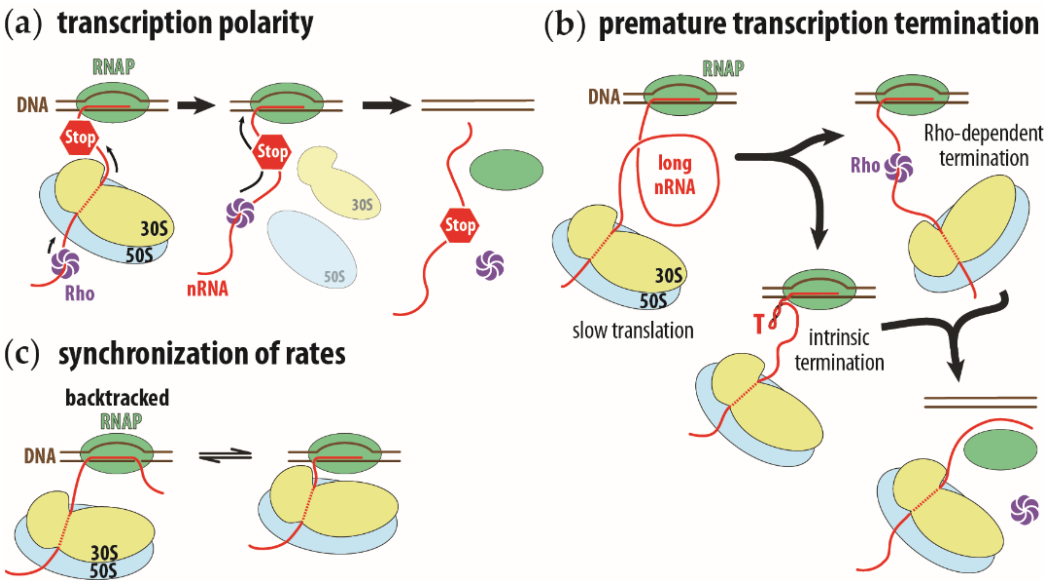

Figure 6.1. Schematic representation of transcription polarity, premature transcription termination on long intervening nascent RNA, and synchronization of transcription and translation rates. (**a**) Transcription polarity is caused by a premature stop codon (STOP sign) on the nascent RNA (nRNA, in red). Translation of the nascent RNA will terminate and the ribosome (in yellow and blue, for small and large ribosomal subunits, respectively) will prematurely dissociate from the nascent RNA. This allows Rho transcription termination factor (in purple) to reach RNAP (in green) and induce premature transcription termination. (**b**) A long intervening nascent RNA allows the Rho factor to bind ahead of the ribosome or allow the intrinsic transcription terminator to fold (hairpin structure indicated with a red capital T). In both instances, transcription terminates. (**c**) Synchronization of transcription rate to translation rate. The running ahead of the RNAP will cause the polymerase to pause and backtrack (complex on the left). The translating ribosome will push the RNAP forward and reactivate its transcription activity (complex on the right). This running ahead and pausing to wait for the ribosome synchronizes the transcription rate to the translation rate.

The proximity between the transcribing RNAP and its trailing ribosome is maintained under different growth conditions (Vogel and Jensen 1994, Iyer, Le et al. 2018). A slowing of translation induced by either an antibiotic or a mutation results in a corresponding slowing of transcription (Proshkin, Rahmouni et al. 2010). This slowing of translation allows the RNAP to run ahead of the ribosome, where it is more likely to stall and backtrack. While backtracking, the RNAP slides backwards on the nascent RNA and DNA template strand, rezipping the upstream nascent RNA and template DNA while extruding the 3' end out of the NTP entry site. A ribosome trailing closely behind the RNAP will prevent the polymerase from sliding backwards, biasing the polymerase towards the forward direction, extending the nascent RNA (Proshkin, Rahmouni et al. 2010). This interplay between the RNAP running ahead and stalling and being reactivated by a trailing ribosome, results in the matching of RNAP's speed to that of the ribosome, *i.e.*, the rate of transcription is synchronized to the rate of translation (Figure 6.1C). Therefore, inhibiting translation leads to a genome-wide stalling of transcription (Zhang, Mooney et al. 2014). The stalled RNAP acts as a barrier for the DNA replication machinery, jeopardizing the processivity of replication and with it, the integrity of the genome (Mirkin and Mirkin 2007, Dutta, Shatalin et al. 2011).

Increasing the transcription rate by blocking backtracking occurs also on non-protein encoding genes. Rather than a trailing ribosome, a trailing RNAP suppresses stalling and backtracking of the leading RNAP. The trailing polymerase biasing the leading polymerase towards the forward direction explains the higher overall transcription rate of highly transcribed non-coding operons, such as the rRNA operons

(*i.e.*, 85 nts/sec for rRNA vs. 40-55 nts/sec for mRNA) (Epshtein and Nudler 2003, Bremer and Dennis 2008, Klumpp and Hwa 2009).

Do transcription and translation occur in the same cellular compartment?

Although transcription and translation are assumed to occur in the same compartment, this assumption has been recently challenged. In *E. coli*, the genome is segregated from the cytoplasm, forming a dense, compact structure in the center of the cell, known as the nucleoid. The nucleoid sequesters nearly all of the cellular RNAPs (Shepherd, Dennis et al. 2001, Bakshi, Siryaporn et al. 2012) while expelling most of the ribosomes, forcing them to accumulate on the periphery of the nucleoid, particularly at the poles of the cell (Hobot, Villiger et al. 1985, Cabrera and Jin 2003, Bakshi, Siryaporn et al. 2012). This spatial separation of RNAPs and ribosomes suggests that most of transcription and translation occur apart from each other (Bakshi, Choi et al. 2015).

Tracking of individual ribosomal subunits reveals that most of the translating ribosomes are excluded from the nucleoid, while free ribosomal subunits can enter the nucleoid almost as unhindered as tRNAs and translation factors (Sanamrad, Persson et al. 2014, Bakshi, Choi et al. 2015, Stracy, Lesterlin et al. 2015, Plochowietz, Farrell et al. 2017, Mustafi and Weisshaar 2018). Similarly, tracking of individual RNAP molecules indicates that free RNAPs can move unhindered within the nucleoid at a rate comparable to that of in solution (Stracy, Lesterlin et al. 2015). This unhindered diffusion of the RNAP suggests that RNAP is, in addition to sliding along individual DNA strands, crossing between DNA strands in its search for a transcription start site (von Hippel and Berg 1989). Once a polymerase has found a transcription start site, it initiates and

transcribes approximately 100-150 nucleotides before pausing, *i.e.*, promoter proximal pausing (Mooney, Davis et al. 2009). The polymerase pausing presumably enables one or several ribosomes to initiate translation on the nascent RNA and catch up to the polymerase, thus establishing the coupling of transcription and translation.

Under fast growing conditions, the transcribing RNAPs cluster on the periphery of the nucleoid, while under slow growing conditions they remain distributed throughout the nucleoid (Cabrera and Jin 2003, Stracy, Lesterlin et al. 2015). In a nutrient-rich condition, *E. coli* requires fewer genes to satisfy its metabolic needs, therefore allowing it to redirect its resources towards expressing the genes required for fast growth. This results in the aggregation of RNAPs and ribosomes on these few, highly expressed genes. Possibly driven to increase the nucleoid's conformational flexibility (*i.e.*, entropy) (Mondal, Bratton et al. 2011), these highly expressed genes move to the periphery of the nucleoid where they cluster (Figure 6.2) (Cabrera and Jin 2003, Spahn, Cella-Zannacchi et al. 2015, Stracy, Lesterlin et al. 2015). This suggests that under fast growing conditions all genes are transcribed at the interface between the nucleoid and ribosome-rich cytoplasm, which further implies that all genes that can support coupling, will have transcription and translation coupled.

Under slow growing conditions, RNAP remains evenly distributed in the nucleoid (Cabrera and Jin 2003, Stracy, Lesterlin et al. 2015). Based on the observation that an mRNA undergoes on average 30-60 rounds of translation before it is degraded and only the first round is coupled to transcription (Bremer and Dennis 2008, Mitarai, Sneppen et al. 2008), we estimate that no more than 4 % of ribosomes participate in transcription-

translation coupling. 10-15 % of ribosomes are present as free ribosomal subunits, which can enter the nucleoid nearly unhindered (Sanamrad, Persson et al. 2014). As the nucleoid occupies nearly half the volume of the cell, it implies that at least 5 % of ribosomes are available in the nucleoid. This suggests that even under slow growing conditions transcription and translation are coupled. Note that we are implicitly assuming that all protein-encoding genes require or support transcription-translation coupling – an assumption that has not yet been tested.

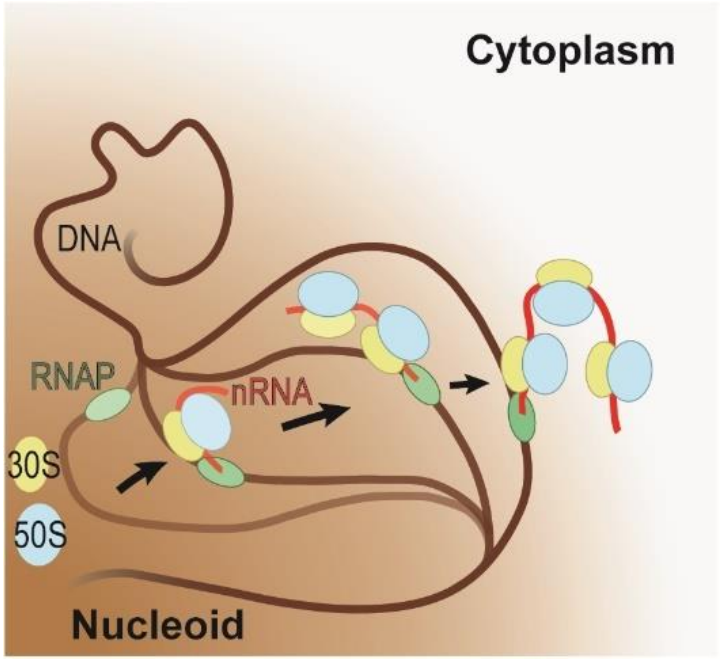

Figure 6.2. Schematic representation of the coupling of transcription and translation on highly expressed genes under fast growing conditions. RNA polymerase (RNAP, in green) initiates transcription on the DNA (in brown) within the nucleoid (brown shaded area). As soon as the polymerase has transcribed a sufficiently long nascent RNA (in red), translation will ensue (large and small ribosomal subunits in blue and yellow, respectively). During coupling the active gene is relocalized to the interface of the nucleoid and cytoplasm. The progression of this relocalization is indicated by arrows and by the progressive increase in opacity of the DNA, RNAP, nascent RNA, and ribosomal subunits.

Does transcription-translation coupling result only from the colocalization of RNAP and ribosomes on nascent RNA?

The above described observations of transcription-translation coupling can be explained by the binding of ribosomes to the nascent RNA of a transcribing RNAP; no physical interactions between the transcribing RNAP and the first trailing ribosome must be evoked. This assumption was first challenged by the NMR structure of the complex of ribosomal protein uS10 bound to transcription factor NusG (Burmann, Schweimer et al. 2010). (Ribosomal protein uS10 is also known as ribosomal protein S10 and as transcription factor NusE. Here we follow the naming convention for ribosomal proteins as set forth in Ban *et al.* (Ban, Beckmann et al. 2014).)

NusG stimulates transcription (Burova, Hung et al. 1995, Burns, Richardson et al. 1998) as well as translation (Zellars and Squires 1999). Of the two domains of NusG, the N-terminal domain binds to RNAP, while the C-terminal domain can bind either transcription termination factor Rho (Mooney, Schweimer et al. 2009) or ribosomal protein uS10 (Burmann, Schweimer et al. 2010). The binding of the N-terminal domain of NusG to the RNAP prevents the polymerase from entering long-lived pauses, thereby increasing the overall transcription rate (Herbert, Zhou et al. 2010). On the other hand, the binding of Rho factor to the C-terminal domain places the transcription termination factor near the nascent RNA. This proximity facilitates the loading of Rho factor onto the nascent RNA only a short distance away from the RNAP, thereby promoting Rho-dependent transcription termination. NusG's ability to prevent prolonged transcription pausing and to recruit Rho factor to the RNAP explains the apparently contradictory

effects NusG exerts on transcription, stimulating both transcription elongation and transcription termination (Li, Mason et al. 1992, Sullivan and Gottesman 1992).

The binding interface of NusG on ribosomal protein uS10 within the NusG:uS10 complex is accessible on the ribosome (Burmann, Schweimer et al. 2010) and residues within this interface are critical for binding of NusG to ribosomes both *in vitro* and *in vivo* (Saxena, Myka et al. 2018). NusG appears not only to bind RNAP and ribosome on their own, but also to form a physical link between the transcribing RNAP and the trailing ribosome during transcription-translation coupling (Burmann, Schweimer et al. 2010). Since ribosomal protein uS10 competes with Rho factor for overlapping sites on NusG's C-terminal domain (Burmann, Schweimer et al. 2010, Lawson, Ma et al. 2018), coupling of RNAP and ribosomes via NusG suppresses the recruitment of Rho factor and with it its mediated transcription termination.

Another transcription factor known to physically link RNAP and ribosomes is the NusG-paralog RfaH. While NusG associates with RNAP during expression of almost all genes (Mooney, Davis et al. 2009), RfaH regulates the expression of a handful of operons with a specific signal sequence in the 5' untranslated region (*i.e.*, operon polarity suppressor or *ops* signal) (Bailey, Hughes et al. 1997). The coupling brought about by RfaH enables the expression of exogenous, horizontally transferred genes even if they are not codon-optimized and are missing the translation initiation signals specific for *E. coli* (Burmann, Knauer et al. 2012).

Like NusG, RfaH consists of two domains. Its N-terminal domain is highly similar to NusG's and equally reduces transcription pausing. Both proteins even compete

for binding to overlapping sites on the RNAP, resulting in a mutually exclusive binding of the factors to RNAP *in vivo* (Belogurov, Mooney et al. 2009). The C-terminal domains of both factors, however, are strikingly different. While the C-terminal domain of NusG adopts an all β-sheet structure and is connected via a flexible linker to its N-terminal domain (Steiner, Kaiser et al. 2002), the C-terminal domain of RfaH folds into an all α-helical structure and intimately interacts with its N-terminal domain (Belogurov, Vassylyeva et al. 2007). RNAP will pause upon transcribing the *ops* signal. This allows RfaH to recognize the *ops* sequence on the non-template DNA strand and bind to the polymerase (Artsimovitch and Landick 2002, Kang, Mooney et al. 2018). Upon binding of the N-terminal domain, RfaH's C-terminal domain is released and adopts the all β-sheet structure of NusG (Burmann, Knauer et al. 2012). The transformed C-terminal domain then allows RfaH to recruit ribosomal protein uS10 at the same interface that NusG does (Belogurov, Mooney et al. 2009).

Unlike NusG, RfaH does not bind Rho factor (Burmann, Knauer et al. 2012). Therefore, RfaH hampers Rho-dependent transcription termination in two ways. First, it blocks Rho factor from reaching the RNAP by mediating a tight coupling between RNAP and the first trailing ribosome. Second, it diminishes NusG's stimulatory effect on Rho-dependent termination by competing with NusG for binding to RNAP.

Are RNAP and ribosome only linked together by NusG and RfaH or can they directly interact with each other?

Early genetic studies uncovered an interaction between RNAP and the small ribosomal subunit (Chakrabarti and Gorini 1975, Chakrabarti and Gorini 1977),

indicating that mediating factors such as NusG or RfaH may not be required for the coupling of transcription and translation. Additionally, several ribosomal proteins also serve as transcription factors on their own. For example, ribosomal protein uS4 inhibits premature termination of ribosomal RNA transcription (Torres, Condon et al. 2001), while ribosomal protein uL2 promotes transcription of genes driven from ribosomal RNA promoters (Rippa, Cirulli et al. 2010). Ribosomal protein uS10, which binds the C-terminal domain of NusG as discussed above, is an integral part of a transcription antitermination complex and can bind RNAP on its own (Burmann, Schweimer et al. 2010, Drogemuller, Strauss et al. 2015, Drogemuller, Strauss et al. 2015, Said, Krupp et al. 2017). Finally, ribosomal protein bS1 stimulates the recycling of RNAP during *in vitro* transcription (Sukhodolets, Garges et al. 2006). Although bS1 binds only weakly to ribosomes, it is critical for translation initiation (Boni, Isaeva et al. 1991). By capturing the mRNA in its unfolded form, bS1 provides the ribosome access to the ribosomal binding site (aka Shine-Dalgarno sequence) buried in local secondary structure (Studer and Joseph 2006, Qu, Lancaster et al. 2012). This unfolding of the structured mRNA extends not only downstream towards the Shine-Dalgarno region, but also upstream of the bS1 binding site. In some cases, the upstream unfolding is large enough to accommodate a second ribosome, priming the mRNA for a second round of translation (Andreeva, Belardinelli et al. 2018). Once translation has ensued, it is unable to dissociate from the ribosome (Sørensen, Fricke et al. 1998). This suggests that ribosome-bound bS1 interacts with RNAP during transcription-translation coupling.

Direct interactions between RNAP and ribosomes were also observed in the cryo-EM studies of the small ribosomal subunit bound to RNAP (*i.e.*, the 30S•RNAP complex) and of the ribosome in complex with RNAP, in which the ribosome is translating the nascent RNA being transcribed by the RNAP (*i.e.*, the expressome) (Demo, Rasouly et al. 2017, Kohler, Mooney et al. 2017). In reconstructions of both complexes, the RNAP binds to the ribosome with its nascent RNA exit site while the RNAP binding sites on the ribosome are distinct and non-overlapping (Figure 6.3B-E).

In reconstructions of the 30S•RNAP complex, the RNAP is bound close to the 30S subunit site that recognizes the Shine-Dalgarno sequence of mRNAs. The interface between RNAP and 30S subunit consists of regions of the β' and β subunits close to the nascent RNA exit site on the RNAP and of ribosomal proteins uS2, bS6:bS18 heterodimer, and bS21, and ribosomal RNA helices 26 and 40. Due to the flexibility of ribosomal protein bS1, only parts of the protein were visualized in one of the reconstructed 30S•RNAP particles. In this reconstruction, the C-terminal half of ribosomal protein bS1 interacts with the bound RNAP. In our own studies of the RNAP-30S subunit interface, we found by chemical crosslinking that the β' subunit of RNAP is close to ribosomal proteins bS1, uS2, bS6, uS7, uS9, and uS11; all proteins surrounding the mRNA exit site of the 30S subunit (Figure 6.3B and D) (Fan, Conn et al. 2017).

The 30S subunit of all three reconstructed 30S•RNAP particles adopts the same conformation, in which the diameter of the mRNA exit site is widened. This widening of the 30S subunit's mRNA exit site may allow the nascent RNA to better access the mRNA path on the 30S subunit during translation initiation (Demo, Rasouly et al. 2017). Please

note that in all 30S•RNAP particles the RNAP is neither transcribing a nascent RNA nor bound to DNA (Demo, Rasouly et al. 2017). Therefore, these complexes may not recapitulate a step during translation initiation of the nascent RNA, but simply reflect interactions between 30S subunits and *free* RNAP that may occur in the nucleoid.

In the reconstruction of the expressome, the RNAP docks to the mRNA entry site of the ribosome, allowing the nascent RNA exiting the RNAP to immediately enter the ribosome. The binding interface on the RNAP consists of regions close to the nascent RNA exit site from all subunits and on the ribosome it includes ribosomal proteins uS2, uS3, uS4, uS5, and uS10, and helix 16 of the 30S subunit's ribosomal RNA (Kohler, Mooney et al. 2017) (Figure 6.3C and E). In addition, the C-terminal domain of one of the two α subunits of the bound RNAP is bound to ribosomal protein uS9 and helices 38 and 39 of the 30S subunit's ribosomal RNA. This RNAP binding site is more than 75 Å distant from that seen in the 30S•RNAP particles (Demo, Rasouly et al. 2017, Kohler, Mooney et al. 2017). Please note that the expressome complex was prepared by translating all of the nascent RNA of a preformed, stable RNAP complex. Furthermore, the physical contact between RNAP and the ribosome was favored by the presence of the chemical cross-linker glutaraldehyde during the purification of the complex (Stark 2010, Kohler, Mooney et al. 2017). Therefore, the expressome structure may only reflect a complex with minimal nascent RNA between the RNAP and ribosome (Kohler, Mooney et al. 2017).

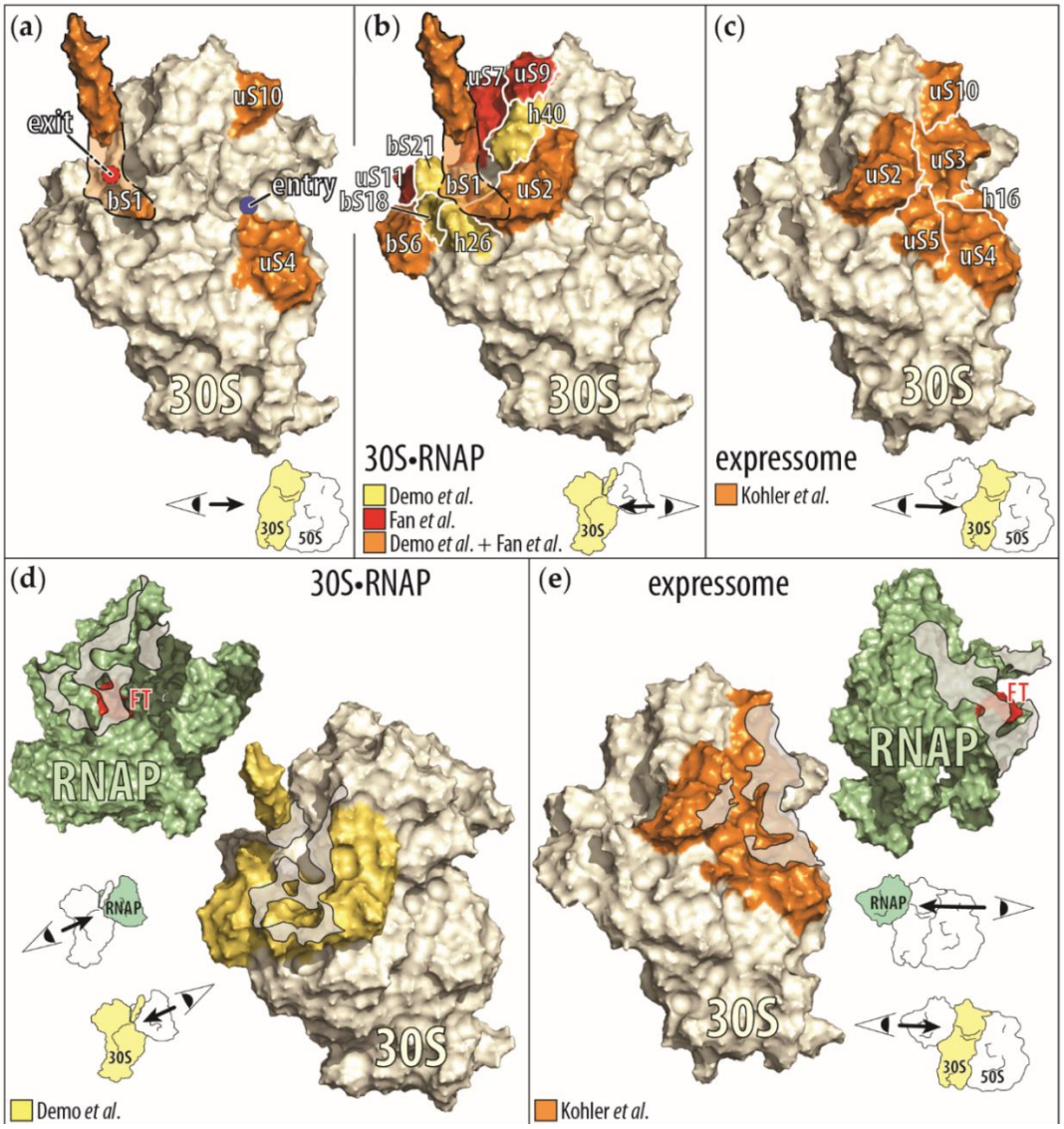
(a)
exit
uS10
entry
bS1
uS4
30S
30S
50S
(b)
uS7
uS9
h40
bS21
uS11
bS18
bS1
uS2
bS6
h26
30S
30S•RNAP
Demo et al.
Fan et al.
Demo et al. + Fan et al.
30S
(c)
uS10
uS2
uS3
h16
uS5
uS4
30S
expressome
Kohler et al.
30S
50S
(d)
30S•RNAP
FT
RNAP
RNAP
30S
30S
Demo et al.
(e)
expressome
FT
RNAP
RNAP
30S
30S
50S
Kohler et al.

Figure 6.3. Display of the RNAP-ribosome interactions and contact points identified by biochemical and cryo-EM studies. (**a**) Ribosomal proteins (in orange) that influence RNAP activity by themselves (bS1 (Sukhodolets, Garges et al. 2006), uS4 (Torres, Condon et al. 2001), and uS10 (Drogemuller, Strauss et al. 2015)) are mapped onto the small ribosomal subunit (30S) derived from the cryo-EM structure of the small ribosomal subunit bound to RNAP (30S•RNAP) (Demo, Rasouly et al. 2017). Because ribosomal protein bS1 is only partially resolved in this structure, we outlined the approximate position of the remaining protein (orange shaded area). In addition, the mRNA entry (blue circle) and exit (red circle with dashed black border indicating its positions behind bS1) sites on the small ribosomal subunit are indicated. In the right corner is a cartoon representation of the direction of the view displayed of the small ribosomal subunit. (**b**) Ribosomal proteins and RNA helices contacting the RNAP upon binding of the small ribosomal subunit to RNAP. Shown are the proteins identified to be close to RNAP in the cryo-EM structure of 30S•RNAP in Demo *et al.* (Demo, Rasouly et al. 2017) and by chemical crosslinking in Fan *et al.* (Fan, Conn et al. 2017). (Proteins observed only in Demo *et al.* are in yellow, those shared by Demo *et al.* and Fan *et al.* are in orange and those observed only in Fan *et al.* are in red). (**c**) Ribosomal proteins (in orange) contacting the RNAP in the cryo-EM structure of a ribosome translating a nascent RNA as it is being synthesized, aka expressome (Kohler, Mooney et al. 2017). Interactions between the C-terminal domain of one of the two α subunits of the RNAP with the ribosome were omitted for clarity. (**d**) and (**e**) Contact interfaces between RNAP and small ribosomal subunit as seen in the cyro-EM structures of the 30S•RNAP complex (d) and the expressome (e). In both representations the view is onto the contact areas (gray shaded areas) on the RNAP (green) and on the small ribosomal subunit (yellow). Also indicated is the β flap-tip of the RNAP (red, marked with FT), past which the nascent RNA exits the RNAP to enter the small ribosomal subunit.

Although the RNAP positions in both structures are distinct, they may be part of a single, overarching cycle of transcription-translation coupling. We propose that similar to translation initiation of a structured mRNA, during which the 3' end is repositioned on the 30S subunit from the mRNA exit to the mRNA entry site (de Smit and Van Duin 2003, Marzi, Myasnikov et al. 2007), the RNAP is repositioned during translation initiation of the nascent RNA. Therefore, the RNAP-binding site seen in the 30S•RNAP may reflect a state during the beginning phase of the coupling, while the one seen in the expressome may reflect a state during ongoing coupling along a gene or operon.

In both structures, the NusG- and RfaH-binding sites on the RNAP and the ribosome are too far apart to allow NusG or RfaH to bridge both macromolecules. Therefore, another spatial arrangement between RNAP and ribosome must exist that complements already captured and visualized arrangements.

Does the length of intervening RNAs influence the interaction between RNAP and ribosome during coupling?

The structure of the expressome, suggests a continuous, static physical connection between RNAP and the ribosome during coupling. Such a close connection provides a simple explanation for the effects the coupling of translation exerts on transcription. However, the length of intervening nascent RNA between RNAP and ribosome is constantly fluctuating. Because the ribosome steps three nucleotides at a time along the nascent RNA, the ribosome must wait for the RNAP to add three nucleotides, one by one, before taking a step. This causes the length of the intervening RNA to fluctuate between one, two, three, and no extra nucleotides between RNAP and ribosome. Such small

variations in the length of the nascent RNA may be scrunched in between the RNAP and ribosome without breaking the interface.

Larger variations are more difficult to reconcile with a static model of RNAP-ribosome arrangement of the expressome. The transcription and translation rates are dependent on the cellular concentration of different metabolites, *i.e.*, nucleotides and amino acids, respectively. Therefore, these rates will respond differently to concentration fluctuations of these metabolites. These independent responses of transcription and translation will result in varying lengths of intervening nascent RNA. The rate differences are further aggravated by the apparent independent distribution of transcription and translation regulatory elements along genes. (For more specific information on the different regulatory elements for translation, see review by Rodnina (Rodnina 2016) and for those for transcription, see review by Artsimovitch (Artsimovitch 2018).) These larger fluctuations in the length of the intervening RNA can be accommodated by a repeated breaking and forming of the expressome depending on the length of the intervening RNA.

Because the interactions between RNAP and ribosomes can be repeatedly formed and broken, it suggests that the interactions between both are dynamic. Such a dynamic view of the interactions is supported by the moderate strength of the RNAP affinity for ribosomes (*i.e.*, a low micromolar dissociation constant of the RNAP•ribosome complex (Fan, Conn et al. 2017)). We suggest that the interactions between the RNAP and ribosomes are not only more dynamic but are possibly independent of the length of the intervening nascent RNA. Due to the tethering via the nascent RNA, the local

concentration of the first trailing ribosome close to the RNAP will exceed the dissociation constant of the RNAP•ribosome complex even with thousands of nucleotides of intervening nascent RNA (Figure 6.4A) (Conant, Goodarzi et al. 2008). To accommodate such long intervening RNA, the RNA has to loop out and away from the RNAP-ribosome complex (Figure 6.4B). Similar looping of the nascent RNA has been attributed to the antitermination observed during transcription of ribosomal RNA (Condon, Squires et al. 1995, Krupp, Said et al. 2019) and during transcription of lambda bacteriophage genome (Conant, Goodarzi et al. 2008, Said, Krupp et al. 2017). Such dynamic binding and dissociation of the RNAP-ribosome complex could explain the stochastic behavior of transcription-translation coupling observed *in vivo* (Li, Zhang et al. 2016, Chen and Fredrick 2018). These lines of argument should also apply to the RNAP-ribosome complex formation mediated by NusG and RfaH.

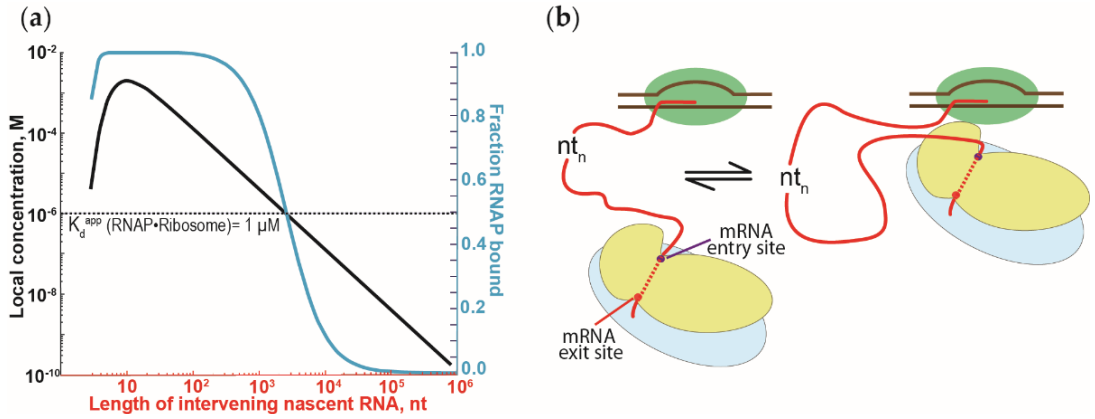

Figure 6.4. The effect of tethering of RNAP and ribosomes by nascent RNA on the RNAP•ribosome complex formation. (**a**) Dependence of RNAP•ribosome complex formation on length of intervening nascent RNA. The intervening nascent RNA was modeled as a freely jointed chain. The local concentration of the first trailing ribosome around the RNAP that it is tethered to (left y-axis) and the fraction of RNAP-ribosome complex formation (in blue, right y-axis) are plotted against the length of the intervening nascent RNA. Local concentration and fraction of complex formation were calculated following Conant *et al.* (Conant, Goodarzi et al. 2008) and Rippe (Rippe 2001). (**b**) Schematic representation of the binding equilibrium dynamics between the first trailing ribosome (in blue and yellow for large and small ribosomal subunits, respectively) and the RNAP (in green), tethered via the nascent RNA (red). Binding of the RNAP and ribosome will cause the intervening nascent RNA to loop out and away from the RNAP-ribosome complex.

What is the current framework for transcription-translation coupling?

We can discern two possible modes of transcription-translation coupling, factor-free and factor-mediated coupling; a distinction also eluded to by others, *e.g.* (Artsimovitch 2018).

In factor-free coupling, the RNAP is initially recruited to the mRNA exit site of the 30S subunit (Demo, Rasouly et al. 2017). During translation initiation, the RNAP relocalizes from the mRNA exit to the mRNA entry site of the 30S subunit (Kohler, Mooney et al. 2017). Due to tethering by the nascent RNA and a moderate affinity of the ribosome for RNAP, the complex between the first trailing ribosome and RNAP will repeatedly form and dissociate. These frequent encounters between RNAP and ribosome enable the coupling to accommodate a fluctuating length of intervening nascent RNA.

Factor-mediated coupling is most apparent for coupling mediated by RfaH. Here, the coupling also affects translation of the nascent RNA, in particular its initiation (Burmann, Knauer et al. 2012). This therefore points to RfaH already being bound to the RNAP during the first step of translation initiation when the 30S subunit recruits the nascent RNA. Due to RfaH linkage of RNAP and the trailing ribosome, the spatial arrangement of RNAP and the ribosome differs from those captured for factor-free coupling.

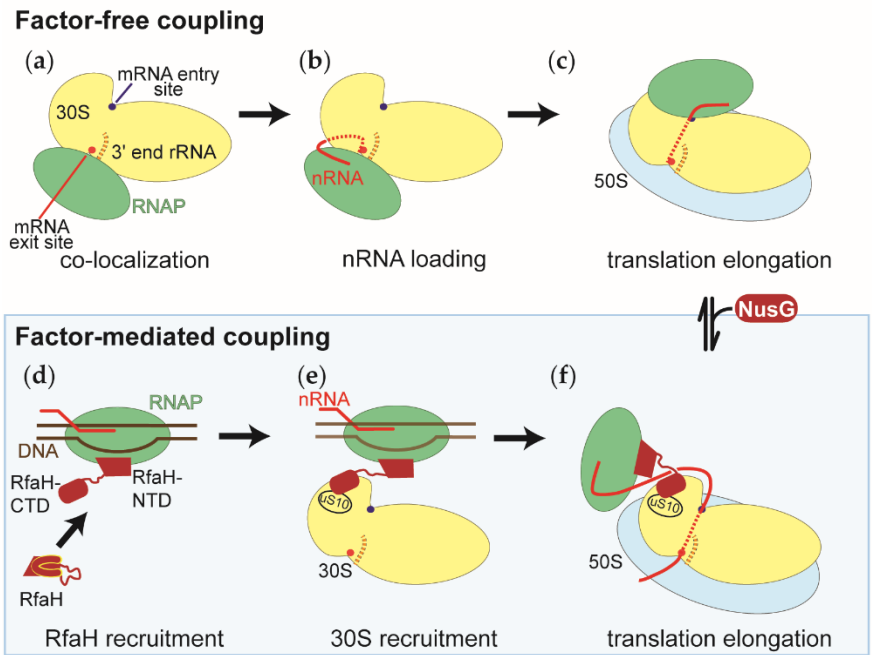

Figure 6.5. Model of RNAP-ribosome arrangements during factor-free and factor-mediated coupling of transcription and translation. The representation of the small ribosomal subunit (30S in yellow) is the same in all panels, with both RNAP binding sites facing the reader. RNAP, the large ribosomal subunit (50S), DNA, and nascent RNA are shown in green, blue, brown, and red, respectively. NusG and RfaH, the factors that physically link RNAP and ribosomes during factor-mediated coupling are shown in dark red. (**a**) Co-localization of RNAP and small ribosomal subunits within the nucleoid. (**b**) Recruitment of nascent RNA to the small ribosomal subunit during the first step of translation initiation. Also shown is the positioning of the 5' end of the nascent RNA relative to the 3' end of the ribosomal RNA of the small ribosomal subunit (3' end rRNA). In many cases, both ends engage in base pairing interactions. (**c**) During translation initiation, RNAP relocalizes on the 30S subunit from the mRNA exit site shown in (a) and (b) to the mRNA entry site. Shown is the RNAP-ribosome complex with the shortest intervening nascent RNA. (**d**) Recruitment of transcription factor RfaH to the RNAP which has transcribed and paused at the *ops* signal sequence. RfaH's C-terminal domain undergoes a conformational change from an all α helical to an all β sheet structure. (**e**) Recruitment of the small ribosomal subunit (30S) to RNAP-RfaH complex before initiation of translation. (**f**) During factor-mediated coupling, the RNAP and ribosome are held close to each other by either transcription factor RfaH or NusG. The NuG-mediated coupling is established by binding of NusG to the factor-free coupled RNAP and ribosome.

NusG-mediated coupling appears to be a hybrid of factor-mediated and factor-free coupling. Unlike RfaH, NusG is not recruited at a defined point during transcription of a gene, but is recruited after the RNAP has cleared a promoter proximal pausing site (Mooney, Davis et al. 2009). This implies that NusG is recruited to RNAP after translation of the nascent RNA has assisted the polymerase in clearing the pause site. Therefore, NusG can reorganize the RNAP-ribosome arrangement from factor-free to factor-mediated coupling (Figure 6.5).

Which questions remain?

The discovery of direct physical interactions between RNAP and ribosomes hints that individual transcription events can immediately be relayed to the ribosome, affecting its translational activity. Conversely, individual translation events can be relayed to the RNAP, thus affecting its transcriptional activity. The mutual influence of transcription and translation on coupling raises the tantalizing prospective of a novel mechanism of regulation. Any mechanism of the mutual regulation will have to specify: 1) the phases of transcription and translation that are coupled, 2) the functional states of the RNAP and ribosome that interact, and 3) the effect this regulation exerts on the coupled processes.

Most of our current understanding of transcription-translation coupling was gained from work with a narrow set of model genes and operons under a few conditions. A comprehensive list of genes that support or require coupling for expression remains elusive. Modern genome-wide approaches may overcome this shortcoming in the foreseeable future. It will be interesting to see how this list of genes depends on the presence of NusG or varies with environmental and growth conditions.

Although we focused in this review on transcription-translation coupling alone, it is important to realize transcription and translation couples with other critical cellular processes. For example, transcription couples to DNA repair (Spivak 2016, Pani and Nudler 2017) and translation couples to protein folding (Seligmann and Warthi 2017, Thommen, Holtkamp et al. 2017) and protein translocation (Woldringh 2002, Elvekrog and Walter 2015). The integration of all these coupled processes into a comprehensive view will be required to gain a full appreciation of the effects that transcription-translation coupling exert on the physiology of the bacterial cell. With the resurgence of interest in transcription-translation coupling, we look forward to new exciting insights into all aspects of coupling and the ramifications for regulation of gene expression in bacteria.

Acknowledgments: We would like to apologize sincerely for failing to cite the work of many colleagues whose contributions have shaped our current understanding and made the recent advances possible. We also would like to thank Tim Rowsell and Dr. Sean O'Leary for critical discussions.

References:

Adelman, K., Porta, A. La, Santangelo, T. J., Lis, J. T., Roberts, J. W., Wang, M. D. (2002) "Single Molecule Analysis of RNA Polymerase Elongation Reveals Uniform Kinetic Behavior." Proceedings of the National Academy of Sciences ***99*** (21), 13538–13543.

Adhya, S., Gottesman, M. (1978). "Control of transcription termination." Annu. Rev. Biochem. **47**: 967-996.

Adhya, S., Gottesman, M., Crombrugghe, B. de, Court, D. (1976). Transcription Termination Regulates Gene Expression. RNA Polymerase. R. Losick and M. Chamberlin, Cold Spring Harbor Laboratory**,** 719-730.

Agirrezabala, X., Liao, H. Y., Schreiner, E., Fu, J., Ortiz-Meoz, R. F., Schulten, K., Green, R., Frank, J. (2012). "Structural characterization of mRNA-tRNA translocation intermediates." Proc Natl Acad Sci U S A **109**(16): 6094-6099.

Aitken, C. E., Beznoskova, P., Vlckova, V., Chiu, W. L., Zhou, F., Valasek, L. S., Hinnebusch, A. G., Lorsch, J. R. (2016). "Eukaryotic translation initiation factor 3 plays distinct roles at the mRNA entry and exit channels of the ribosomal preinitiation complex." Elife **5**.

Allen, G. S., Zavialov, A., Gursky, R., Ehrenberg, M., Frank, J. (2005). "The cryo-EM structure of a translation initiation complex from *Escherichia coli*." Cell, **121**(5): 703-712.

Alpi, E., Griss, J., Silva, A. W. da, Bely, B., Antunes, R., Zellner, H., Rios, D., O'Donovan, C., Vizcaino, J. A., Martin, M. J. (2015). "Analysis of the tryptic search space in UniProt databases." Proteomics **15**(1): 48-57.

Andreeva, I., Belardinelli, R., Rodnina, M. V. (2018). "Translation initiation in bacterial polysomes through ribosome loading on a standby site on a highly translated mRNA." Proc Natl Acad Sci U S A **115**(17): 4411-4416.

Antoun, A., Pavlov, M. Y., Lovmar, M., Ehrenberg, M. (2006). "How initiation factors tune the rate of initiation of protein synthesis in bacteria." The EMBO journal, ***25***(11), 2539–2550.

Antoun, A., Pavlov, M. Y., Tenson, T., Ehrenberg, M. (2004). "Ribosome formation from subunits studied by stopped-flow and Rayleigh light scattering." Biological procedures online, ***6***:35–54.

Arora, S., Bhamidimarri, S. P., Weber, M. H., Varshney, U. (2013). "Role of the ribosomal P-site elements of m(2)G966, m(5)C967, and the S9 C-terminal tail in maintenance of the reading frame during translational elongation in *Escherichia coli*." J Bacteriol **195**(16): 3524-3530.

Artsimovitch, I. (2018). "Rebuilding the bridge between transcription and translation." Mol Microbiol **108**(5): 467-472.

Artsimovitch, I., Landick, R. (2002). "The transcriptional regulator RfaH stimulates RNA chain synthesis after recruitment to elongation complexes by the exposed nontemplate DNA strand." Cell **109**(2): 193-203.

Artsimovitch, I., Knauer, S.H. (2019). "Ancient transcription factors in the news." mBio, **10**(1): 1547.

Artsimovitch, I., Svetlov, V., Murakami, K. S., Landick, R. (2003). "Co-overexpression of *Escherichia coli* RNA Polymerase Subunits Allows Isolation and Analysis of Mutant Enzymes Lacking Lineage-specific Sequence Insertions." J Biol Chem **278**(14): 12344-12355.

Aylett, C. H., Boehringer, D., Erzberger, J. P., Schaefer, T., Ban, N. (2015). "Structure of a yeast 40S-eIF1-eIF1A-eIF3-eIF3j initiation complex." Nat Struct Mol Biol **22**(3): 269-271.

Ayyub, S. A., Dobriyal, D., Varshney, U. (2017) "Contributions of the N- and C-Terminal Domains of Initiation Factor 3 to Its Functions in the Fidelity of Initiation and Antiassociation of the Ribosomal Subunits." J Bacteriol ***199*** (11), e00051-17, e00051-17.

Baggett, N. E., Zhang, Y., Gross, C. A. (2017). "Global analysis of translation termination in *E. coli*." PLoS Genet **13**(3): e1006676.

Bailey, M. J., Hughes, C., Koronakis, V. (1997). "RfaH and the ops element, components of a novel system controlling bacterial transcription elongation." Mol. Microbiol. **26**(5): 845-851.

Bakshi, S., Siryaporn, A., Goulian, M., Weisshaar, J. (2012). "Superresolution imaging of ribosomes and RNA polymerase in live *Escherichia coli* cells." Mol Microbiol **85**(1): 21-38.

Bakshi, S., Choi, H., Weisshaar, J. C. (2015). "The spatial biology of transcription and translation in rapidly growing *Escherichia coli*." Front. Microbiol. **6**: 636.

Ban, N., Beckmann, R., Cate, J. H., Dinman, J. D., Dragon, F., Ellis, S. R., Lafontaine, D. L., Lindahl, L., Liljas, A., Lipton, J. M., McAlear, M. A., Moore, P. B., Noller, H. F., Ortega, J., Panse, V. G., Ramakrishnan, V., Spahn, C. M., Steitz, T. A., Tchorzewski, M., Tollervey, D., Warren, A. J., Williamson, J. R., Wilson, D., Yonath, A., Yusupov, M. (2014). "A new system for naming ribosomal proteins." Curr. Opin. Struct. Biol. **24**: 165-169.

Ban, N., Nissen, P., Hansen, J., Moore, P. B., Steitz, T. A. (2000). "The complete atomic structure of the large ribosomal subunit at 2.4 A resolution." Science, ***289***(5481), 905–920.

Basu, R. S., Warner, B. A., Molodtsov, V., Pupov, D., Esyunina, D., Fernández-Tornero, C., Kulbachinskiy, A., A.,, Murakami, K. S. (2014) "Structural Basis of Transcription Initiation by Bacterial RNA Polymerase Holoenzyme." J. Biol. Chem. ***289*** (35), 24549–24559.

Bayfield, M. A., Dahlberg, A. E., Schulmeister, U., Dorner, S., Barta, A. (2001) "A conformational change in the ribosomal peptidyl transferase center upon active/inactive transition." Proceedings of the National Academy of Sciences of the United States of America, ***98***(18), 10096–10101.

Belogurov, G. A., Artsimovitch, I. (2015). "Regulation of Transcript Elongation." Annual review of microbiology, ***69***:49–69.

Belogurov, G. A., Sevostyanova, A., Svetlov, V., Artsimovitch, I. (2010). "Functional regions of the N-terminal domain of the antiterminator RfaH." Mol Microbiol **76**(2): 286-301.

Belogurov, G. A., Vassylyeva, M. N., Svetlov, V., Klyuyev, S., Grishin, N. V., Vassylyev, D. G., Artsimovitch, I. (2007). "Structural basis for converting a general transcription factor into an operon-specific virulence regulator." Mol. Cell **26**(1): 117-129.

Belogurov, G. A., Mooney, R. A., Svetlov, V., Landick, R., Artsimovitch, I. (2009). "Functional specialization of transcription elongation factors." EMBO J. **28**(2): 112-122.

Berg, D., Chamberlin, M. (1970). "Physical studies on ribonucleic acid polymerase from *Escherichia coli* B." Biochemistry **9**(26): 5055-5064.

Bhattacharyya, S., Jacobs, W. M., Adkar, B. V., Yan, J., Zhang, W., Shakhnovich, E.I (2018). "Accessibility of the Shine-Dalgarno Sequence Dictates N-Terminal Codon Bias in E. coli." Mol Cell, **70**(5): 894–905.e5.

Blaha, G., Stelzl, U., Spahn, C. M., Agrawal, R. K., Frank, J., Nierhaus, K. H. (2000) “Preparation of functional ribosomal complexes and effect of buffer conditions on tRNA positions observed by cryoelectron microscopy.” Methods Enzymol. **317**(1):292-309.

Bocharov, E. V., Sobol, A. G., Pavlov, K. V., Korzhnev, D. M., Jaravine, V. A., Gudkov, A. T., Arseniev, A. S. (2004). "From structure and dynamics of protein L7/L12 to molecular switching in ribosome." J Biol Chem **279**(17): 17697-17706.

Boni, I. V., Isaeva, D. M., Musychenko, M. L., Tzareva, N. V. (1991). "Ribosome-messenger recognition: mRNA target sites for ribosomal protein S1." Nucleic Acids Res. **19**(1): 155-162.

Borin, B. N., Tang, W., Krezel, A. M. (2014). "*Helicobacter pylori* RNA polymerase alpha-subunit C-terminal domain shows features unique to varepsilon-proteobacteria and binds NikR/DNA complexes." Protein Sci **23**(4): 454-463.

Box, G. E. P., Hunter, J. S., Hunter, W. G. (2005). “Statistics for experimenters: design, innovation, and discovery.” Hoboken, N.J., Wiley-Interscience.

Bratton, B. P., Mooney, R. A., Weisshaar, J. C. (2011). "Spatial distribution and diffusive motion of RNA polymerase in live *Escherichia coli*." J Bacteriol **193**(19): 5138-5146.

Bremer, H., Dennis, P. P. (2008). "Modulation of Chemical Composition and Other Parameters of the Cell at Different Exponential Growth Rates." EcoSal Plus **3**(1).

Britten, R. J., Roberts, R. B. (1960). “High-Resolution Density Gradient Sedimentation Analysis.” Science. **131**(3392):32-3

Buckingham, R. H., Grentzmann, G., Kisselev, L. (1997) "Polypeptide Chain Release Factors." Molecular Microbiology ***24*** (3), 449–456.

Burmann, B. M., Schweimer, K., Luo, X., Wahl, M. C., Stitt, B. L., Gottesman, M. E., Rösch, P. (2010). "A NusE:NusG complex links transcription and translation." Science **328**(5977): 501-504.

Burmann, B., Knauer, S., Sevostyanova, A., Schweimer, K., Mooney, R., Landick, R., Artsimovitch, I., Rösch, P. (2012). "An α helix to β barrel domain switch transforms the transcription factor RfaH into a translation factor." Cell **150**(2): 291-303.

Burns, C. M., Richardson, L. V., Richardson, J. P. (1998). "Combinatorial effects of NusA and NusG on transcription elongation and Rho-dependent termination in *Escherichia coli*." J. Mol. Biol. **278**(2): 307-316.

Burova, E., Hung, S. C., Sagitov, V., Stitt, B. L., Gottesman, M. E. (1995). "*Escherichia coli* NusG protein stimulates transcription elongation rates *in vivo* and *in vitro*." J. Bacteriol. **177**(5): 1388-1392.

Byrgazov, K., Manoharadas, S., Kaberdina, A., C.,, Vesper, O., Moll, I. (2012). "Direct Interaction of the N-Terminal Domain of Ribosomal Protein S1 with Protein S2 in *Escherichia coli*." PLoS ONE.

Caban, K., Gonzalez, R. L. (2015). “The emerging role of rectified thermal fluctuations in initiator aa-tRNA- and start codon selection during translation initiation.” Biochimie, **114**: 30-38.

Cabrera, J. E., Jin, D. J. (2003). "The distribution of RNA polymerase in *Escherichia coli* is dynamic and sensitive to environmental cues." Mol. Microbiol. **50**(5): 1493-1505.

Caliskan, N., Katunin, V. I., Belardinelli, R., Peske, F., Rodnina, M. V. (2014). "Programmed -1 frameshifting by kinetic partitioning during impeded translocation." Cell **157**(7): 1619-1631.

Calogero, R. A., Pon, C. L., Canonaco, M. A., Gualerzi, C. O. (1988). “Selection of the mRNA translation initiation region by *Escherichia coli* ribosomes.” Proc Natl Acad Sci, **85**(17): 6427-6431.

Campbell, E. A., Muzzin, O., Chlenov, M., Sun, J. L., Olson, C. A., Weinman, O., Trester-Zedlitz, M. L., Darst, S. A. (2002) "Structure of the Bacterial RNA Polymerase Promoter Specificity σ Subunit." Molecular Cell ***9*** (3), 527–539.

Carson, M. (1991) “Ribbons 2 0.” J Appl Crystallogr, **24**:958-961.

Carter, A. P. (2001) "Crystal Structure of an Initiation Factor Bound to the 30S Ribosomal Subunit." Science ***291*** (5503), 498–501.

Carter, A. P., Clemons, W.M., Jr, D. E. Brodersen, Morgan-Warren, R. J., Hartsch, T., Wimberly, B. T., Ramakrishnan, V. (2001). “Crystal structure of an initiation factor bound to the 30S ribosomal subunit.” Science, **291**(5503): 498–501.

Chakrabarti, S. L., Gorini, L. (1975). "A link between streptomycin and rifampicin mutation." Proc. Natl. Acad. Sci. USA **72**(6): 2084-2087.

Chakrabarti, S. L., Gorini, L. (1977). "Interaction between mutations of ribosomes and RNA polymerase: a pair of strA and rif mutants individually temperature-insensitive but temperature-sensitive in combination." Proc. Natl. Acad. Sci. USA **74**(3): 1157-1161.

Chen, J., Petrov, A., Johansson, M., Tsai, A., O'Leary, S. E., Puglisi, J. D. (2014). "Dynamic pathways of -1 translational frameshifting." Nature **512**(7514): 328-332.

Chen, M., Fredrick, K. (2018). "Measures of single- versus multiple-round translation argue against a mechanism to ensure coupling of transcription and translation." Proc. Natl. Acad. Sci. USA **115**(42): 10774-10779.

Christian, T., Evilia, C., Williams, S., Hou, Y. M. (2004). "Distinct origins of tRNA(m1G37) methyltransferase." J Mol Biol **339**(4): 707-719.

Chen, S. S., Williamson, J. R. (2013). “Characterization of the ribosome biogenesis landscape in E. coli using quantitative mass spectrometry.” Journal of molecular biology, ***425***(4), 767–779.

Conant, C. R., Goodarzi, J. P., Weitzel, S. E., Hippel, P. H. von (2008). "The antitermination activity of bacteriophage lambda N protein is controlled by the kinetics of an RNA-looping-facilitated interaction with the transcription complex." J. Mol. Biol. **384**(1): 87-108.

Condon, C., Squires, C., Squires, C. L. (1995). "Control of rRNA transcription in *Escherichia coli*." Microbiol. Rev. **59**(4): 623-645.

Conn, A. B., Diggs, S., Tam, T. K., Blaha, G. M. (2019). “Two Old Dogs, One New Trick: A Review of RNA Polymerase and Ribosome Interactions during Transcription-Translation Coupling.” International journal of molecular sciences, ***20***(10), 2595.

Cox, J., Mann, M. (2008). "MaxQuant enables high peptide identification rates, individualized p.p.b.-range mass accuracies and proteome-wide protein quantification." Nat Biotechnol **26**(12): 1367-1372.

Das, H. K., Goldstein, A., Lowney, L. I. (1967). "Attachment of ribosomes to nascent messenger RNA in *Escherichia coli*." J. Mol. Biol. **24**(2): 231-245.

de Smit, M. H., Duin, J. Van (2003). Ribosomes on Standby: A Prelude to Translational (Re)Initiation. Translation mechanisms. J. Lapointe and L. Brakier-Gingras. Georgetown, TX and New York, NY, Eurekah.com : Landes Bioscience and Kluwer Academic/Plenum Publishers**:** 298-321.

de Smit, M. H., Verlaan, P. W., Duin, J. van, Pleij, C. W. (2008). "Intracistronic transcriptional polarity enhances translational repression: a new role for Rho." Mol. Microbiol. **69**(5): 1278-1289.

Demo, G., Rasouly, A., Vasilyev, N., Svetlov, V., Loveland, A. B., Diaz-Avalos, R., Grigorieff, N., Nudler, E., Korostelev, A. A. (2017). "Structure of RNA polymerase bound to ribosomal 30S subunit." eLife **6**: e28560.

Drogemuller, J., Strauss, M., Schweimer, K., Wohrl, B. M., Knauer, S. H., Rosch, P. (2015). "Exploring RNA polymerase regulation by NMR spectroscopy." Sci. Rep. **5**: 10825.

Drogemuller, J., Strauss, M., Schweimer, K., Jurk, M., Rosch, P., Knauer, S. H. (2015). "Determination of RNA polymerase binding surfaces of transcription factors by NMR spectroscopy." Sci. Rep. **5**: 16428.

Dunkle, J. A., Wang, L., Feldman, M. B., Pulk, A., Chen, V. B., Kapral, G. J., Noeske, J., Richardson, J. S., Blanchard, S. C., Cate, J. H. D. (2011) "Structures of the Bacterial Ribosome in Classical and Hybrid States of TRNA Binding." Science ***332*** (6032), 981–984.

Dutta, D., Shatalin, K., Epshtein, V., Gottesman, M. E., Nudler, E. (2011). "Linking RNA polymerase backtracking to genome instability in *E. coli*." Cell **146**(4): 533-543.

Eiler, D., Lin, J., Simonetti, A., Klaholz, B. P., Steitz, T. A. (2013) "Initiation Factor 2 Crystal Structure Reveals a Different Domain Organization from Eukaryotic Initiation Factor 5B and Mechanism among Translational GTPases." Proceedings of the National Academy of Sciences ***110*** (39), 15662–15667.

Elgamal, S., Artsimovitch, I., Ibba, M. (2016). "Maintenance of Transcription-Translation Coupling by Elongation Factor P." MBio **7**(5).

Elvekrog, M. M., Walter, P. (2015). "Dynamics of co-translational protein targeting." Curr Opin Chem Biol **29**: 79-86.

Endesfelder, U., Finan, K., Holden, S. J., Cook, P. R., Kapanidis, A. N., Heilemann, M. (2013). "Multiscale spatial organization of RNA polymerase in *Escherichia coli*." Biophys J **105**(1): 172-181.

Epshtein, V., Nudler, E. (2003). "Cooperation between RNA polymerase molecules in transcription elongation." Science **300**(5620): 801-805.

Eriksen, M., Sneppen, K., Pedersen, S., Mitarai, N. (2017). "Occlusion of the Ribosome Binding Site Connects the Translational Initiation Frequency, mRNA Stability and Premature Transcription Termination." Frontiers in microbiology, ***8***:362.

Fan, H., Conn, A. B., Williams, P. B., Hahm, J., Gamper, H. B., Hou, Y. M., O'Leary, S. E., Wang, Y., Blaha, G. M. (2017). "Transcription-translation coupling: direct interactions of RNA polymerase with ribosomes and ribosomal subunits." Nucleic Acids Res. **45**(19): 11043-11055.

Feklistov, A., Darst, S. A. (2011) "Structural Basis for Promoter −10 Element Recognition by the Bacterial RNA Polymerase σ Subunit." Cell ***147*** (6), 1257–1269.

Finn, R. D. (2000) "Escherichia Coli RNA Polymerase Core and Holoenzyme Structures." The EMBO Journal ***19*** (24), 6833–6844.

Fong, B. A., Gillies, A. R., Ghazi, I., LeRoy, G., Lee, K. C., Westblade, L. F., Wood, D. W. (2010). "Purification of *Escherichia coli* RNA polymerase using a self-cleaving elastin-like polypeptide tag." Protein Sci **19**(6): 1243-1252.

Franklin, N. C., Luria, S. E. (1961). "Transduction by bacteriophage P-1 and the properties of the lac genetic region in *E. coli* and *S. dysenteriae*." Virology **15**: 299-311.

French, S. L., Santangelo, T. J., Beyer, A. L., Reeve, J. N. (2007). "Transcription and translation are coupled in Archaea." Mol. Biol. Evol. **24**(4): 893-895.

Fu, Z., Kaledhonkar, S., Borg, A., Sun, M., Chen, B., Grassucci, R. A., Ehrenberg, M., Frank, J. (2016) "Key Intermediates in Ribosome Recycling Visualized by Time-Resolved Cryoelectron Microscopy." Structure ***24*** (12), 2092–2101.

Gibbs, M. R., Moon, K. M., Chen, M., Balakrishnan, R., Foster, L. J., Fredrick, K. (2017). "Conserved GTPase LepA (Elongation Factor 4) functions in biogenesis of the 30S subunit of the 70S ribosome." Proc Natl Acad Sci U S A **114**(5): 980-985.

Gill, S., Weitzel, S., Hippel, P. von (1991). "*Escherichia coli* sigma 70 and NusA proteins. I. Binding interactions with core RNA polymerase in solution and within the transcription complex." J Mol Biol **220**(2): 307-324.

Gordiyenko, Y., Deroo, S., Zhou, M., Videler, H., Robinson, C. V. (2008). "Acetylation of L12 increases interactions in the *Escherichia coli* ribosomal stalk complex." J Mol Biol **380**(2): 404-414.

Griffin, N. M., Yu, J., Long, F., Oh, P., Shore, S., Li, Y., Koziol, J. A., Schnitzer, J. E. (2010). "Label-free, normalized quantification of complex mass spectrometry data for proteomic analysis." Nat Biotechnol **28**(1): 83-89.

Grigoriadou, C., Marzi, S., Pan, D., Gualerzi, C. O., Cooperman, B. S. (2008) "The Translational Fidelity Function of IF3 During the Transition from 30S to 70S Initiation Complex." J. Mol Biol **373**(3): 551-561.

Grunberg-Manago, M., Dessen, P., Pantaloni, D., Godefroy-Colburn, T., Wolfe, A. D., D., A., Dondon, J. (1975). "Light-scattering studies showing the effect of initiation factors on the reversible dissociation of *Escherichia coli* ribosomes." Journal of molecular biology, ***94***(3), 461–478.

Gualerzi, C. O., Pon, C. L. (2015). "Initiation of mRNA translation in bacteria: structural and dynamic aspects." Cell Mol Life Sci **72**(22): 4341-4367.

Harris, S. J., Williams, R. C., Jr.,, Lee, J. C. (1995). "Self-association of *Escherichia coli* DNA-dependent RNA polymerase core enzyme." Biochemistry **34**(27): 8752-8762.

Hartz, D., McPheeters, D. S., Gold, L. (1989). "Selection of the initiator tRNA by Escherichia coli initiation factors." Genes & development, ***3***(12A), 1899–1912.

Hawley, D. K., McClure, W. R. (1983) "Compilation and Analysis of *Escherichia Coli* Promoter DNA Sequences." Nucl Acids Res ***11*** (8), 2237–2255.

Herbert, K. M., Zhou, J., Mooney, R. A., Porta, A. L., Landick, R., Block, S. M. (2010). "*E. coli* NusG inhibits backtracking and accelerates pause-free transcription by promoting forward translocation of RNA polymerase." J. Mol. Biol. **399**(1): 17-30.

Hobot, J. A., Villiger, W., Escaig, J., Maeder, M., Ryter, A., Kellenberger, E. (1985). "Shape and fine structure of nucleoids observed on sections of ultrarapidly frozen and cryosubstituted bacteria." J. Bacteriol. **162**(3): 960-971.

Holschuh, K., Gassen, H. G. (1982). "Mechanism of translocation. Binding equilibria between the ribosome, mRNA analogues, and cognate tRNAs." J Biol Chem **257**(4): 1987-1992.

Hussain, T., Llácer, J. L., Wimberly, B. T., Kieft, J. S., Ramakrishnan, V. (2016). "Large-Scale Movements of IF3 and tRNA during Bacterial Translation Initiation." Cell, **167**(1): 133–144.e13.

Iyer, S., Le, D., Park, B. R., Kim, M. (2018). "Distinct mechanisms coordinate transcription and translation under carbon and nitrogen starvation in *Escherichia coli*." Nat. Microbiol. **3**(6): 741-748.

Jacob, F., Monod, J. (1961). "On the Regulation of Gene Activity. Cellular Regulatory Mechansims." L. Frisch. Cold Spring Harbor, L.I., New York, The Biological Laboratory. **XXVI:** 193-211.

Jain, C. (2008). "The *E. coli* RhlE RNA helicase regulates the function of related RNA helicases during ribosome assembly." RNA **14**(2): 381-389.

Jiang, M., Sullivan, S. M., Walker, A. K., Strahler, J. R., Andrews, P. C., Maddock, J. R. (2007). "Identification of novel *Escherichia coli* ribosome-associated proteins using isobaric tags and multidimensional protein identification techniques." Journal of bacteriology, ***189***(9), 3434–3444.

Julián, P., Milon, P., Agirrezabala, X., Lasso, G., Gil, D., Rodnina, M. V., Valle, M. (2011). "The cryo-EM structure of a complete 30S translation initiation complex from escherichia coli." PLoS Biol, **9**(7): e1001095.

Kaempfer, R. (1974). "The Ribosome Cycle" Ribosomes. M. Nomura, A. Tissieres and P. Lengyel, Cold Spring Harbor Laboratory**:** 679-704.

Kang, J. Y., Olinares, P. D., Chen, J., Campbell, E. A., Mustaev, A., Chait, B. T., Gottesman, M. E., Darst, S. A. (2017). "Structural basis of transcription arrest by coliphage HK022 Nun in an *Escherichia coli* RNA polymerase elongation complex." eLife **6**.

Kang, J. Y., Mooney, R. A., Nedialkov, Y., Saba, J., Mishanina, T. V., Artsimovitch, I., Landick, R., Darst, S. A. (2018). "Structural Basis for Transcript Elongation Control by NusG Family Universal Regulators." Cell **173**(7): 1650-1662 e1614.

Kansara, S. G., Sukhodolets, M. V. (2011). "Oligomerization of the *E. coli* core RNA polymerase: formation of (alpha2betabeta'omega)2-DNA complexes and regulation of the oligomerization by auxiliary subunits." PLoS One **6**(4): e18990.

Karimi, R., Pavlov, M. Y., Buckingham, R. H., Ehrenberg, M. (1999) "Novel Roles for Classical Factors at the Interface between Translation Termination and Initiation." Molecular Cell ***3*** (5), 601–609.

Kashkina, E., Anikin, M., Tahirov, T. H., Kochetkov, S. N., Vassylyev, D. G., Temiakov, D. (2005). "Elongation complexes of *Thermus thermophilus* RNA polymerase that possess distinct translocation conformations." Nucleic Acids Res **34**(14): 4036-4045.

Kato, T., Yoshida, H., Miyata, T., Maki, Y., Wada, A., Namba, K. (2010). "Structure of the 100S ribosome in the hibernation stage revealed by electron cryomicroscopy." Structure **18**(6): 719-724.

Katunin, V. I., Savelsbergh, A., Rodnina, M. V., Wintermeyer, W. (2002). "Coupling of GTP hydrolysis by elongation factor G to translocation and factor recycling on the ribosome." Biochemistry **41**(42): 12806-12812.

Kim, H. K., Liu, F., Fei, J., Bustamante, C., Gonzalez, R. L., Jr.,, Tinoco, I., Jr., (2014). "A frameshifting stimulatory stem loop destabilizes the hybrid state and impedes ribosomal translocation." Proc Natl Acad Sci U S A **111**(15): 5538-5543.

Klaholz, B. P. (2017). "The Ribosome Holds the RNA Polymerase on Track in Bacteria." Trends Biochem. Sci. **42**(9): 686-689.

Klumpp, S., Hwa, T. (2009). "Traffic patrol in the transcription of ribosomal RNA." RNA Biol. **6**(4): 392-394.

Kohler, R., Mooney, R. A., Mills, D. J., Landick, R., Cramer, P. (2017). "Architecture of a transcribing-translating expressome." Science **356**(6334): 194-197.

Komarova, A. V., Tchufistova, L. S., Dreyfus, M., Boni, I. V. (2005) "AU-rich sequences within 5' untranslated leaders enhance translation and stabilize mRNA in *Escherichia coli*." Journal of bacteriology, ***187***(4), 1344–1349.

Korostelev, A., Trakhanov, S., Asahara, H., Laurberg, M., Lancaster, L., Noller, H. F. (2007). "Interactions and dynamics of the Shine–Dalgarno helix in the 70S ribosome." Proc Natl Acad Sci, **104**(43): 16840-16843.

Korostelev, A., Trakhanov, S., Laurberg, M., Noller, H. F. (2006). "Crystal structure of a 70S ribosome-tRNA complex reveals functional interactions and rearrangements." Cell, **126**(6): 1065–1077.

Kraulis, P.J. (1991) "MOLSCRIPT: A program to produce both detailed and schematic plots of proteins structures." J. Appl. Cryst, **24**:946–950.

Krupp, F., Said, N., Huang, Y. H., Loll, B., Burger, J., Mielke, T., Spahn, C. M. T., Wahl, M. C. (2019). "Structural Basis for the Action of an All-Purpose Transcription Anti-termination Factor." Mol. Cell **74**(1): 143-157 e145.

Landick, R., Turnbough, C. L., Jr.,, Yanofsky, C. (1996). "Transcription attenuation. Escherichia coli and Salmonella:" Cellular and Molecular Biology. F. C. Neidhardt. Washington, D.C., USA, ASM**:** 1263-1286.

Landick, R., Carey, J., Yanofsky, C. (1985). "Translation activates the paused transcription complex and restores transcription of the trp operon leader region." Proc. Natl. Acad. Sci. USA **82**(14): 4663-4667.

Larson, M. H., Mooney, R. A., Peters, J. M., Windgassen, T., Nayak, D., Gross, C. A., Block, S. M., Greenleaf, W. J., Landick, R., Weissman, J. S. (2014). "A pause sequence enriched at translation start sites drives transcription dynamics *in vivo*." Science **344**(6187): 1042-1047.

Lawson, M. R., Ma, W., Bellecourt, M. J., Artsimovitch, I., Martin, A., Landick, R., Schulten, K., Berger, J. M. (2018). "Mechanism for the Regulated Control of Bacterial Transcription Termination by a Universal Adaptor Protein." Mol. Cell **71**(6): 911-922 e914.

Lee, S. J., Gralla, J. D. (2004). "Osmo-regulation of bacterial transcription via poised RNA polymerase." Mol Cell **14**(2): 153-162.

Lesnik, E. A., Sampath, R., Levene, H. B., Henderson, T. J., McNeil, J. A., Ecker, D. J. (2001). "Prediction of rho-independent transcriptional terminators in *Escherichia coli*." Nucleic Acids Res **29**(17): 3583-3594.

Lewicki, B. T., Margus, T., Remme, J., Nierhaus, K. H. (1993) "Coupling of rRNA transcription and ribosomal assembly in vivo. Formation of active ribosomal subunits in Escherichia coli requires transcription of rRNA genes by host RNA polymerase which cannot be replaced by bacteriophage T7 RNA polymerase." Journal of molecular biology, ***231***(3), 581–593.

Li, G. W., Oh, E., Weissman, J. S. (2012). "The anti-Shine-Dalgarno sequence drives translational pausing and codon choice in bacteria." Nature **484**(7395): 538-541.

Li, J., Mason, S. W., Greenblatt, J. (1992). "Elongation factor NusG interacts with termination factor rho to regulate termination and antitermination of transcription." Genes Dev. **7**(1): 161-172.

Li, R., Zhang, Q., Li, J., Shi, H. (2016). "Effects of cooperation between translating ribosome and RNA polymerase on termination efficiency of the Rho-independent terminator." Nucleic Acids Res. **44**(6): 2554-2563.

Lide, R. D. "CRC Handbook of Chemistry, Physics,, Raton, 88th Edition." Boca, Press, Fla: CRC

Liu, B., Zuo, Y., Steitz, T. A. (2015). "Structural basis for transcription reactivation by RapA." Proc Natl Acad Sci U S A **112**(7): 2006-2010.

López-Alonso, J. P., Fabbretti, A., Kaminishi, T., Iturrioz, I., Brandi, L., Gil-Carton, D., Gualerzi, C. O., Fucini, P., Connell, S. R. (2017). "Structure of a 30S pre-initiation complex stalled by GE81112 reveals structural parallels in bacterial and eukaryotic protein synthesis initiation pathways." Nucleic acids research, ***45***(4), 2179–2187.

Lowery-Goldhammer, C., Richardson, J. P. (1974) "An RNA-Dependent Nucleoside Triphosphate Phosphohydrolase (ATPase) Associated with Rho Termination Factor." Proceedings of the National Academy of Sciences ***71*** (5), 2003–2007.

Lubkowska, L., Maharjan, A. S., Komissarova, N. (2011) "RNA Folding in Transcription Elongation Complex: Implication for Transcription Termination." J. Biol. Chem. ***286*** (36), 31576–31585.

Ma, C., Mobli, M., Yang, X., Keller, A. N., King, G. F., Lewis, P. J. (2015). "RNA polymerase-induced remodelling of NusA produces a pause enhancement complex." Nucleic Acids Res, **43**(5): 2829-2840.

Mangiarotti, G., Schlesinger, D. (1966) "Polyribosome Metabolism in *Eschericia coli*. I. Extraction of Polyribosomes and Ribosomal Subunits from Fragile, Growing *Eschericia coli*." J. Mol. Biol. **20**(1):123-143.

Maracci, C., Peske, F., Dannies, E., Pohl, C., Rodnina, M. V. (2014). "Ribosome-induced tuning of GTP hydrolysis by a translational GTPase." Proc Natl Acad Sci U S A **111**(40): 14418-14423.

Martin, R. G., Gillette, W. K., Martin, N. I., Rosner, J. L. (2002). "Complex formation between activator and RNA polymerase as the basis for transcriptional activation by MarA and SoxS in *Escherichia coli*." Mol Microbiol **43**(2): 355-370.

Marzi, S., Myasnikov, A. G., Serganov, A., Ehresmann, C., Romby, P., Yusupov, M., Klaholz, B. P. (2007). "Structured mRNAs regulate translation initiation by binding to the platform of the ribosome." Cell **130**(6): 1019-1031.

McGary, K., Nudler, E. (2013). "RNA polymerase and the ribosome: the close relationship." Curr. Opin. Microbiol. **16**(2): 112-117.

Merritt, E. A., Bacon, D. J. (1997). "Raster3D: photorealistic molecular graphics." Methods in enzymology, **277**:505–524.

Miller, O., Hamkalo, B., Thomas, C. (1970). "Visualization of bacterial genes in action." Science **169**(3943): 392-395.

Mirkin, E. V., Mirkin, S. M. (2007). "Replication fork stalling at natural impediments." Microbiol. Mol. Biol. Rev. **71**(1): 13-35.

Mishanina, T. V., Palo, M. A., Nayak, D., Mooney, R. A., Landick, R. (2017) "Trigger Loop of RNA Polymerase Is a Positional, Not Acid–Base, Catalyst for Both Transcription and Proofreading." Proc Natl Acad Sci USA 201702383.

Miskin, R., Zamir, A., Elson, D. (1970). "Inactivation and reactivation of ribosomal subunits: The peptidyl transferase activity of the 50 s subunit of *Escherichia coli*." J Mol Biol, **54**(2): 355-378.

Mitarai, N., Sneppen, K., Pedersen, S. (2008). "Ribosome collisions and translation efficiency: optimization by codon usage and mRNA destabilization." J. Mol. Biol. **382**(1): 236-245.

Moazed, D., Stolk, B. J. Van, Douthwaite, S., Noller, H.F. (1986). "Interconversion of active and inactive 30 S ribosomal subunits is accompanied by a conformational change in the decoding region of 16 S rRNA." J Mol Biol, **191**(3): 483-493.

Mohammad, F., Woolstenhulme, C. J., Green, R., Buskirk, A. R. (2016). "Clarifying the Translational Pausing Landscape in Bacteria by Ribosome Profiling." Cell Rep **14**(4): 686-694.

Mohan, S., Donohue, J. P., Noller, H. F. (2014). "Molecular mechanics of 30S subunit head rotation." Proc Natl Acad Sci, **111**(37): 13325-13330.

Mondal, J., Bratton, B. P., Li, Y., Yethiraj, A., Weisshaar, J. C. (2011). "Entropy-based mechanism of ribosome-nucleoid segregation in *E. coli* cells." Biophys. J. **100**(11): 2605-2613.

Monro, R. E., Staehelin, T., Celma, M. L., Vazquez, D. (1969). "The peptidyl transferase activity of ribosomes." Cold Spring Harbor symposia on quantitative biology, ***34***:357–368.

Mooney, R. A., Schweimer, K., Rösch, P., Gottesman, M., Landick, R. (2009). "Two structurally independent domains of *E. coli* NusG create regulatory plasticity via distinct interactions with RNA polymerase and regulators." J. Mol. Biol. **391**(2): 341-358.

Mooney, R., Davis, S., Peters, J., Rowland, J., Ansari, A., Landick, R. (2009). "Regulator trafficking on bacterial transcription units *in vivo*." Mol. Cell **33**(1): 97-108.

Morrison, C. A., Tischendorf, G., Stoffler, G., Garrett, R. A. (1977). "Accessibility of proteins in 50S ribosomal subunits of *Escherichia coli* to antibodies: an ultracentrifugation study." Mol Gen Genet **151**(3): 245-252.

Murakami, K. S. (2002) "Structural Basis of Transcription Initiation: An RNA Polymerase Holoenzyme-DNA Complex." Science ***296*** (5571), 1285–1290.

Murakami, K. S., Darst, S. A. (2003) "Bacterial RNA Polymerases: The Wholo Story." Current Opinion in Structural Biology ***13*** (1), 31–39.

Mustafi, M., Weisshaar, J. C. (2018). "Simultaneous Binding of Multiple EF-Tu Copies to Translating Ribosomes in Live *Escherichia coli*." MBio **9**(1).

Nedialkov, Y. A., Opron, K., Assaf, F., Artsimovitch, I., Kireeva, M. L., Kashlev, M., Cukier, R. I., Nudler, E., Burton, Z. F. (2013). "The RNA polymerase bridge helix YFI motif in catalysis, fidelity and translocation." Biochim Biophys Acta **1829**(2): 187-198.

Neuhoff, V., Arold, N., Taube, D., Ehrhardt, W. (1988) "Improved staining of proteins in polyacrylamide gels including isoelectric focusing gels with clear background at nanogram sensitivity using Coomassie Brilliant Blue G-250 and R-250." Electrophoresis. **9**(6):255-62.

Nevskaya, N., Tishchenko, S., Gabdoulkhakov, A., Nikonova, E., Nikonov, O., Nikulin, A., Platonova, O., Garber, M., Nikonov, S., Piendl, W. (2005). "Ribosomal protein L1 recognizes the same specific structural motif in its target sites on the autoregulatory mRNA and 23S rRNA." Nucleic Acids Res **33**(2): 478-485.

Noll, M., Schreier, M. H., Noll, H. (1973) "Structural dynamics of bacterial ribosomes. I. Characterization of vacant couples and their relation to complexed ribosomes." J. Mol. Biol. **75**(2):281-294.

Ogle, J. M., Ramakrishnan, V. (2005) "Structural Insights into Translation Fidelity." Annu. Rev. Biochem. ***74*** (1), 129–177.

Ogle, J. M., Murphy, F. V., Tarry, M. J., Ramakrishnan, V. (2002) "Selection of TRNA by the Ribosome Requires a Transition from an Open to a Closed Form." Cell ***111*** (5), 721–732.

O'Reilly, F. J., Xue, L., Graziadei, A., Sinn, L., Lenz, S., Tegunov, D., Blötz, C., Singh, N., Hagen, W., Cramer, P., Stülke, J., Mahamid, J., Rappsilber, J. (2020). “In-cell architecture of an actively transcribing-translating expressome.“ Science, ***369***(6503), 554–557.

Pan, T., Artsimovitch, I., Fang, X. W., Landick, R., Sosnick, T. R. (1999) "Folding of a Large Ribozyme during Transcription and the Effect of the Elongation Factor NusA." Proceedings of the National Academy of Sciences ***96*** (17), 9545–9550.

Pani, B., Nudler, E. (2017). "Mechanistic insights into transcription coupled DNA repair." DNA Repair (Amst) **56**: 42-50.

Park, J. S., Roberts, J. W. (2006) "Role of DNA Bubble Rewinding in Enzymatic Transcription Termination." Proceedings of the National Academy of Sciences ***103*** (13), 4870–4875.

Petersen, H. U., Kruse, T. A., Worm-Leonhard, H., Siboska, G. E., Clark, B. F. C., Boutorin, A. S., Remy, P., Ebel, J. P., Dondon, J., Grunberg-Manago, M. A. (1981) "Study of the Interaction of *Escherichia Coli* Initiation Factor IF2 with Formylmethionyl-TRNA $^{Met}{}_{f}$ by Partial Digestion with Cobra Venom Ribonuclease." FEBS Letters ***128*** (1), 161–165.

Plochowietz, A., Farrell, I., Smilansky, Z., Cooperman, B. S., Kapanidis, A. N. (2017). "*In vivo* single-RNA tracking shows that most tRNA diffuses freely in live bacteria." Nucleic Acids Res. **45**(2): 926-937.

Proshkin, S., Rahmouni, A. R., Mironov, A., Nudler, E. (2010). "Cooperation between translating ribosomes and RNA polymerase in transcription elongation." Science **328**(5977): 504-508.

Qin, Y., Polacek, N., Vesper, O., Staub, E., Einfeldt, E., Wilson, D. N., Nierhaus, K. H. (2006). "The highly conserved LepA is a ribosomal elongation factor that back-translocates the ribosome." Cell **127**(4): 721-733.

Qu, X., Lancaster, L., Noller, H. F., Bustamante, C., Tinoco, I. (2012). "Ribosomal protein S1 unwinds double-stranded RNA in multiple steps." Proc Natl Acad Sci U S A **109**(36): 14458-14463.

Raguin, O., Gruaz-Guyon, A., Barbet, J. (2002). "Equilibrium expert: an add-in to Microsoft Excel for multiple binding equilibrium simulations and parameter estimations." Anal Biochem **310**(1): 1-14.

Ramakrishnan, V. (2002) “Ribosome Structure and the Mechanism of Translation.” *Cell*, ***108*** (4), 557–572.

Ratje, A. H., Loerke, J., Mikolajka, A., Brünner, M., Hildebrand, P. W., Starosta, A. L., Dönhöfer, A., Connell, S. R., Fucini, P., Mielke, T., Whitford, P. C., Onuchic, J. N., Yu, Y., Sanbonmatsu, K. Y., Hartmann, R. K., Penczek, P. A., Wilson, D. N., Spahn, C. M. T. (2010) "Head Swivel on the Ribosome Facilitates Translocation by Means of Intra-Subunit tRNA Hybrid Sites. Nature ***468*** (7324), 713–716.

Ray-Soni, A., Bellecourt, M. J., Landick, R. (2016). "Mechanisms of Bacterial Transcription Termination: All Good Things Must End." Annu. Rev. Biochem. **85**: 319-347.

Richardson, J. P. (2002) "Rho-Dependent Termination and ATPases in Transcript Termination." Biochimica et Biophysica Acta - Gene Structure and Expression ***1577*** (2), 251–260.

Richardson, J. P., Grimley, C., Lowery, C. (1975). "Transcription termination factor rho activity is altered in *Escherichia coli* with *suA* gene mutations." Proc. Natl. Acad. Sci. USA **72**(5): 1725-1728.

Rippa, V., Cirulli, C., Palo, B. Di, Doti, N., Amoresano, A., Duilio, A. (2010). "The ribosomal protein L2 interacts with the RNA polymerase alpha subunit and acts as a transcription modulator in *Escherichia coli*." J. Bacteriol. **192**(7): 1882-1889.

Rippe, K. (2001). "Making contacts on a nucleic acid polymer." Trends Biochem. Sci. **26**(12): 733-740.

Robertson, J. M., Wintermeyer, W. (1981). “Effect of Translocation on Topology and Conformation of Anticodon and D Loops of $tRNA^{Phe}$.” J. Mol. Biol. **151**(1):57-90

Robertson, J. M., Paulsen, H., Wintermeyer, W. (1988). "Pre-steady-state kinetic studies on ribosomal translocation." Methods Enzymol **164**: 581-597.

Rodnina, M. V. (2016). "The ribosome in action: Tuning of translational efficiency and protein folding." Protein Sci **25**(8): 1390-1406.

Rodnina, M. V. (2018). “Translation in prokaryotes.” Cold Spring Harb Perspect Biol, **10**(9), a032664.

Ron, E. Z., Kohler, R. E., Davis, B. D. (1968). “Magnesium Ion Dependence of Free and Polysomal Ribosomes from *Eschericia coli*.” J. Mol Biol. **36**(1):83-89.

Ruff, E. F., Record, M. T., Jr.,, Artsimovitch, I. (2015). "Initial events in bacterial transcription initiation." Biomolecules **5**(2): 1035-1062.

Ruff, E. F., Kontur, W. S., Record, M. T., Jr. (2015). "Using solutes and kinetics to probe large conformational changes in the steps of transcription initiation." Methods Mol Biol **1276**: 241-261.

Saecker, R. M., Record, M. T., deHaseth, P. L. (2011) "Mechanism of Bacterial Transcription Initiation: RNA Polymerase - Promoter Binding, Isomerization to Initiation-Competent Open Complexes, and Initiation of RNA Synthesis." Journal of Molecular Biology ***412*** (5), 754–771.

Said, N., Krupp, F., Anedchenko, E., Santos, K. F., Dybkov, O., Huang, Y. H., Lee, C. T., Loll, B., Behrmann, E., Burger, J., Mielke, T., Loerke, J., Urlaub, H., Spahn, C. M. T., Weber, G., Wahl, M. C. (2017). "Structural basis for lambdaN-dependent processive transcription antitermination." Nat. Microbiol. **2**: 17062.

Salah, P., Bisaglia, M., Aliprandi, P., Uzan, M., Sizun, C., Bontems, F. (2009). "Probing the relationship between Gram-negative and Gram-positive S1 proteins by sequence analysis." Nucleic Acids Res **37**(16): 5578-5588.

Sanamrad, A., Persson, F., Lundius, E. G., Fange, D., Gynna, A. H., Elf, J. (2014). "Single-particle tracking reveals that free ribosomal subunits are not excluded from the *Escherichia coli* nucleoid." Proc. Natl. Acad. Sci. USA **111**(31): 11413-11418.

Saxena, S., Myka, K. K., Washburn, R., Costantino, N., Court, D. L., Gottesman, M. E. (2018). "*Escherichia coli* transcription factor NusG binds to 70S ribosomes." Mol. Microbiol. **108**(5): 495-504.

Schilling-Bartetzko, S., Franceschi, F., Sternbach, H., Nierhaus, K. H. (1992). "Apparent association constants of tRNAs for the ribosomal A, P, and E sites." J Biol Chem **267**(7): 4693-4702.

Schmeing, T. M., Ramakrishnan, V. (2009) "What Recent Ribosome Structures Have Revealed about the Mechanism of Translation." Nature ***461*** (7268), 1234–1242.

Schmeing, T. M., Huang, K. S., Kitchen, D. E., Strobel, S. A., Steitz, T. A. (2005) "Structural Insights into the Roles of Water and the 2′ Hydroxyl of the P Site TRNA in the Peptidyl Transferase Reaction." Molecular Cell ***20*** (3), 437–448.

Schneider, C.A., Rasband, W. S., Eliceri, K. W. (2012) “NIH Image to ImageJ: 25 years of image analysis.” Nature Methods. **9**(7):671-675

Seligmann, H., Warthi, G. (2017). "Genetic Code Optimization for Cotranslational Protein Folding: Codon Directional Asymmetry Correlates with Antiparallel Betasheets, tRNA Synthetase Classes." Comput Struct Biotechnol J **15**: 412-424.

Selmer, M., Dunham, C., Murphy, F., Weixlbaumer, A., Petry, S., Kelley, A., Weir, J., Ramakrishnan, V. (2006). "Structure of the 70S ribosome complexed with mRNA and tRNA." Science **313**(5795): 1935-1942.

Shaner, S. L., Piatt, D. M., Wensley, C. G., Yu, H., Burgess, R. R., Record, M. T., Jr., (1982). "Aggregation equilibria of *Escherichia coli* RNA polymerase: evidence for anion-linked conformational transitions in the protomers of core and holoenzyme." Biochemistry **21**(22): 5539-5551.

Sharma, M. R., Barat, C., Wilson, D. N., Booth, T. M., Kawazoe, M., Hori-Takemoto, C., Shirouzu, M., Yokoyama, S., Fucini, P., Agrawal, R. K. (2005). "Interaction of Era with the 30S ribosomal subunit implications for 30S subunit assembly." Mol Cell **18**(3): 319-329.

Shepherd, N., Dennis, P., Bremer, H. (2001). "Cytoplasmic RNA Polymerase in *Escherichia coli*." J. Bacteriol. **183**(8): 2527-2534.

Shi, X., Khade, P. K., Sanbonmatsu, K. Y., Joseph, S. (2012) "Functional Role of the Sarcin-Ricin Loop of the 23S rRNA in the Elongation Cycle of Protein Synthesis." Journal of Molecular Biology. **419**(3-4): 125-138

Shoji, S., Walker, S. E., Fredrick, K. (2009) "Ribosomal Translocation: One Step Closer to the Molecular Mechanism." ACS Chem. Biol. ***4*** (2), 93–107.

Simonetti, A., Marzi, S., Fabbretti, A., Hazemann, I., Jenner, L., Urzhumtsev, A., Gualerzi, C. O., Klaholz, B. P. (2013). "Structure of the protein core of translation initiation factor 2 in apo, GTP-bound and GDP-bound forms." Acta crystallographica. Section D, Biological crystallography, ***69***(Pt 6), 925–933.

Simonetti, A., Marzi, S., Myasnikov, A. G., Fabbretti, A., Yusupov, M., Gualerzi, C. O., Klaholz, B.P (2008). "Structure of the 30S translation initiation complex." Nature, **455**(7211): 416-420.

So, A.G., Davie,, E.W.,, Epstein,, R.,, Tissieres,, A., (1967) "Effects of cations on DNAdependent RNA polymerase." Proc Natl Acad Sci U S A, **58**, 1739-1746.

Sørensen, M. A., Fricke, J., Pedersen, S. (1998). "Ribosomal protein S1 is required for translation of most, if not all, natural mRNAs *in Escherichia coli in vivo*." J. Mol. Biol. **280**(4): 561-569.

Spahn, C., Cella-Zannacchi, F., Endesfelder, U., Heilemann, M. (2015). "Correlative super-resolution imaging of RNA polymerase distribution and dynamics, bacterial membrane and chromosomal structure in *Escherichia coli*." Methods Appl. Fluoresc. **3**(1): 014005.

Spivak, G. (2016). "Transcription-coupled repair: an update." Arch Toxicol **90**(11): 2583-2594.

Stark, H. (2010). "GraFix: stabilization of fragile macromolecular complexes for single particle cryo-EM." Methods Enzymol. **481**: 109-126.

Steiner, T., Kaiser, J. T., Marinkoviç, S., Huber, R., Wahl, M. C. (2002). "Crystal structures of transcription factor NusG in light of its nucleic acid- and protein-binding activities." EMBO J. **21**(17): 4641-4653.

Steitz, T. A. (1998) "A Mechanism for All Polymerases." Nature ***391*** (6664), 231–232.

Stevens, A., Emery, A. J., Jr.,, Sternberger, N. (1966). "Sedimentation properties of *E. coli* RNA polymerase and its complexes with polyuridylic acid." Biochem Biophys Res Commun **24**(6): 929-936.

Stevenson-Jones, F., Woodgate, J., Castro-Roa, D., Zenkin, N. (2020). “Ribosome reactivates transcription by physically pushing RNA polymerase out of transcription arrest.” Proceedings of the National Academy of Sciences of the United States of America, ***117***(15), 8462–8467.

Stoffler, G., Hasenbank, R., Lutgehaus, M., Maschler, R., Morrison, C. A., Zeichhardt, H., Garrett, R. A. (1973). "The accessibility of proteins of the *Escherichia coli* 30S ribosomal subunit to antibody binding." Mol Gen Genet **127**(2): 89-110.

Stracy, M., Lesterlin, C., Leon, F. Garza de, Uphoff, S., Zawadzki, P., Kapanidis, A. N. (2015). "Live-cell superresolution microscopy reveals the organization of RNA polymerase in the bacterial nucleoid." Proc. Natl. Acad. Sci. USA **112**(32): E4390-4399.

Studer, S. M., Joseph, S. (2006). "Unfolding of mRNA secondary structure by the bacterial translation initiation complex." Mol Cell **22**(1): 105-115.

Suh, W.C., Leirmo,, S.,, Record,, M.T.,, Jr., (1992) “Roles of Mg2+ in the mechanism of formation and dissociation of open complexes between Escherichia coli RNA polymerase and the lambda PR promoter: kinetic evidence for a second open complex requiring Mg^{2+}” . Biochemistry, **31**, 7815-7825.

Sukhodolets, M. V., Garges, S. (2003). "Interaction of *Escherichia coli* RNA polymerase with the ribosomal protein S1 and the Sm-like ATPase Hfq." Biochemistry **42**(26): 8022-8034.

Sukhodolets, M. V., Garges, S., Adhya, S. (2006). "Ribosomal protein S1 promotes transcriptional cycling." RNA **12**(8): 1505-1513.

Sullivan, S. L., Gottesman, M. E. (1992). "Requirement for *E. coli* NusG protein in factor-dependent transcription termination." Cell **68**(5): 989-994.

Sussman, J. K., Simons, E. L., Simons, R. W. (1996) "*Escherichia Coli* Translation Initiation Factor 3 Discriminates the Initiation Codon *in Vivo*." Molecular Microbiology ***21*** (2), 347–360.

Thommen, M., Holtkamp, W., Rodnina, M. V. (2017). "Co-translational protein folding: progress and methods." Curr Opin Struct Biol **42**: 83-89.

Tomsic, J. (200) "Late Events of Translation Initiation in Bacteria: A Kinetic Analysis." The EMBO Journal ***19*** (9), 2127–2136.

Torres, M., Condon, C., Balada, J. M., Squires, C., Squires, C. L. (2001). "Ribosomal protein S4 is a transcription factor with properties remarkably similar to NusA, a protein involved in both non-ribosomal and ribosomal RNA antitermination." EMBO J. **20**(14): 3811-3820.

Tsai, Y. C., Du, D., Domínguez-Malfavón, L., Dimastrogiovanni, D., Cross, J., Callaghan, A. J., García-Mena, J., Luisi, B. F. (2012). “Recognition of the 70S ribosome and polysome by the RNA degradosome in *Escherichia coli*.” Nucleic acids research, ***40***(20), 10417–10431.

Turnbough, C. L., Jr.,, Hicks, K. L., Donahue, J. P. (1983). "Attenuation control of pyrBI operon expression in *Escherichia coli* K-12." Proc. Natl. Acad. Sci. USA **80**(2): 368-372.

Turtola, M., Belogurov, G. A. (2016). "NusG inhibits RNA polymerase backtracking by stabilizing the minimal transcription bubble." Elife **5**.

Valle, M., Zavialov, A., Li, W., Stagg, S. M., Sengupta, J., Nielsen, R. C., Nissen, P., Harvey, S. C., Ehrenberg, M., Frank, J. (2003) "Incorporation of Aminoacyl-TRNA into the Ribosome as Seen by Cryo-Electron Microscopy." Nat Struct Mol Biol ***10*** (11), 899–906.

Vassylyev, D. G., Vassylyeva, M. N., Perederina, A., Tahirov, T. H., Artsimovitch, I. (2007) "Structural Basis for Transcription Elongation by Bacterial RNA Polymerase." Nature ***448*** (7150), 157–162.

Villa, E., Sengupta, J., Trabuco, L. G., LeBarron, J., Baxter, W. T., Shaikh, T. R., Grassucci, R. A., Nissen, P., Ehrenberg, M., Schulten, K., Frank, J. (2009) "Ribosome-Induced Changes in Elongation Factor Tu Conformation Control GTP Hydrolysis." PNAS **106**(4), 1063-1068.

Vizcaino, J. A., Csordas, A., Del-Toro, N., Dianes, J. A., Griss, J., Lavidas, I., Mayer, G., Perez-Riverol, Y., Reisinger, F., Ternent, T., Xu, Q. W., Wang, R., Hermjakob, H. (2016). "2016 update of the PRIDE database and its related tools." Nucleic Acids Res **44**(22): 11033.

Vogel, U., Jensen, K. F. (1994). "The RNA chain elongation rate in *Escherichia coli* depends on the growth rate." J. Bacteriol. **176**(10): 2807-2813.

von Hippel, P. H., Berg, O. G. (1989). "Facilitated target location in biological systems." J. Biol. Chem. **264**(2): 675-678.

Wang, C., Molodtsov, V., Firlar, E., Kaelber, J. T., Blaha, G., Su, M., Ebright, R. H. (2020). "Structural basis of transcription-translation coupling." Science, **369**(6509): 1359-1365.

Webster, M. W., Takacs, M., Zhu, C., Vidmar, V., Eduljee, A., Abdelkareem, M., Weixlbaumer, A. (2020). "Structural basis of transcription-translation coupling and collision in bacteria." Science, **369**(6509): 1355-1359.

Weiel, J., Hershey, J. W. (1981). "Fluorescence polarization studies of the interaction of Escherichia coli protein synthesis initiation factor 3 with 30S ribosomal subunits." Biochemistry, ***20***(20), 5859–5865.

Weixlbaumer, A., Leon, K., Landick, R., Darst, S. A. (2013) "Structural Basis of Transcriptional Pausing in Bacteria." Cell ***152*** (3), 431–441.

Westermeier, R. (2006) "Sensitive, quantitative, and fast modifications for Coomassie Blue staining of polyacrylamide gels." Proteomics.**6** (Suppl 2):61-4.

Windgassen, T. A., Mooney, R. A., Nayak, D., Palangat, M., Zhang, J., Landick, R. (2014) "Trigger-Helix Folding Pathway and SI3 Mediate Catalysis and Hairpin-Stabilized Pausing by Escherichia Coli RNA Polymerase." Nucleic Acids Research ***42*** (20), 12707–12721.

Wintermeyer, W., Gualerzi, C. (1983). "Effect of *Escherichia coli* initiation factors on the kinetics of N-Acphe-tRNAPhe binding to 30S ribosomal subunits. A fluorescence stopped-flow study." Biochemistry, ***22***(3), 690–694.

Woldringh, C. L. (2002). "The role of co-transcriptional translation and protein translocation (transertion) in bacterial chromosome segregation." Mol Microbiol **45**(1): 17-29.

Xia, T., Santa-Lucia, J., Burkard, M. E., Kierzek, R., Schroeder, S. J., Jiao, X., Cox, C., Turner, D. H. (1998) "Thermodynamic Parameters for an Expanded Nearest-Neighbor Model for Formation of RNA Duplexes with Watson−Crick Base Pairs." Biochemistry ***37*** (42), 14719–14735.

Yan, S., Wen, J. D., Bustamante, C., Tinoco, I., Jr., (2015). "Ribosome excursions during mRNA translocation mediate broad branching of frameshift pathways." Cell **160**(5): 870-881.

Yanofsky, C. (1999). "Transcription attenuation: once viewed as a novel regulatory strategy." J. Bacteriol. **182**(1): 1-8.

Yanofsky, C., Ito, J. (1966). "Nonsense codons and polarity in the tryptophan operon." J. Mol. Biol. **21**(2): 313-334.

Yokogawa, T., Kitamura, Y., Nakamura, D., Ohno, S., Nishikawa, K. (2010). “Optimization of the hybridization-based method for purification of thermostable tRNAs in the presence of tetraalkylammonium salts.” Nucleic Acids Res, **38**(6) E89

Yokota, T., Arai, K. I., Kaziro, Y. (1977). “Involvement of 30S ribosomal protein S1 in poly(U)-directed polyphenylalanine synthesis.” Journal of biochemistry, ***82***(5), 1485–1489.

Yusupova, G., Jenner, L., Rees, B., Moras, D., Yusupov, M. (2006). "Structural basis for messenger RNA movement on the ribosome." Nature **444**(7117): 391-394.

Zamir, A., Miskin,, R.,, Elson,, D., (1971) “Inactivation and reactivation of ribosomal subunits: amino acyl-transfer RNA binding activity of the 30S subunit of *Escherichia coli*.” J Mol Biol, **60**, 347-364.

Zamir, A., Miskin,, R.,, Vogel,, Z.,, Elson,, D., (1974) “The inactivation and reactivation of *Escherichia coli* ribosomes.” Methods Enzymol, **30**, 406-426.

Zavialov, A. V., Buckingham, R. H., Ehrenberg, M. A. (2001) "Posttermination Ribosomal Complex Is the Guanine Nucleotide Exchange Factor for Peptide Release Factor RF3." Cell ***107*** (1), 115–124.

Zellars, M., Squires, C. L. (1999). "Antiterminator-dependent modulation of transcription elongation rates by NusB and NusG." Mol. Microbiol, **32**(6): 1296-1304.

Zhang, Y., Mooney, R., Grass, J., Sivaramakrishnan, P., Herman, C., Landick, R., Wang, J. (2014). "DksA guards elongating RNA polymerase against ribosome-stalling-induced arrest." Mol. Cell, **53**(5): 766-778.

Zhang, Y., Feng, Y., Chatterjee, S., Tuske, S., Ho, M. X., Arnold, E., Ebright, R. H. (2012) "Structural Basis of Transcription Initiation." Science, ***338*** (6110), 1076–1080.

Zhen, H.J., Krumins,, V.,, Fennell,, D.E.,, Mainelis,, G., (2015) “Development of a dualinternal-reference technique to improve accuracy when determining bacterial 16S rRNA:16S rRNA gene ratio with application to Escherichia coli liquid and aerosol samples.” J Microbiol Meth, **117**, 113-121.

Zucker, F. H., Hershey, J. W. (1986). “Binding of *Escherichia coli* protein synthesis initiation factor IF1 to 30S ribosomal subunits measured by fluorescence polarization.” Biochemistry, ***25***(12), 3682–3690.

Appendix:

Background subtraction macro written for ImageJ (full)

```
background = 10; //number of pixels height background defined as
a_temp= newArray(background*2); //stores values of background column temporarily, used for
a_backsub to store background average intensity
a = newArray(0,0,0,0);//defines the highlighted area
a1 = newArray(14000*1000);  //makes large array; may need to increase size with image.
a_background = newArray(14000); //average values of background colum; to be subtracted from intensity
of sample; may need to enlarge with large images
a1_backsub = newArray(1400*1000); //a1 with background subtraction; may need to enlarge for large
images.
timeout =0;
SafetyLock=0;
title= getTitle();

print ("Operation Instructions:");
print ("First: Shift Click-top left corner of region of interest");
print ("Second: Alt-click bottom right corner of region of interest");
print ("Lastly: Hit Space-bar to perform background subtraction");
print ("The file saves in the imageJ folder");

//keeps program active while running
while (timeout <150000) {
	timeout++;
	wait (1);
	getCursorLoc(x,y,z,flags);                    //allows us to track cursor movement
	//makeRectangle(a[0], a[1], a[2], a[3]);     //highlight and add location to (x,y,w,h)

//warning of timing out.
	if (timeout ==120000) {
		print ("You will be timed out in 1 minute.");
		print ("Run background subtraction or rerun program");
	}

//define top left corner of ROI
	if (isKeyDown("shift")) {
		a[0] =x;
		a[1]=y;
		wait (1000);
		print (a[0], a[1], a[2], a[3]);
		timeout =0;
		Overlay.remove;
		Overlay.drawLine(a[0],a[1],a[0]+800,a[1]);
		Overlay.drawLine(a[0],a[1],a[0],a[1]+40);
		Overlay.show;
	}
```

```
//define bottom right corner of ROI

	if (isKeyDown("alt")) {
		a[2] =x-a[0];
		a[3] =y-a[1];
		wait (1000);
		print (a[0], a[1], a[2], a[3]);
		Overlay.remove;
		if (a[0]!=0) {
			Overlay.drawLine(a[0],a[1],a[0]+800,a[1]);
			Overlay.drawLine(a[0],a[1],a[0],a[1]+40);
		}
		Overlay.drawLine(a[0]+a[2],a[1]+a[3],a[0]+a[2]-800,a[1]+a[3]);
		Overlay.drawLine(a[0]+a[2],a[1]+a[3],a[0]+a[2],a[1]+a[3]-40);
		Overlay.show;
	}

//start body of background subtraction program
	if (isKeyDown("space")) {
	SafetyLock= 1;
	}

//define background pixels as average of ten pixels above and below column
//saves values into a_background
	if (SafetyLock==1) {
	makeRectangle(a[0], a[1], a[2], a[3]);
		print ("success!");
		for (i=0;i<(a[2]);i++) {
			for (j=0;j<background;j++) {
				a_temp[j] = getPixel(a[0]+i, a[1]+j-background); //records values above
ROI
				a_temp[j+background] = getPixel(a[0]+i, a[1]+a[3]+j); //records below
ROI
				if (j==(background-1)) {     // way to determine average and load in
a_background
					average =0;
					for (k=0; k<(background*2);k++) {
						average = average + a_temp[k];
						if (k==background*2-1) {
							average = average/(background*2);
							a_background[i]= average;
						}
					}
				}
			}
		}
```

```
//calls each pixel intensity around ROI, then stores in 1d array
//subtracts background from sample columns

                for (i=0;i<(a[2]);i++) {
                        for (j=0;j<(a[3]);j++) {
                                a1[(j+a[3]*i)] = getPixel(a[0]+i, a[1]+j);
                                a1_backsub[(j+a[3]*i)] = a1[(j+a[3]*i)]-a_background[i]; //creates
updated matrix with background subtraction
                                if (a1_backsub[(j+a[3]*i)] <0) {
                                        a1_backsub[(j+a[3]*i)]= 0;
                                }
                                setPixel(a[0]+i, a[1]+j,a1_backsub[(j+a[3]*i)]);
                                updateDisplay();
                        }
                }

//displays and plots background subtraction

                run("Select First Lane");
                //setTool("line");
                run("Plot Lanes");
                timeout =155000;
        }
}
```